Unione Europea
Fondo Sociale Europeo

Ministero dell'Università e della Ricerca

Università degli studi di Palermo

Facoltà di Ingegneria - Dipartimento di Ingegneria Chimica dei Processi e dei Materiali
Dottorato di ricerca in "Tecnologie chimiche e dei nuovi materiali", XVIII Ciclo
Settore Scientifico Disciplinare ING-IND/25 Impianti Chimici

Gas-liquid dispersions in mechanically agitated contactors

PhD Thesis by
Francesca Scargiali

Supervisor
Prof. Alberto Brucato

Head of PhD Board
Prof. Alberto Brucato

Academic Year 2006/2007

Programma Operativo Nazionale 2000/2006
"Ricerca Scientifica, Sviluppo Tecnologico, Alta Formazione"
Misura III.4 Formazione Superiore e Universitaria" – Dottorati di Ricerca - (CCI: 1999 IT 16 1 PO 003)

TABLE OF CONTENTS

PREFACE

Gas-liquid reactors are widely used in the process industry to carry out conventional gas-liquid reactions, such as hydrogenations, oxidations, chlorination and biotech fermentations. Suitable devices for this purpose include:

Bubble columns and air lift reactors, in which gas is sparged into the liquid at the bottom of the contactor and mixing is accomplished in the absence of rotating mechanical devices;

Mechanically agitated vessels, in which an impeller rotates in a tank to give enhanced rates of mixing and mass transfer.

In the case of mechanical agitated contactors the usual way for injecting the gas in the liquid phase is that of dispersing it through suitable distributors placed below the lowermost impeller. In this configuration, the gas that has reached the vessel top has little chances to be further involved in the reactions occurring in the liquid phase, and has therefore to be withdrawn from vessel top to be subsequently discharged (as it is usually done in the case of air) or compressed and fed back to the sparger, through a purposely made external circuitry.

An interesting alternative is that of using "*self-inducing*" impellers or *"self–aspirating"* vessels. In this equipment when the impeller is operated at sufficiently high rotational speed the gas phase in the headspace is injected and re-dispersed into the liquid phase, through suitably exploited hollow shafts or surface vortexes. These systems have the advantage that they can operate in *dead-end* mode, so that all of the gas fed may eventually be absorbed in the liquid, a useful feature especially for reactions involving pure gases (e.g. hydrogenations, chlorinations etc.). In this case in fact not only the external circuitry and compressor are saved, but also the hazards connected to its operation are avoided, therefore leading to safer operation.

It is worth noting that these systems have received so far less attention than other gas-liquid contactors, as for instance sparged vessels and bubble column. This is probably due to their strong sensitivity to fine geometrical and operational details, that results into serious scale-up and design uncertainties. As a consequence, applications are somewhat lagging behind the potential of these apparatuses. Clearly the availability of improved modelling tools might well revert the situation.

As concerns bubble columns and gas-liquid stirred tanks, these have been the subject of significant research efforts for several decades, which have led to better understanding of the complex two-phase phenomena involved. The art is anyway far from being satisfactory and, also for this type of equipment, the design of full scale apparatuses is still affected by significant uncertainties. There clearly is a strong need for reliable and general models for the scale-up, development and design of gas-liquid systems..

A fairly new and very promising tool for modelling gas-liquid systems is Computational Fluid Dynamics (CFD). This, being based on a fundamental phenomenological description of system fluid dynamics, is expected to give rise to a new generation of modelling tools, characterized by a very wide applicability. When these approaches will be properly developed and validated, it will be possible to run reliable fully-predictive simulations of full scale apparatuses, that will make pilot-plant experimentation redundant.

It is worth noting, however, that as a difference from single phase systems, the development of CFD models of gas-liquid systems is still at its early stages. As a matter of fact, the simulation of gas-liquid systems not only shares the intrinsic complexity of other multiphase systems, such as solid-liquid systems, but is further complicated by the presence of a non-predefined bubble size distribution as well as by the greater complexity of forces exchanged between phases.

Among these, it is usually the drag force that accounts for most of the force inter-exchange, and therefore deserves special attention. It can be modelled on the basis of *bubble drag coefficient*, which is therefore a critical parameter for the correct prediction of global and local gas hold-up. This estimation is usually made with reference to bubble terminal velocity in quiescent liquids, although the fluid dynamic situation in the industrial units is typically far from that of a quiescent liquid.

This raises the problem of estimating the influence of free stream turbulence on the drag coefficient. As a matter of fact, in analogy with particle-liquid experimental information, turbulence might well have an important effect

on bubble drag. Although indirect and direct evidence shows that bubble terminal rise velocity in liquids may be severely affected by free-stream turbulence, there is a general lack of information on the subject, as well as a lack of viable experimental techniques to suitably quantify the phenomenon.

On the basis of the above considerations, the present work was aimed at contributing to the field by developing the following points:

- Development and evaluation of a new variant of the dynamic technique for the mass transfer coefficient k_La measurement and comparison with other conventional dynamic techniques.

- Design and development of a new self-ingesting stirred vessel; collection of relevant experimental data (mass transfer coefficients, gas hold-up, specific power input) and evaluation of the new reactor performance.

- Measurement of free-stream turbulence effects on bubble drag, through development of a novel experimental technique.

- Development and test of CFD models for gas-liquid systems. Simulations are carried out for both non stirred gas-liquid systems (in particular an air-lift reactor) and stirred tanks, Model validation is carried out through comparison with literature experimental data.

In particular, the thesis is organised in the following chapters:

Chapter 1:

A general introduction on gas-liquid systems and on their hydrodynamic characteristics is reported.

Chapter 2:

An investigation on some variants of the well established *oxygen dynamic technique* is carried out, with the aim of setting up a reliable measurement technique to be employed in the followings of the work. In particular, comparison is made between k_La values determined in presence or in absence of inert gases such as nitrogen. The relevant experimentation is carried out with a *standard* gas-liquid

stirred vessel. Results show that the gas-liquid mass transfer coefficient values obtained either in presence or in absence of dissolved nitrogen are significantly different. Possible reasons behind this discrepancy and the reliability of most of the available literature information (almost invariantly obtained in the presence of dissolved nitrogen) are discussed.

Chapter 3:

A novel self-inducing gas-liquid reactor, the *"Long Draft Tube Self-ingesting Reactor"* (LDTSR), suitable for two and three-phase operations, is proposed.

The difference between k_La values determined in presence or in absence of nitrogen is found to be much larger here than in the case of the standard tank, as it might have been expected.

The performance of the LDTSR in terms of power consumption, gas hold-up and gas-liquid mass transfer is compared with literature data on other self-inducing devices.

Chapter 4:

Chapter 4 describes the attempts made to set up a novel experimental technique aimed at collecting data on the free stream turbulence effects on bubble drag. The technique is based on the use of a vertical water channel where a suitable grid acts as a turbulence generator.
Preliminary experimental results and the difficulties encountered are discussed.

Chapter 5:

Chapter 5 concerns CFD modelling of gas-liquid systems. In the first part general information on the modelling approaches adopted is presented. Then the gas-liquid CFD simulations of an air-lift reactor and of a standard stirred vessel are presented and validated by comparison with literature experimental data.

Chapter 6:

The results obtained and future work perspectives are summarised.

CHAPTER 1:

INTRODUCTION TO STIRRED GAS LIQUID DISPERSIONS

1.1 Selection and configuration of gas-liquid equipment

The cylindrical tank, either stirred or unstirred, is the most common reactor in processing and bio-processing engineering. Yet, a vast array of reactor configurations is in use in different process industries. Novel reactors are constantly being developed for special applications. Much of the challenge in reactor design lies in the provision of adequate mixing and gas distribution.

The first classification of gas-liquid mixing problems is according to liquid viscosity, since this dictates the basic mixing mechanics and types of equipment applicable in practice.

For low viscosities (say < 0.2 Pa*s), turbulence can be used to obtain good mixing, high interfacial area and high mass transfer coefficients, while degassing can be achieved by gravity. Suitable devices include (see Fig.1.1):

- simple bubble columns, in which gas is sparged into the liquid at the bottom of the contactor;
- plate columns, in which gas is redispersed at each plate up the column;
- mechanically agitated vessels, where an impeller rotates in a tank (usually baffled) to give enhanced rates of mass transfer;
- in line static mixers, where mixing energy is derived from the pressure drop across the mixer;
- jet devices, where gas is dispersed into the liquid by liquid jets;
- surface aerators, in which agitators at the liquid surface entrain gas from the head space into the liquid.

In this discussion, attention is focused upon gas dispersion in mechanically agitated vessels, which are generally the most effective and flexible contactors for many duties. However the fundamental concepts set down for these systems also have some relevance to the other gas dispersing devices.

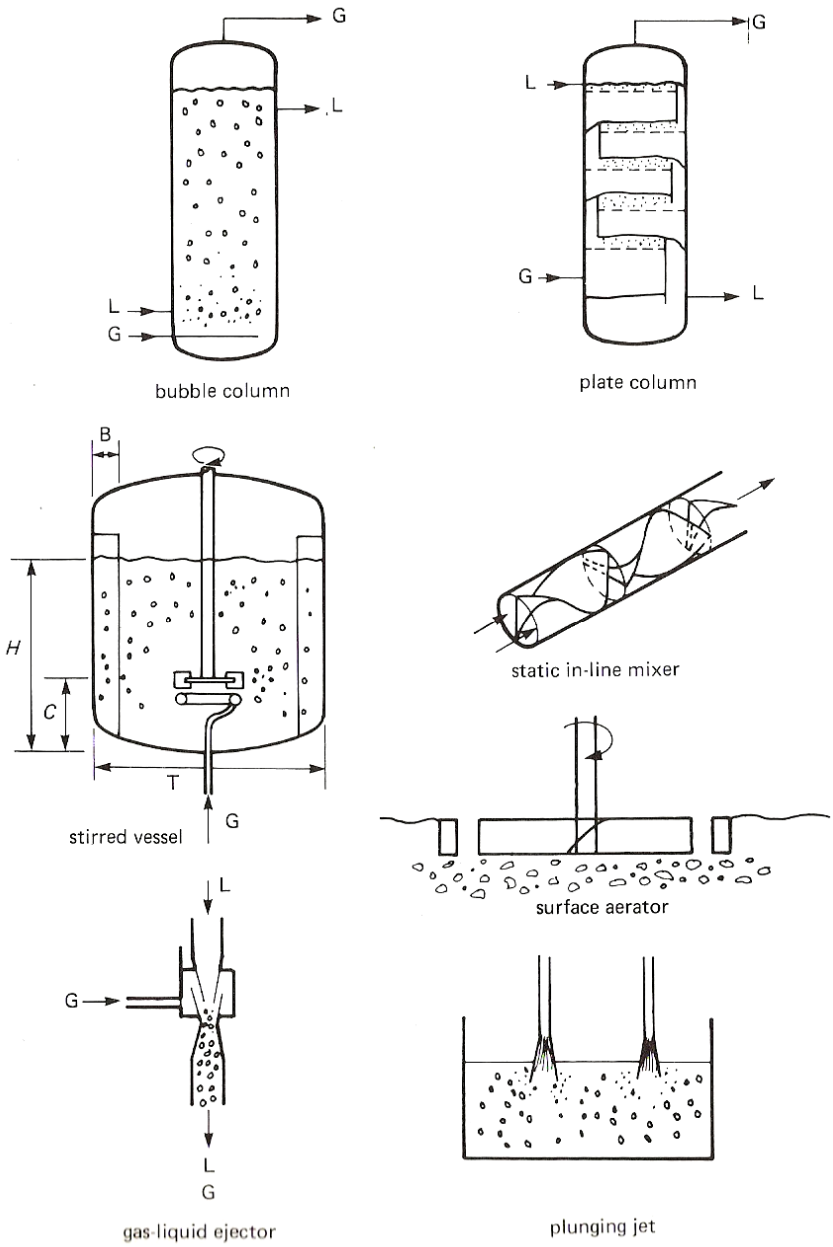

Fig. 1.1: Gas-liquid contacting devices for low-viscosity systems (after Middleton, 1985, fig.17.1)

1.2 Flow patterns and operating regimes in standard gas-liquid stirred vessels

In gas-liquid stirred reactors mechanical agitation is used to break the gas in small bubbles for high interfacial area, to disperse the bubbles throughout the liquid, to keep the bubbles in the liquid for sufficient time providing a good gas hold-up, to mix the liquid inside the vessel, to maximize heat and mass transfer coefficients, to maintain particles (when present) in suspension. This is obtained by providing high energy turbulence (shear rate controlled systems) and high flows at the agitator.

An effective and widely proven impeller for gas-liquid stirred tanks is the 6-blade disc turbine, also known as *Rushton* turbine (Fig. 1.2a). However improved disc turbine agitators with 12 or 18 blades, or with concave rather than flat blades (Fig. 1.2 b, c, d),, have shown to have better gas handling capacity than Rushton turbines and are therefore increasingly employed (Middleton, 1985).

The general range of application of such vessels is:
Liquid viscosity up to about 0.2 Pa s (Re > 104);
Gas superficial velocity up to about 0.2 m/s;
Shaft power input from 1 to 7 kW/m3;
Volume up to 100 m3;
Small particle concentration up about 30 % wt.

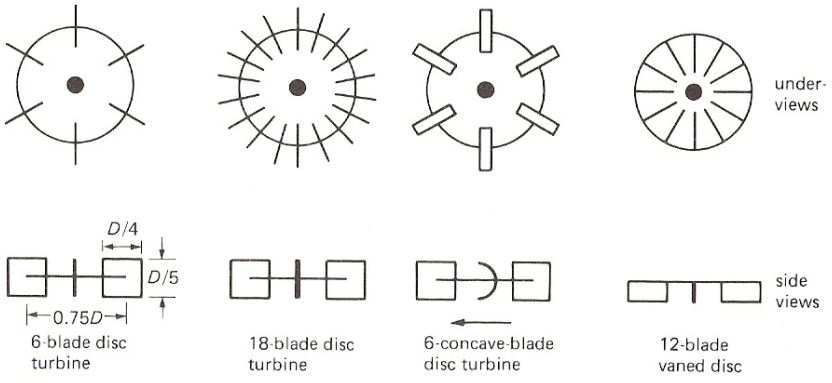

Fig. 1.2 Agitators for gas-liquid dispersions (after Middleton, 1985, fig.17.1)

The nature of the gas inlet device is relatively unimportant if the design is such that the gas is effectively captured and dispersed by the agitator. Multiple orifice ring spargers are often recommended to obtain efficient mass transfer. However they are only marginally better than a single open pipe sparging centrally beneath the disc. To make sure that all entering gas is immediately processed by the impeller, the inlet distance from impeller plane is usually smaller than D/2 (D = impeller diameter).
Apart from the type of the impeller used, for a given gas flow rate entering the reactor, different flow regimes can be observed when agitation speed is increased. For six bladed disk turbine impellers, five flow regimes in the vessel can be defined, as shown in Fig. 1.3 (Nienow *et al.*, 1978):

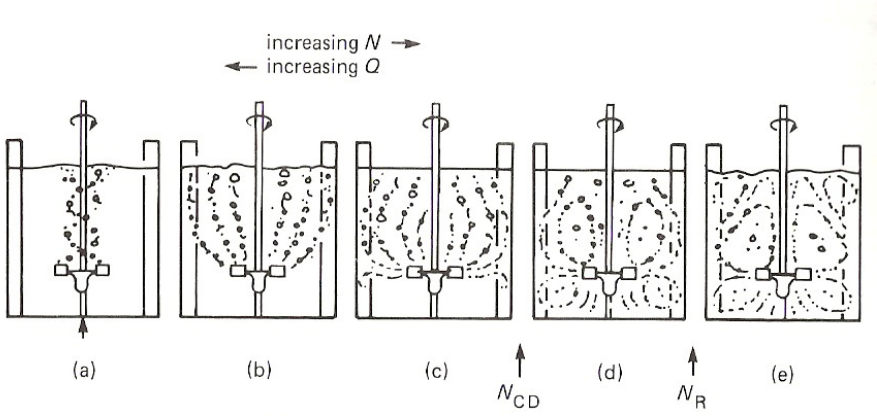

Fig. 1.3: Regimes of bubble flow (after Nienow et al., 1978)

(a) *Flooding*: at the lowest agitation speed (N) the gas passes through the agitator region mainly as large bubbles that are not broken into smaller ones by the impeller action.

(b) *First loading regime*:: as N increases the gas phase begins to be dispersed in smaller bubbles which pervade the superior section of the reactor where the gas flow can be modelled as a plug flow.

(c) *Second loading*: the gas phase is dispersed in smaller and smaller bubbles Part of the bubbles are entrained by the downward liquid velocities and are therefore recirculated to the impeller region. A few bubbles may occasionally enter the lower part of the reactor, which is however occupied in practice by the liquid phase only.

(d) *Complete aeration*: Gas recirculation is present both above and below the impeller. Gas dispersion concerns the entire volume of the reactor.

(e) *Secondary recirculation*: An unstable regime in which the impeller is oversupplied with gas and secondary gas recirculation loops appear inside the reactor.

The most important transition is that from C to D the minimum speed to just completely disperse the gas. Nienow *et al.* (1978) proposed the following correlation to calculate the relevant critical stirrer revolution rate N_{CD}:

$$N_{CD} = 4\frac{Q_g^{0.5}T^{0.25}}{D^2} \tag{1.1}$$

A correlation is also available to estimate the critical agitation speed from regime D (complete aeration) to regime E (recirculation) (Nienow *et al.* , 1978):

$$N_R = 1.5\frac{Q_g^{0.2}T}{D^2} \tag{1.2}$$

1.3 Power consumption

Knowledge of the power, Pg, absorbed by the gas-liquid dispersion from the agitator is required for good mechanical design. The ungassed power is readily obtained from:

$$P = N_p \rho N^3 D^5 \tag{1.3}$$

where the *ungassed power number* N_p may be easily obtained from literature information (Middleton and Smith, 2004).
When gas is sparged the power drawn by the impeller decreases (see Fig. 1.4) mainly due to the formation of gas pockets (called *cavities*) behind the blades (Fig. 1.5). These quite effectively "streamline" the blades, thus reducing fluid drag and in turn shaft torque and power. Several workers have attempted to correlate Pg as a function of system and operating variables (e.g. Michell and Miller, 1965, Hassan and Robbinson, 1977).

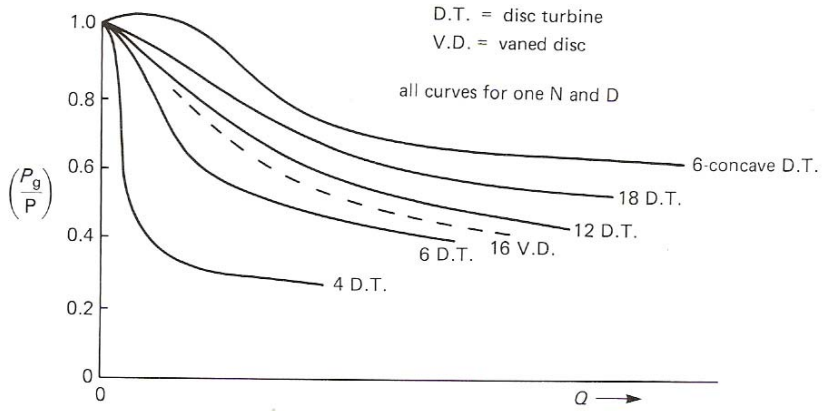

Fig. 1.4: Typical power curves for gassed agitators (after Middleton, 1985, fig.17.4)

In more recent work, Pg/P has been related to the different flow regimes. These regimes can be associated closely with a graph of (Pg/P) *vs* Gas Flow Number, Q_G/ND^3, with increasing N when Q_G is held constant (Fig. 1.5). At the lowest values of N (region a) gassed power is not much less than the

blades and dispersed and Pg first decreases as captured gas "streamlines" the blades, forming "large cavities".

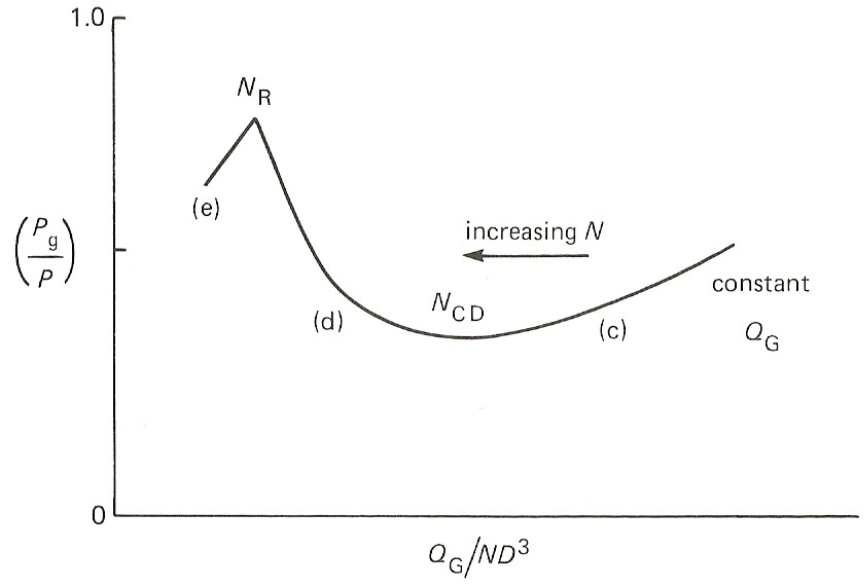

Fig. 1.5: Power curves at constant gas rate (after Nienow et al., 1978)

Further increase of N diminishes the size of cavities and changes their form to "vortex" cavities (Fig. 1.6). The curve passes through a minimum at N_{CD}, the minimum speed for complete dispersion of the gas. It then rises when small recirculation patterns start to emerge. The maximum is attained at about the speed N_R, at which gross recirculation of gas back into the agitator sets in.

The speed N_{CD} can be predicted from this minimum and this is valuable since it marks the speed below which gas does not penetrate beneath the agitator and the whole is not effectively used. In Fig. 1.5 transition between state (C) and (D) is easily found.

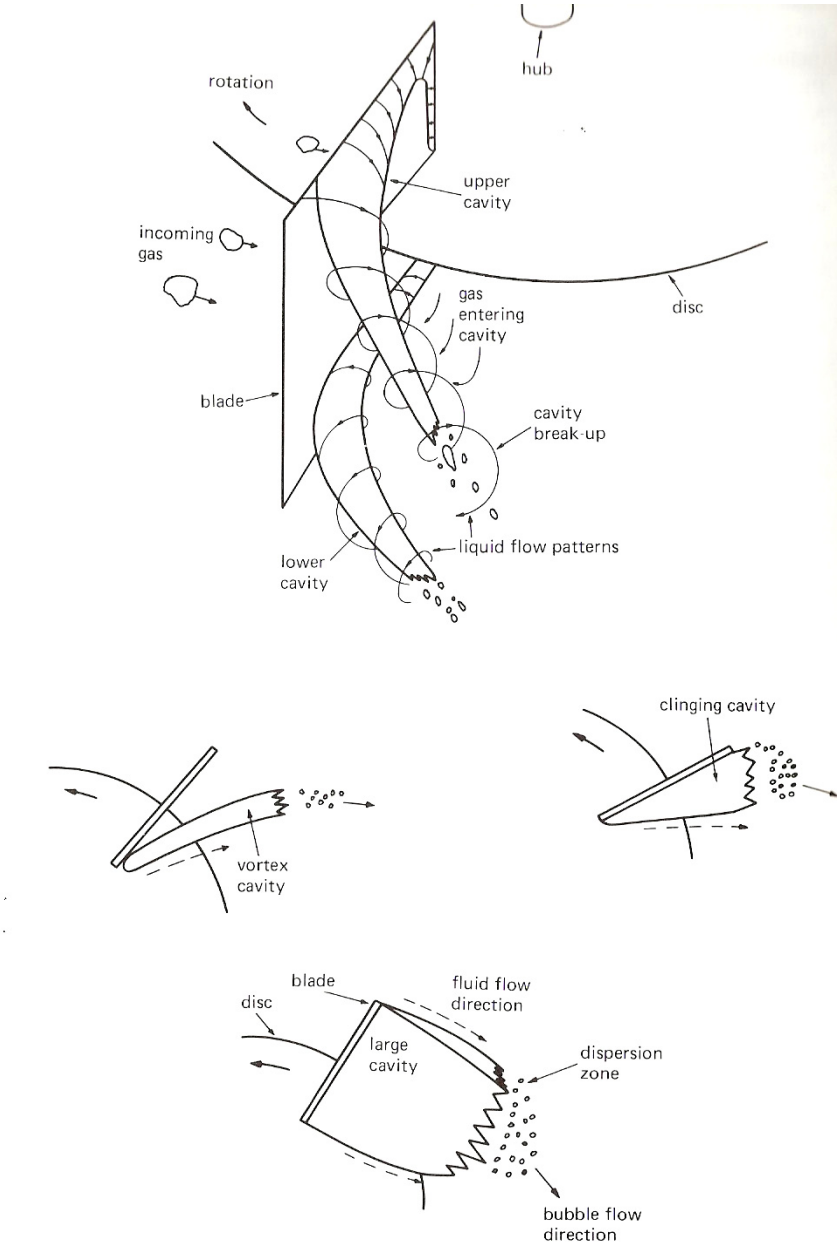

Fig. 1.6: Cavity formation behind blades (after Middleton, 1985, fig.17.4)

The literature on "standard" stirred tanks and gas-liquid characteristics of Rushton turbines is vast and will not be further reviewed here. The interested readers may refer to books such as Harnby *et al.* (1985), Paul *et al.* (2004).

The literature on self-inducing gas-liquid stirred tanks and other specific subjects dealt with in this thesis (k_La measurements, bubble terminal velocity, CFD simulations of gas-liquid systems) is thoroughly reviewed at the beginning of the relevant chapters.

CHAPTER 2

ON THE MEASUREMENTS OF MASS TRANSFER COEFFICIENT ($k_L a$) IN GAS-LIQUID SYSTEMS

2.1 INTRODUCTION

The design, scale-up and optimization of industrial processes conducted in multiphase agitated reactors require, among others, precise knowledge of the hydrodynamics, mass and heat transfer parameters and reaction kinetics. Literature data available indicate that the gas-liquid mass transfer is very often the rate limiting step in many industrial processes (Mills and Chaudhari, 1999). For the design of such systems, knowledge of the mass-transfer coefficient is clearly of primary importance.

2.1.1 Mass transfer coefficient k_La measurement

Experimentally, the mass-transfer coefficient can be determined by physical or chemical methods. The former derive the k_La value from a step change of oxygen concentration in the inlet gas stream, while the latter utilise a constant concentration in the liquid phase above or below saturation. Methods using the first approach are often referred to as unsteady state or dynamic methods ($dC_L/dt \neq 0$), whilst those using the second, are referred to as steady state methods ($dC_L/dt = 0$).

Chemical methods

The principle of steady state methods for the measurement of k_La is to maintain the liquid phase concentration of the gas (oxygen, ozone, CO_2, etc.) at a constant value. different from the saturation concentration. This means that the concentration driving force between gas and liquid is constant. Therefore the liquid has to act as a gas sink or source. This is achieved by chemical or biochemical methods, where the reacting gas is removed or generated by a chemical reaction. If the liquid batch is assumed to be at steady state and perfectly mixed, the oxygen mass balance is:

$$k_La\,(C_G\,/m - C_L) + Rg = 0$$

where Rg is simply related (through stoichiometry) to the reagent consumption rate. The main advantage, compared to the dynamic methods, is that the dynamic behaviour of the oxygen probe does not affect the measurement of oxygen concentration and, therefore, no modelling of this device is required.

The extent to which the macromixing state of the two phases affects the k_La value is not completely clear. As regards the liquid, Linek *et al.* (1982) do implicitly assume that it is irrelevant, while, e.g., Lara Marquez *et al.* (1994) observed that the method requires perfect mixing. When complete homogeneity cannot be assured, proper models of the liquid phase should be adopted (Vasconcelos *et al.*, 1997; Manna, 1997). As for the gas phase, problems similar to those mentioned for the dynamic method can arise: apart from the rough no-depletion/no-enrichment model (where C_G is assumed uniform and equal to the entering gas concentration) the simplest modelling approaches consider perfect mixing and plug flow. Usually, lesser influence of the gas behaviour is recognised for these methods.

A very common technique is the sulphite method (Van't Riet 1979) in which sulphite reacts with oxygen under the presence of a copper or cobalt catalyst. Though this is a popular technique, a significant drawback of it and other chemical techniques (Van't Riet, 1979) is the high ionic concentration (1 – 2 M). This changes the liquid properties, transforming water from a rather coalescent system into a non-coalescent one, characterized by smaller bubbles, hence leading to increased values of the k_La coefficient.

Other chemical techniques include the absorption of CO_2 into different liquids (Mehta and Sharma, 1971; Joshi and Sharma, 1977). This method leads to ionic concentration similar to the sulphite method, and therefore share the same disadvantageous consequences.

The variety of measurement methods is a clear indication that difficulties still exist when reliable measurements of k_La are desired. Great care has to be taken to select the appropriate method and to use the chosen technique correctly.

Physical methods

The dynamic oxygen-electrode method has been widely used for kLa measurements (Van't Riet, 1979; Linek *et al.*,1987). In this method the oxygen concentration in the gas is changed instantaneously and the change of oxygen concentration as a function of time is followed using a dissolved oxygen probe. The gas side mass transfer resistance is usually much smaller than the liquid side, and can therefore be neglected. For a perfectly mixed system, Eqn. 2.1 is obtained:

$$\frac{dC_L}{dt} = k_L a\left(C_L^* - C_L\right) \tag{2.1}$$

where C_L^* is the equilibrium oxygen concentration. If k_La, and C_L^* are identical for all bubbles at any time throughout the process, equation (2.1) can be integrated to give:

$$\ln\left(\frac{C_L^* - C_L}{C_L^* - C_0}\right) = -k_L a(t - t_0) \qquad (2.2)$$

It follows from equation (2.2) that, if the above hypothesis are reasonably abode by, plots of $\ln(C_L^*-C_L)$ versus t will result into straight lines with a slope equal to $(- k_La)$.

Certain difficulties are encountered when using this method. As a matter of fact, Eqns. 2.1 and 2.2 strictly hold only when both the liquid and gas phases are perfectly mixed. In all other cases precise information on the gas and liquid behaviour is required in order to properly asses the mass transfer parameter.

The influence of the liquid phase flow behaviour on the accuracy of measurements is recognized to be small (Nocentini, 1990). On the contrary, the flow behaviour of the gas phase may significantly affect the results, and should be suitably accounted for. This can be done in several ways, among which are the three idealised models of fully-backmixed, no-depletion, and plug flow. The fully back-mixed model assumes a perfectly mixed gas phase where all bubbles share the same concentration, equal to the exit gas concentration. The other extreme is the no-depletion model, where all bubbles are assumed to practically maintain the inlet concentration. Between these two extreme cases lies the plug-flow model, in which the gas phase concentration varies according to the time spent by each bubble in the system. Clearly in the last two cases eqns. (2.1) and (2.2) have to be properly rewritten.

The choice of a suitable gas behaviour model is also linked to the concentration of the gas phase fed to the system (i.e. pure oxygen or air) and of the liquid phase (i.e. degassed liquid, deoxygenated liquid by nitrogen saturation, etc.). Useful reviews of models devised to describe the gas and the liquid phase behaviour can be found in Linek *et al.* (1982; 1987).

It is worth noting that the only case in which there is no need to resort to models for the behaviour of the gas phase, is when a pure gas is absorbed in a completely degassed liquid (Linek *et al.*,1987). In this case in fact there can be no question about the uniformity of gas concentration in the bubbles and the k_La value obtained using equation (1.2) does certainly coincide with the real value. The present authors are aware of only one example of application and

comparison of this method in the open literature, namely that reported by Linek *et al.* (1987). They compared the k_La values obtained by the traditional dynamic method in a standard stirred reactor with the values obtained by the above variant. Notably, in the latter case the resulting k_La values were found to be larger, by about 20% for coalescing systems and up to 50% for non-coalescing systems, than those obtained by the former technique.

In this chapter, the mass transfer performance in a conventional stirred vessels is investigated. Comparison is made between k_La values determined by the dynamic method, performed in two different variants.

2.2 EXPERIMENTAL APPARATUS

A schematic diagram of the experimental apparatus is reported in Fig. 2.1. It consisted of a "standard" stirred reactor with ID = 190 mm, H= 300 mm, thickness s= 5 mm. A "Rushton turbine" (six flat blade disk mounted) of 65 mm dia. (Fig.2.2) was mounted on the 17 mm dia. shaft., leaving a clearance of T/3 from vessel bottom. The vessel was equipped with 4 vertical baffles 3 mm thick and 19 mm wide, deployed along wessel walls at 90° from each other. The vessel was filled with deionized water up to an eight of 190 mm (H=T).

The shaft was driven by a 1200W DC motor (Mavilor MSS-12), equipped with tacho and speed control unit (Infranor SMVEN 1510) so that rotational speed was maintained constant, within $\pm$ 0.1%.

A Venturi vacuum pump (Vaccon HVP 100) was used to evacuate the vessel down to 0.1 atm. Oxygen flow was controlled by a "Dynaval" fluximeter.

Oxygen concentration was measured by means of an electrode sensor (WTW CellOx 325) and control unit (WTW Oxi 340i). The electrode time constant was experimentally measured to be about 3.0 s. By means of a peristaltic pump liquid was continuously withdrawn from the vessel and returned to it after having passed over the oxygen electrode. This external loop added a (negligible) almost-pure delay of the order of few seconds to the measurements made. The output of the oxygen measurement unit were recorded with a data acquisition system and finally processed to yield the relevant value of the mass transfer coefficient k_La.

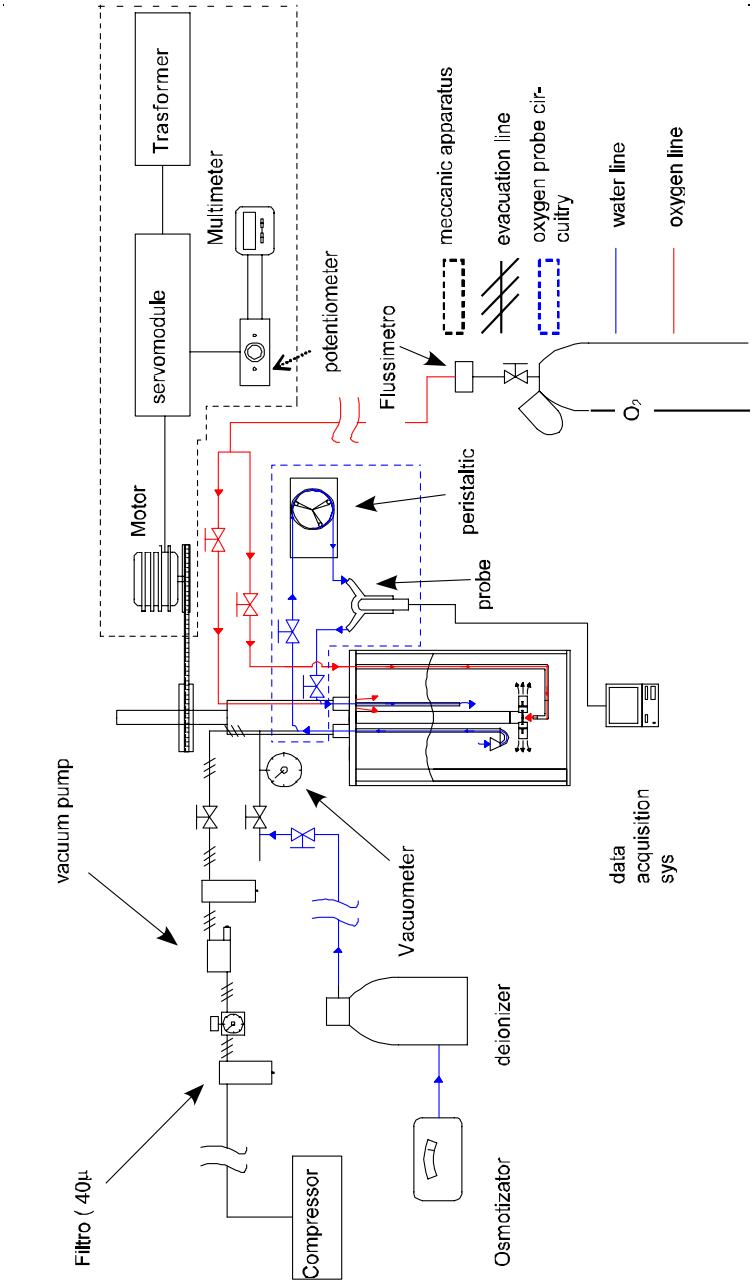

Figura 2.1 – Experimental apparatus

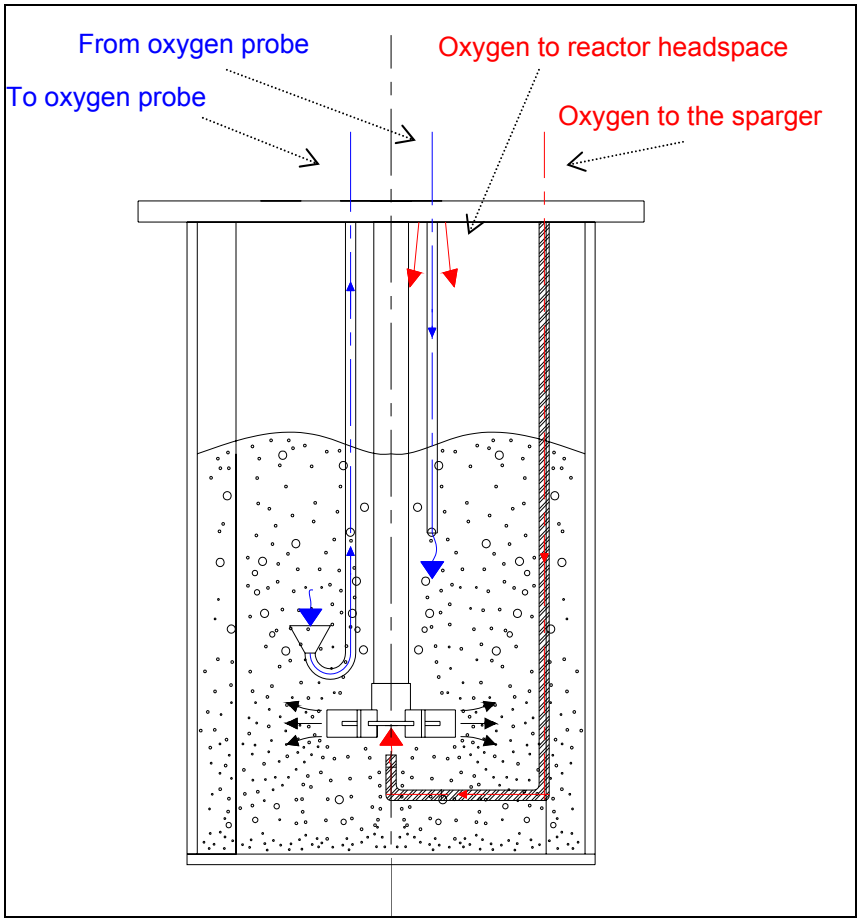

Fig. 2.2 –Reactor

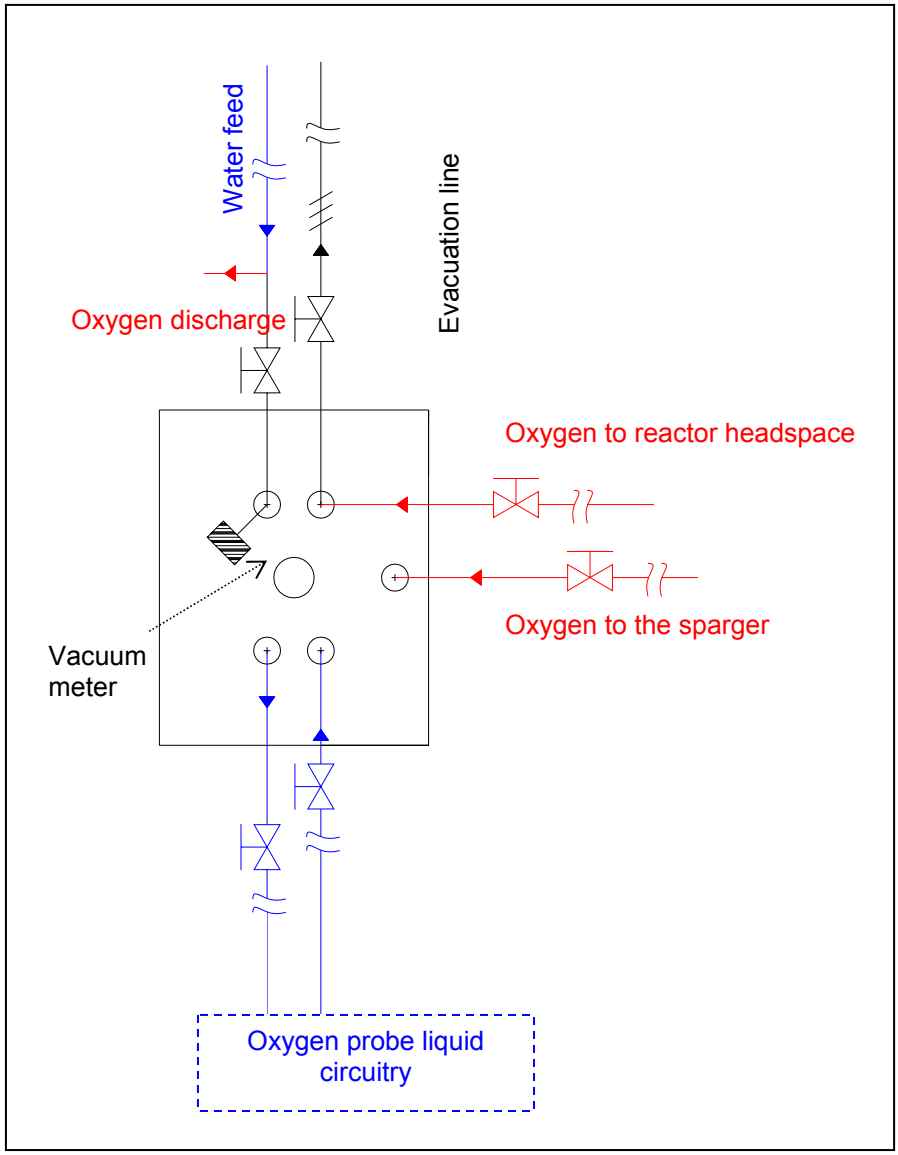

Figura 2.3 – Top plate.

Oxygen sensor CellOx325

The most important components of the oxygen sensor are reported in Fig.2.4:

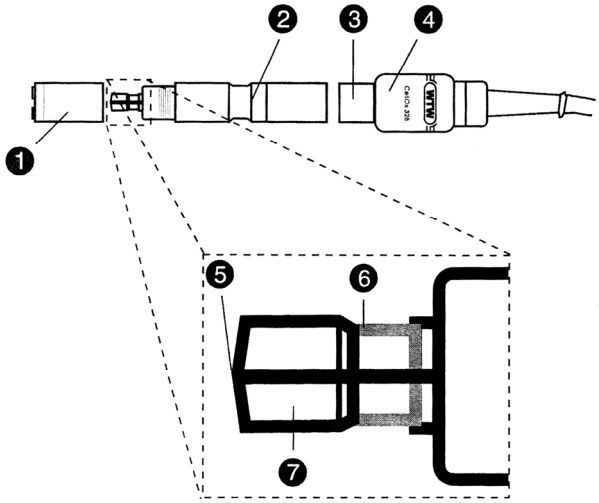

1 Membrane head
2 Temperature sensor
3 shaft
4 closing head
5 working electrode (gold cathode)
6 Counter electrode (lead anode)
7 Isolator

Fig 2.4 – Construction of the oxygen sensor CellOx325

It consists essentially of a pair of polarized electrodes, respectively a gold cathode and a lead anode, and an electrolyte separated from the sample by a gas-permeable membrane.

Oxygen diffuses across the electrode membrane and is reduced to hydroxyl ions at a Silver cathode according to the reaction:

$$0_2 + 2H_2 0 + 4e^- \longrightarrow 40H^-$$

The electrones needed for this process are provided by a reaction at the lead anode. Because the electrolyte contains chloride ions, this reaction may be written as:

$$Pb + Cl^- \longrightarrow PbCl + e^-$$

At any given temperature the electric current which flows between cathode and anode is directly proportional to oxygen concentration outside the membrane. A temperature compensation circuit corrects for changes in the permeability of the membrane to oxygen with temperature.

2.3 EXPERIMENTAL MEASUREMENTS

2.3.1 Power consumption

A "static-frictionless" turntable (Grisafi *et al.* 1998) was devised for the measurement of the mechanical power dissipated by the impeller at various agitation speeds and gas flow rates. The apparatus employed is depicted in Fig. 2.4 and consists of a granite dish (D), polished on the lower side and facing the polished side of a larger table of granite (C). The upper dish was provided with a hard steel pivot pin (OD=5 mm) placed in the centre and protruding from the dish lower surface (see inset in Fig. 2.5). The pivot pin was tightly coupled with a hard steel tube inserted in the granite table, so that the upper dish could only rotate about its centre.

A small flow rate of a fairly viscous oi! was then fed trough the lower end of the tubing coupled with the pivot, therefore lubricating first the pin-tubing coupling and then the coupling between the polished sides of the dish and the table, while flowing radially towards and over the dish border, to be finally collected in a small reservoir. The oi! Flow rate was generated by pressurising the oil reservoir (B) with compressed air. With over pressures of about 2 atm, flow rates of about 2 mL/min were obtained, so that many measurements could be taken before refilling the oi! reservoir.

By this arrangement the static friction between the rotating surfaces was virtually eliminated. Moreover, a dynamic friction useful for damping the unavoidable oscillations of the torque itself was supplied. The tank rotation was hampered by a flexible string (E), fixed to the external tank wall, and connected through a pulley (F) to a weight (G) put over an electronic balance (H). The torque exerted by the stirrer on the vesseI was assessed by measuring the force acting on the flexible string (E) in order to inhibit vessel rotation. This force was measured by subtracting the reading of the balance (H) in agitation conditions from that observed without agitation (still stirrer). On these grounds, the only uncertainty in the measurements is introduced by the static friction between the string and the pulley (F). The error, estimated of the order of 0.05 N, did not significantly affect the precision of the measurements performed. In any case, especially at the lowest stirrer speeds, measurements were taken by approaching the desired agitator speed from both higher and lower speeds, and then taking the arithmetic mean of the two readings obtained.

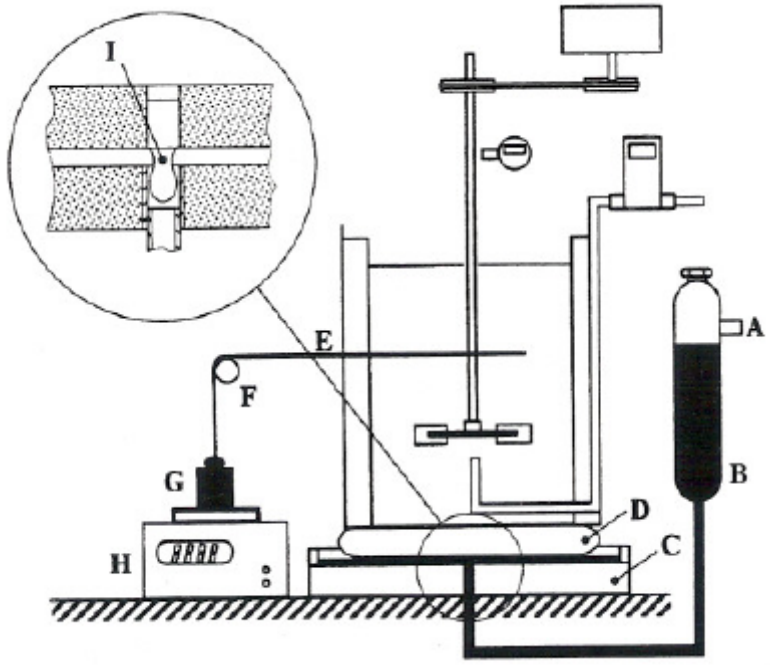

Fig. 2.5: Experimental equipment for power consumption measurements: A) compressed air inlet, B) pressurised oil tank, C) oil duct, D) rotating plates, E) flexible wire, F) pulley, G) weight, H) electronic balance, I) pivot pin.

Results obtained are shown in Fig. 2.6, where it can be observed that, as expected, power consumption increases when increasing agitation speed.

The resulting gassed power number, calculated from Eqn. 1.3, shows two levels, it is lower at low agitation speed and higher at high agitation, as shown in Fig. 2.7, which seems not perfectly convincible. Plotting the gassed power number versus the gas flow number, as done in Fig. 2.8, a trend similar (though not identical) to that described by Nienow *et al.* (1978) (see chapter 1, Fig. 1.5) is obtained, in which a relative maximum in the proximity of N_R and a minimum in correspondence of N_{CD} are clearly visible.

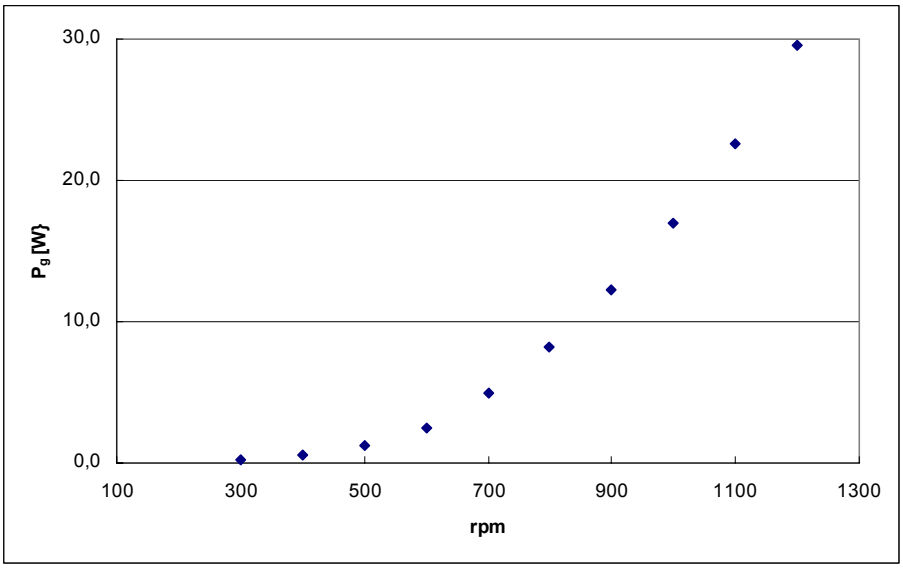

Fig. 2.6: Power consumption for gassed conditions versus agitation speed.

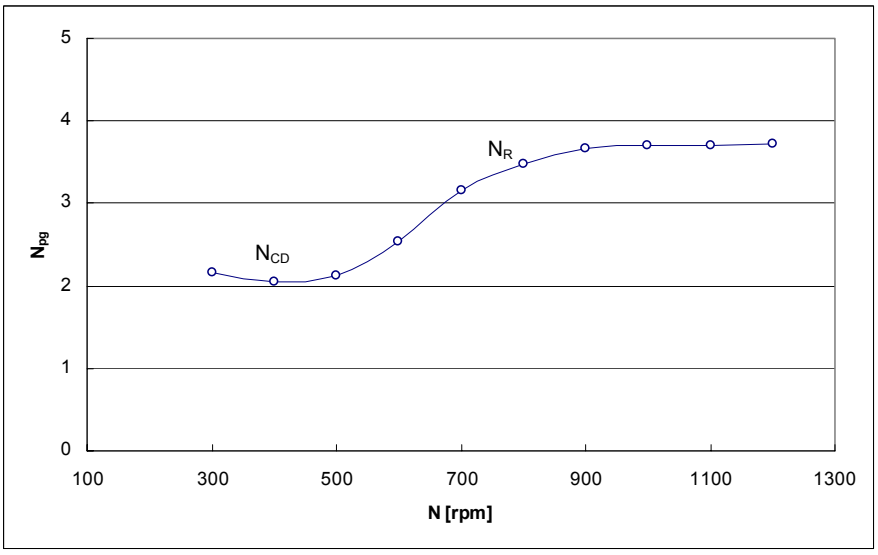

Fig. 2.7: Gassed power number versus agitation speed.

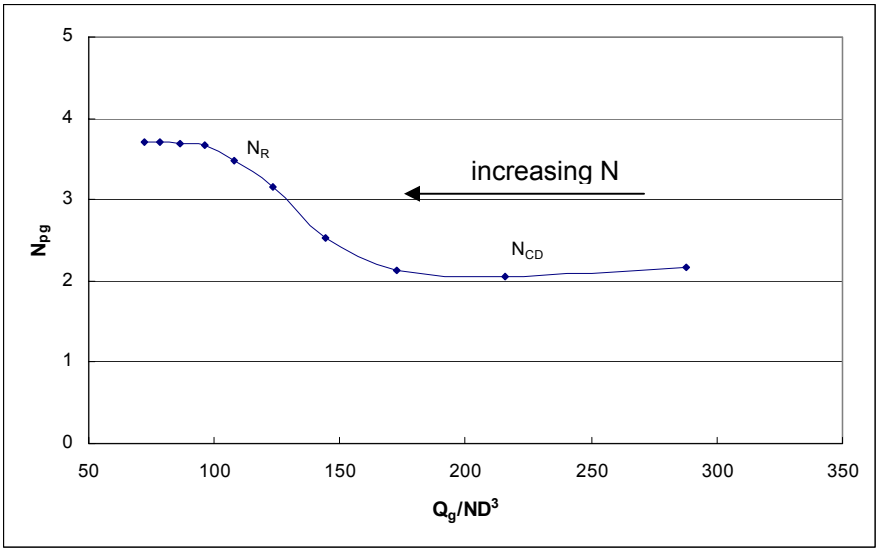

Fig.2.8: Gassed power number versus gas flow number

2.3.2 k_La measurements

Influence of electrode response time

The volumetric mass transfer coefficient, k_La, was assessed by unsteady state experiments on the basis of pure oxygen absorption and desorption dynamics.

As already pointed out, the oxygen sensing electrode was found to have a first order lag of about 3.0 s, thus a value significantly smaller than the expected time dynamics for oxygen absorption, so that neglecting the probe time dynamics should have negligible effects on the resulting k_La values (Van't Riet, 1979).

In order to confirm these expectations, model computations were carried out in which the probe response time t_p was taken into account via the DO probe dynamics equation:

$$\frac{dC_p}{dt} = \frac{\left(C_L - C_p\right)}{t_p} \tag{2.4}$$

where c_p is the measured probe concentration. By solving simultaneously eqn. 2.2 and 2.4, equation 2.5 is obtained (Conway *et al.*, 2002):

$$\frac{C_L^* - C_p}{C_L^*} = \frac{\exp\left(-k_L a\, t\right) - k_L a\, t_p \exp\left(-t/t_p\right)}{1 - k_L a\, t_p} \tag{2.5}$$

Equation 2.5 has been plotted on a semi-log plot, versus the non-dimensional product $t_p{*}k_La$, in Fig. 2.9. It can be seen there that, even for the highest k_La value obtained in this work (0.09 s^{-1} i.e. $t_p{*}k_La$ = 3*0.09 = 0.27) , the final slope of the curve (the one always employed in this work) is completely unaffected by probe dynamics.

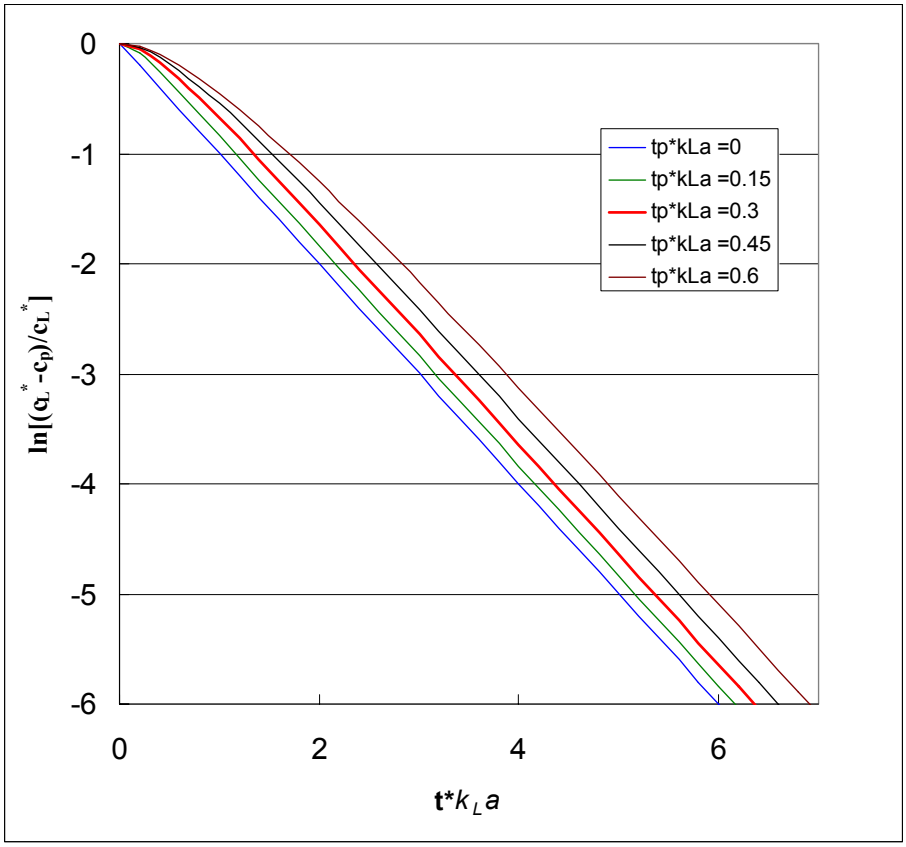

Fig. 2.9: Trend of the measured oxygen concentration in the liquid vs dimensionless time, for various response times of oxygen probe.

The same result can be better quantified by plotting the derivative of eqn. 2.5, resulting in eqn. 2.6, versus non-dimensional time:

$$\frac{d}{d(k_L a\, t)}\left(\frac{C_L^{*}-C_p}{C_L^{*}}\right)=-1+\frac{\left(\left(1-k_L a\, t_p\right)\exp(k_L a\, t)\left(1-1/(k_L a\, t_p)\right)\right)}{1-k_L a\, t_p\,\exp\left(k_L a\, t(1-1/(k_L a\, t_p))\right)} \quad (2.6)$$

As it can be seen, all the curves reported in Fig. 2.10, for a sufficiently high non–dimensional time (t^*k_La) tend to a value equal to "-1", i.e. to a condition in which the measurement is completely unaffected by probe dynamics.

In particular for a $t_p^*k_La = 0.3$, it is sufficient to read the slope of the curve obtained from eqn. 2.5 (in a semi-log diagram) after a non-dimensional time larger than 1.35 to obtain an error smaller than 3%.

As this was the case for all the measurements of the present work, the quantitative correctness of the final figures obtained, is fully confirmed.

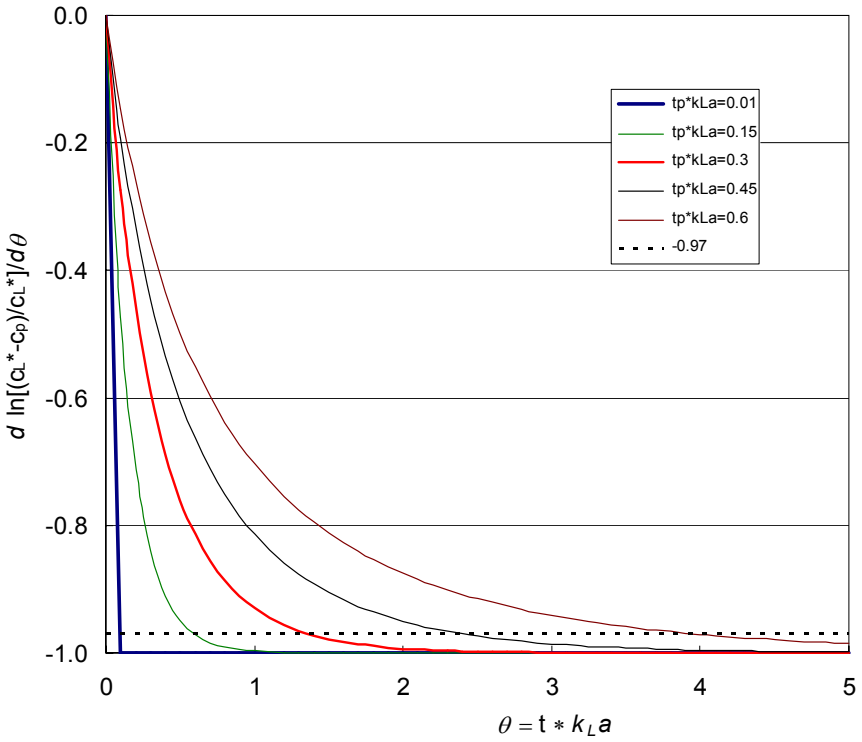

Fig. 2.10: Slope of the oxygen concentration dynamics vs non-dimensional time, for various response time t_p *of the oxygen probe.*

Other k_La measurement interferences

In order to minimize the interferences caused by gas bubbles adhering to the electrode surface, liquid was continuously withdrawn from the vessel by means of a peristaltic pump and returned to it after having passed over the oxygen electrode in such a way that only few bubbles were entrained in the external loop and the majority of these did not interact with the electrode. This external loop was close to a plug flow and therefore added to the measurements an almost-pure delay of about 3 seconds, as experimentally assessed. This resulted in practice in a simple shift of the dynamics response and did not affect the results obtained. The output of the oxygen measurement unit were recorded *via* a data acquisition system and finally processed to yield the relevant value of the mass transfer coefficient k_La. In all runs the temperature inside the reactor was between 24 and 25 °C. This was obtained by adjusting the initial temperature and exploiting the circumstance that, due to the very slow temperature rise dynamics, the temperature increase during each single run was always less than 0.2 °C.

Alternative experimental procedures for the dynamic oxygen technique

As previously stated, under the hypothesis of gas bubbles all made of pure oxygen and perfectly mixed liquid phase, the mass transfer coefficient k_La does simply coincide with the slope of the observed exponential decay (Eqn. 2.2).

It is clear that there are several reasons for the real behaviour to detach from the above idealised model, namely the liquid phase is never perfectly mixed and gas bubbles may not be made of pure oxygen. As a matter of fact, apart from the effectiveness of the air removal from the head space, if there initially is some dissolved nitrogen in the liquid phase, this is unavoidably transferred to the gas bubbles during the run, therefore diluting the oxygen there contained.

For this reason several experimental procedures where employed.

Pure oxygen absorption in air saturated water (procedure "OAS")

A typical "OAS" experimental run started from a condition of air-saturated liquid and no agitation conditions. Pure oxygen then started to be fed to the vessel sparger with a flow rate of about 6 l/min (1vvm). Data acquisition was started shortly after agitation. A transitory followed, in which the difference between the equilibrium concentration to pure oxygen and the time dependent

oxygen concentration measured in the liquid phase decayed and eventually vanished.

Pure oxygen absorption in pre-evacuated water (procedure OApE)

This variant was devised in order to free the system form dissolved nitrogen, so avoiding the subsequent contamination of oxygen bubbles. To this end, the liquid inside the tank was almost completely degassed by repeated evacuation of the reactor headspace. In particular, pressure inside the reactor was typically brought down to about 0.1 bars while stirring at medium agitation speeds to fasten the degassing process. Vacuum and agitation were maintained for several minutes (typically 5 min) and then atmospheric pressure was restored by admitting pure oxygen to the reactor headspace. To make sure that practically all nitrogen initially dissolved in the liquid phase had been removed, a sequence of at least three evacuation cycles was carried out before beginning the experimental run. This last was then performed in the same way described in procedure "OAS". After the first run, a single evacuation procedure was employed to partially desorb the oxygen dissolved in liquid phase and a new run could be started.

2.4 RESULTS AND DISCUSSION

A typical experimental oxygen concentration dynamics obtained by pure oxygen absorption in air saturated water (procedure OAS) is shown in Fig.2.11, where the dimensionless driving force for mass transfer is reported versus time in a semi-logarithmic plot. Data acquisition was started first and only after several seconds the agitator was started. As a consequence, time zero in the figure is meaningless. Nevertheless, as previously discussed, on the basis of the simplest concentrated parameter model (bubbles all made of pure oxygen, well mixed liquid phase) it was expected that, after some time, data points did align on a straight line with a slope equal to $-k_La$.

As it can be seen in Fig.2.11, this is actually the case and an estimation of the mass transfer parameter k_La (0.0396 s^{-1} in the particular case under examination) is obtained.

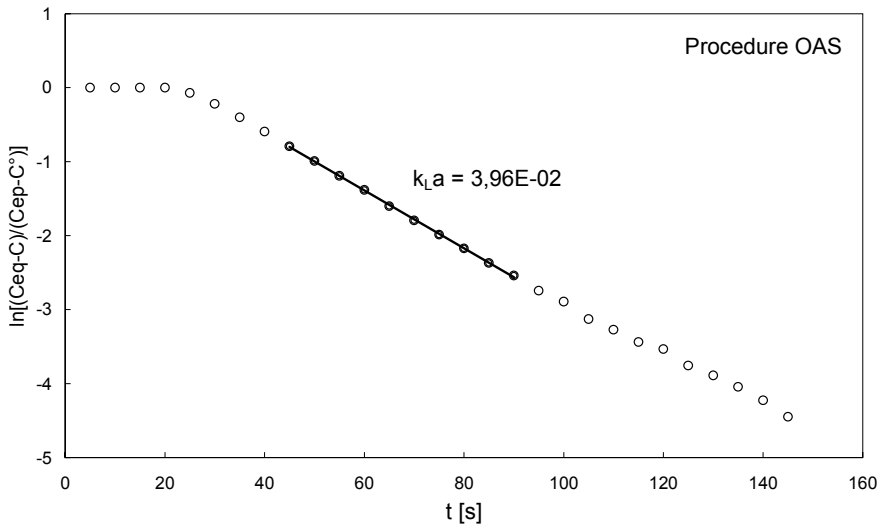

Fig. 2.11: *Typical oxygen concentration dynamics at N=900 rpm, Qg=5.4 lt/min. Procedure OAS (oxygen absorption in air saturated water)*

When the nitrogen-free procedure (OApE) was applied under the same operating conditions, the results reported in Fig. 2.12 were obtained. As it can be seen, once again (after some time) data points did align on a straight line, but

the final slope obtained with OApE procedure (0.0548 s^{-1}) is significantly larger than that obtained with procedure "OAS" (0.0396 s^{-1}) at the same agitation speed.

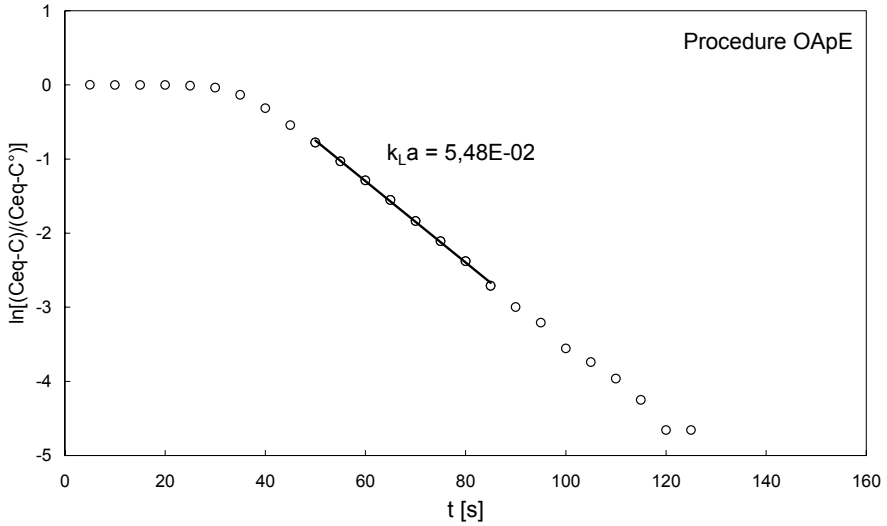

Fig. 2.12: *Typical oxygen concentration dynamics at N=900 rpm, Qg=5.4 lt/min. Procedure OApE (oxygen absorption in pre-evacuated water)*

The same behaviour was observed in all experiments carried out with procedure "OApE", independently of agitation speed, as it can be appreciated in Fig. 2.13 where the k_La values obtained with procedure OAS are reported as solid symbols, while the values obtained with procedure OApE are reported as empty symbols. In this last case, experiments were repeated at least 3 times for each agitation speed, in order to appreciate technique reproducibility. Observation of Fig.2.13, where all the data obtained are reported, leads to the conclusion that the technique provides quite well reproducible results.

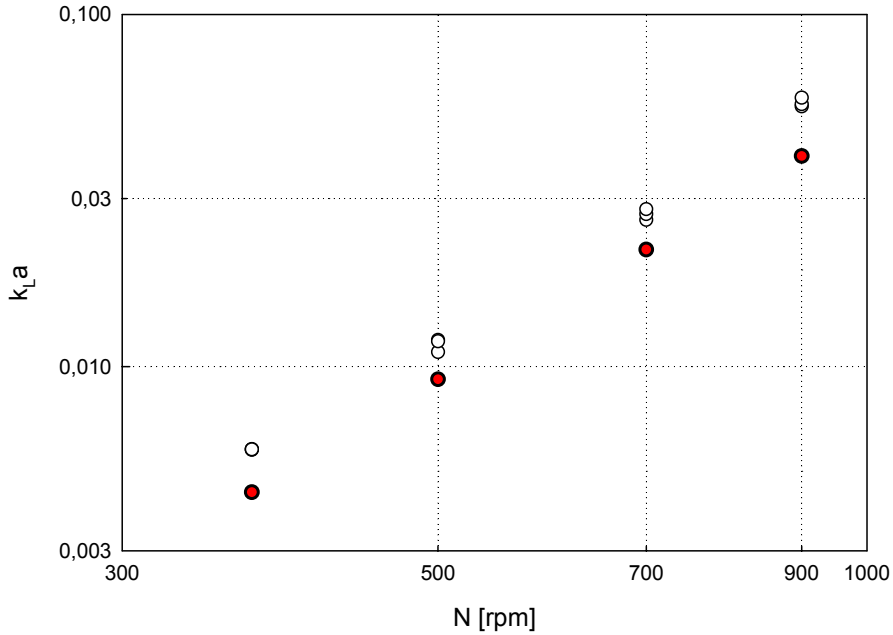

Fig. 2.13: Comparison between k_La values determined with the two variants of the dynamic oxygen absorption method at various agitation speeds. Solid circles: procedure OAS ;open circles: procedure OApE.

It is worth stressing that procedure "OApE" is practically identical to procedure "OAS", the only difference between the two being merely the initial presence of nitrogen in the liquid phase. The fact that values of k_La obtained with the former procedure are from 30 % to 50 % larger than those obtained with the latter is to be entirely attributed to measurement interference by dissolved nitrogen. This result is in accordance to what found by Linek *et al.* (1987).

This can quite easily be explained, as in the case of initially de-aerated liquid (procedure OApE) gas bubbles are all made of pure oxygen, apart from the liquid vapour pressure that is constant throughout the experiment. As a consequence, Oxygen equilibrium concentration in the liquid is constant at any time and the driving force variation is only due to liquid bulk oxygen level variations.

In the other case (procedure "OAS") the initially dissolved nitrogen undergoes transport towards gas bubbles. As a consequence in the gas phase oxygen starts to be diluted, resulting in an oxygen interface concentration smaller than assumed in the simple model employed for results interpretation. This in turn leads to a reduction of mass transfer rates, which are mistakenly seen by the model as a reduction of k_La average values.

It is clear that improving the interpretation model to account for these effects is not easy. As a matter of fact, different bubbles will experience different dilution levels depending on their size, residence time spent in the system (which changes with terminal rise velocity, hence size again, and random occurrences such as whether or not a bubble is entrained by the liquid flow and re-circulated to the impeller). As a consequence, at any instant in the system there many bubbles, with many different sizes and histories, each of which has a more or less diverse oxygen concentration, and taking proper account of this by data interpretation models is very complex if not impossible.

From the above considerations, it can be concluded that the OApE procedure, being free from these disturbances and interpretation difficulties, is the one that leads to reliable results.

It may be worth, however, stressing that although the larger values obtained by procedure "OApE" should be considered as the real mass transfer parameter values, their practical use is straightforward only for systems in which a pure gas has to be absorbed in a liquid phase where no counter diffusing gases are present. For systems where some gaseous component may counter-diffuse, the real value of the k_La parameter should be employed in the framework of a model able to suitably account for the second component concentration into bubbles. As previously outlined, this is bound to be complex, especially considering that properly accounting for it involves explicit consideration of bubble size distribution and possibly different flow models for each class of bubbles.

If, on the contrary, one prefers a simplified modelling of the gas phase behaviour, with no consideration for the counter diffusing component, then using the true value of k_La may be misleading and the erroneous k_La values obtained from procedures "OAS", "ODA" may be better coupled to the similarly erroneous gas model. Clearly, this quite rougher approach is bound to involve larger uncertainties on the final result.

Comparison with literature data

The present results may be compared with the only literature data obtained in absence of initially dissolved nitrogen, namely those reported by

Linek *et al.* (1987). In order to make results meaningful, the k_La data obtained in the two works are to be compared for given specific power inputs, as due to the difference of vessels size (T=0.29 m in the case of Linek's vessel) stirrer speed would not be a suitable comparison basis. This is done in Fig.2.14, where also the regression lines for the data obtained here and those obtained by Linek *et al.* (1987) are reported.

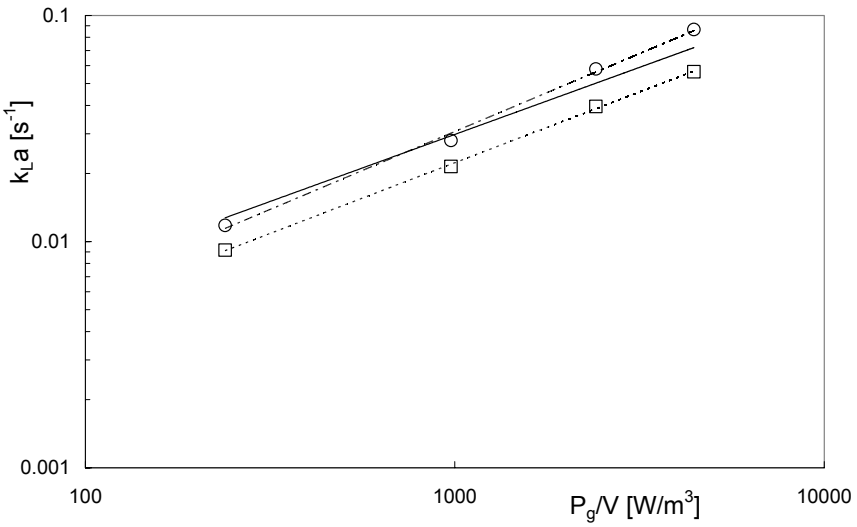

Fig. 2.14: Mass transfer coefficient vs specific power input.
Circles: OApE procedure; dash dotted line: equation 2.7.
Squares: OAS procedure; dotted line: eqn. 2.8;
Solid line: Linek et al. (1987) correlation.

These are respectively given by the following equations:

OApE data power law regression:

$$k_La = \text{const } (Pg/V)^{0.689} \tag{2.7}$$

OAS data power law regression:

$$k_La = \text{const } (Pg/V)^{0.626} \tag{2.8}$$

Linek *et al.* (1987) correlation:

$$k_La = 0.00495\ v_s^{0.4}\ (Pg/V)^{0.593} \qquad (2.9)$$

As it can be seen, Linek *et al.* 1987 correlation, based on experimental measurements obtained with a procedure very similar to procedure OApE, gives rise to results almost coincident with the present OApE data.

At a closer look, the agreement is better at the lowest specific power dissipations, while at the highest specific power dissipations, Linek's correlation underestimates somewhat the present OApE results. The reason behind this discrepancy may lie in the fact that Linek *et al.* (1987) used a topless vessel, therefore nitrogen was present in the gas above the free surface, and this may well have resulted into some nitrogen contamination of the liquid, especially at the highest agitation speeds, where surface areration is likely to occur.

2.5 Conclusions on the standard vessel experimentation

A convenient variant of the dynamic technique for the k_La measurements, characterized by the absence of dissolved inert gases and named Oxygen Absorption in pre-Evacuated liquid (OApE), was developed.

With this variant the simplest two component system (water-oxygen) is dealt with, and therefore the k_La data obtained cannot be affected by gas phase concentration variations. As a consequence there is no need to resort to flow models for the gas phase and reliable information on mass transfer parameter is obtained.

Results show that, for the investigated system, gas-liquid mass transfer coefficients obtained according to procedure OApE are about 30 % - 50 % greater than those (less reliable) measured in the same hydrodynamic conditions but starting with an air-saturated liquid phase.

The data obtained by the OApE technique were also validated by comparison with the (quite scant) literature information available.

Results clearly show that it is extremely important to use correct methods of k_La measurement, able to produce physically consistent data, as only such data with clear physical interpretation can lead to successful design and scale-up of apparatuses.

CHAPTER 3

DEVELOPMENT OF A NOVEL SELF-INDUCING GAS-LIQUID REACTOR

3.1 GAS INDUCING REACTORS

The usual way for introducing the gas stream into the liquid phase is through suitable distributors placed below the impeller (Middleton, 1985). An interesting alternative is that of using a type of "self inducing" gas liquid reactor which features internal recycling of the headspace gas, provided that the impeller is operated at sufficiently high rotational speeds.

These systems have the advantage that they can be operated in "dead-end" mode so that practically all of the feed gas may be absorbed in the liquid, a useful feature whenever reactions involving a gas different than air are to be carried out (e.g. hydrogenations, chlorinations etc.). As a matter of fact, in these cases an external compressor and relevant piping would be required by conventional gas-liquid reactors for recycling the gas phase to the sparger. This additional equipment is saved if a self-inducing/self-ingesting vessel is adopted instead, thus resulting into economic savings as well as safer operation, considering that the hazards connected with the external loop are avoided. In three phase mixing operations, such as hydrometallurgical processes, the blockage of gas spargers by solid particles is a common issue, which can be avoided using a self inducing device.

One of the earliest reported uses of gas inducing impellers is in froth flotation. In this case abrasive solids present in ore flotation can wear the sparger holes or the gangue material present in the ore can form a muddy solid residue that blocks the sparger holes, with adverse effects on the sparger system performance. In such cases, gas inducing impellers are favoured and can adequately deliver the quantity of gas required for the operation.

For similar reasons many biotechnological processes can take advantage from the use of self aspirating devices. As a matter of fact, usual turbine impellers coupled with spargers produce significant shearing stresses in the mixing zone. The effect of these stresses can produce a disintegration of biomass cells and a decrease in process efficiency. If the cells are supported in micro carrier spheres these latter can block the holes of the sparger. Self aspirating impellers have been claimed to enable intensive liquid mixing without the disadvantageous effects (Heim *et al.* 1995).

The main drawbacks of the self inducing devices compared to sparged systems are: (i) the loss of operating flexibility, as the gas flow-rate depends on impeller speed and can no longer be varied independently; (ii) the induced gas flow rate may be sensitive to changes in the liquid level; (iii) large specific power inputs may be required to effect induction of the gas at large scale.

Self-inducing systems include: (i) gas-induction through a hollow shaft and impeller, also called self aspirating impellers (Joshi and Sharma 1977, Rielly *et al.* 1992, Forrester and Rielly 1994, Stelmach & Kunchewicz 2001, Poncin *et al.* 2002); (ii) self-induction through a rotor-stator device and concentric standpipe (Zundelevich 1979, Mundale and Joshi 1995, Saravanan & Joshi 1996, Patwardhan & Joshi 1997, Patil and Joshi 2003); or (iii) "vortex ingesting" vessels (Hsu & Huang 1996, Hsu *et al.* 2001, Conway *et. al.*, 2002) where the gas phase from the headspace is injected and dispersed into the liquid through suitable surface vortices. A detailed description of the various types of existing self-inducing apparatuses is reported in the next three sections.

Patwardan and Joshi (1999) wrote an excellent review of the design criteria to be used in self-inducing reactors. According to Mundale (1993) they classified the gas inducing impellers on the basis of the flow pattern in the impeller zone. The gas enters the impeller zone at one location and leaves at another location. Along with the gas, the liquid can also enter the impeller zone and leaves along with the gas. The nature of the flow entering and leaving the impeller zone is used as the criterion to classify the impellers:

(i) Single-phase flow (gas alone) at the inlet as well as the outlet of the impeller zone (type 11 system). The self aspirating impeller apparatuses belong to this category (Fig. 3.1).

(ii) Single-phase flow (gas alone) at the inlet and two phase flow (gas and liquid) at the outlet of the impeller zone (type 12 system). Many industrial apparatuses equipped with a hollow shaft and special rotating systems which incorporate the liquid phase together with the gas phase coming from the shaft can be included to this category (Fig. 3.2).

(iii) Two-phase flow (gas and liquid) at the inlet as well as at the outlet of the impeller zone (type 22 system). All the apparatuses equipped with a rotor-stator device (Fig. 3.3) as well as the "self-ingesting" apparatuses belong to this category.

After a detailed description of the three different categories and of the apparatuses reported in the open literature, Patwardan and Joshi (1999) accurately analysed the available correlations for estimating the critical impeller speed for the onset of gas-induction (N_{CG}) and the gas-induction rate Q_G . The former is based on Bernoulli's equation while the latter was accurately determined by equating the pressure difference generated by the impeller and the pressure drop required for gas flow. Also, a process design algorithm was presented for the design of type 22 gas inducing impellers (apparatuses equipped with rotor-stator devices).

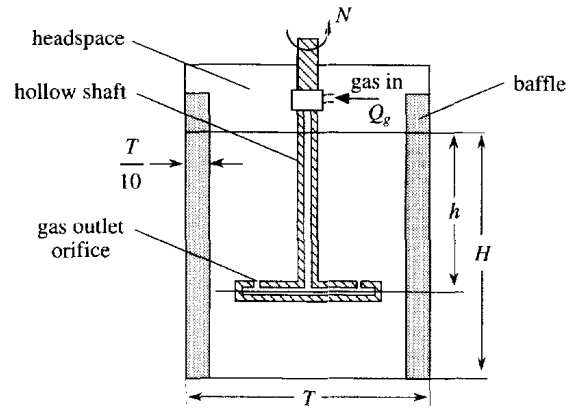

Fig.3.1: Geometry of a self aspirating impeller apparatus (Rielly et al 1992)

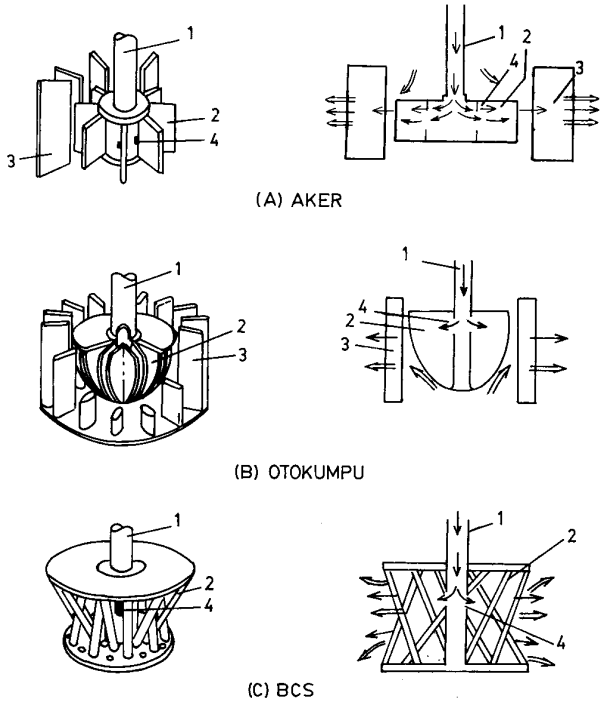

Fig.3.2: Geometry of type 12 impellers (reproduced from Patwardan & Joshi 1999)

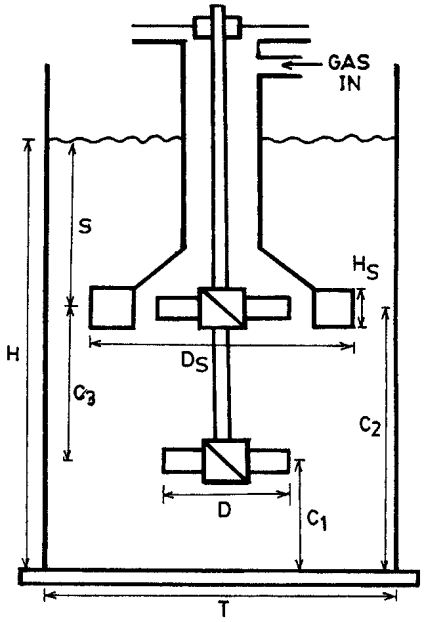

Fig.3.3: Geometry of rotor-stator device (reproduced from Saravanan & Joshi 1995)

3.1.1 Self-aspirating impellers

The simplest kind of self-aspirating impeller is a cylindrical, hollow pipe with one or more orifices (Fig. 3.4). The hollow pipe is mounted on a hollow shaft. This kind of configuration has been studied extensively (Martin 1972, Joshi and Sharma 1977, Rielly *et al.* 1992, Forrester and Rielly 1994, Forrester *et al.* 1998, Heim *et al* 1995).

When this impeller rotates in the fluid, the sudden acceleration of the fluid elements causes a reduction in the static pressure, as quantified by Bernoulli's equation. If the reduced pressure area is connected to the gas space, then the gas will be induced if pressure reduction is sufficient to overcome all the resistances in gas path.

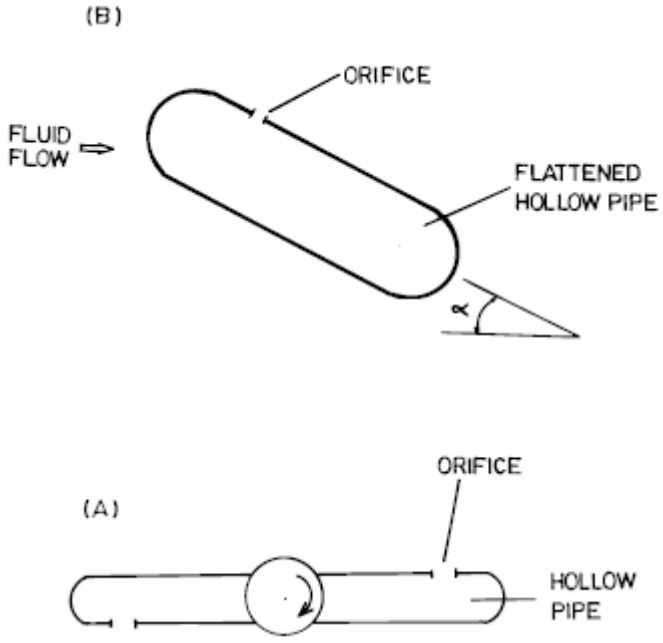

Fig. 3.4: Hollow pipe gas-inducing impeller (Martin, 1972)

Martin (1972) carried out one of the first studies on these apparatuses. He measured pressure difference for different locations of the orifice and tried to find the orifice angle and position that maximized gas induction. Moreover he created an aerofoil shape by flattening the cylinder, which improved the gas induction rate by about 50-100%.
Joshi and Sharma (1977) varied the total orifice area by changing the orifice diameter and/or the number of orifices obtaining a similar increase in gas-induction rate.

Rielly *et al.* (1992) and Forrester and Rielly (1994) investigated hollow concave-bladed impellers (Fig. 3.1). The blades in such a type of impellers were mounted on a disk and connected to a hollow shaft through which the gas induction occurred. Rigby (1994) located the orifice not on the blade but slightly off it varying the distance of the orifice from the blade surface to achieve the maximum gas-induction rate. Forrester and Rielly (1994) and Forrester *et al.* (1998) (Fig. 3.5) used multiple orifices on the blades to improve gas induction characteristics. Increasing the number of orifices was found to significantly increase the rate of gas induction, though this effect diminishes as

the number of orifices increases. Furthermore this method of increasing gas capacity is not at the expense of generating bigger bubbles, and thus larger gas-liquid interfacial areas are obtained.

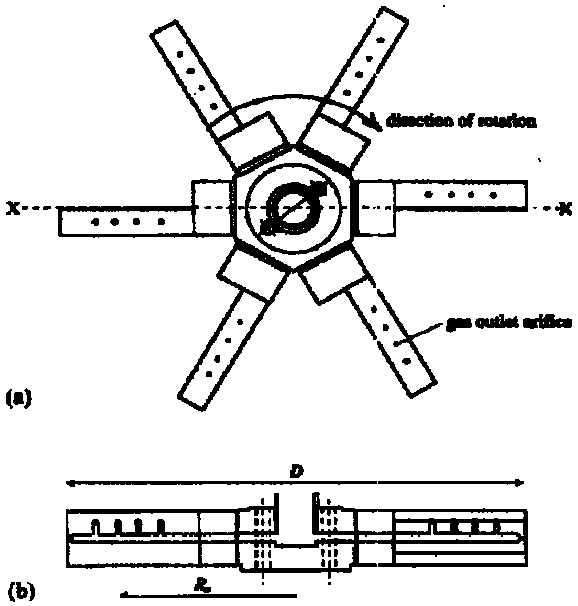

Fig. 3.5: Schematic view of a six-bladed impeller . (a) plan view; (b) section through X-X (Forrester et al. 1994)

Heim *et al.* (1995) used four-pipe, six-pipe and disk impellers for self-inducing aeration in bioreactors. The disk impeller, although operating in a less efficient manner, was claimed to be of interest because it doesn't harm biomass structure. Stelmach and Kuncewitz (2001) investigated the performances of disk impellers (Fig. 3.6) by measuring power consumption and gas flow rate on a cylindrical vessel 300 mm in diameter. They concluded that from the point of view of mass transfer rate, the operating efficiency of the self-aspirating impellers is more than twice that for conventional surface aerators.

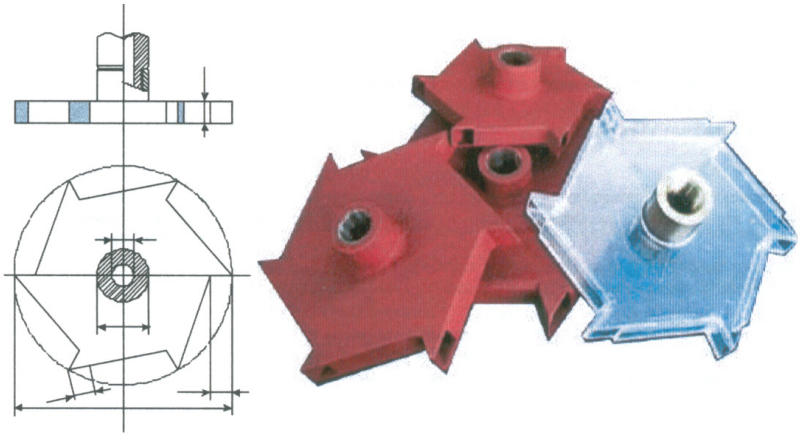

Fig. 3.6: Self-inducing disk-impeller (Stelmach and Kuncewicz, 2001)

Poncin *et al.* (2002) designed and investigated a novel hollow shaft gas inducing turbine resembling centrifugal pumps (Fig. 3.7). According to the classification proposed by Patwardan and Joshi (1999), the impeller used in this study may be classified in type 12 systems for which a two phase flow (gas and liquid) and a single-phase flow (gas) are obtained at the outlet and at the inlet of the impeller respectively The measured global parameters were correlated by means of a modified Froude number.

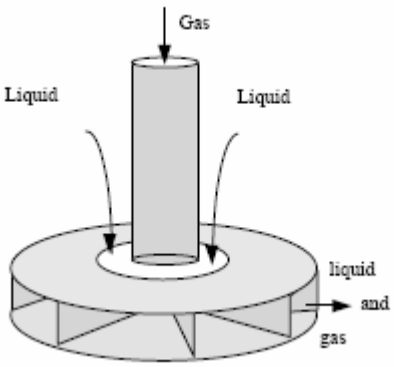

Fig. 3.7: Gas-inducing turbine used by Poncin et al., 2002

3.1.2 Rotor-stator systems

A large variety of these systems has been proposed and studied. These include flotation cells as well as traditional gas-liquid chemical reactors. According to the classification proposed by Patwardan and Joshi (1999) they can be classified as type 22 systems.
Some of the main designs are turbo aerators (Zundelevich, 1979) (Fig. 3.8), pitched turbine impellers covered with a stator-standpipe assembly (Saravanan *et al.*, 1994; Mundale and Joshi, 1995), multiple impeller systems (Saravanan and Joshi, 1995; Saravanan *et al.* 1996; Patil and Joshi, 1999; Patil and Joshi, 2003) and multiple impeller systems equipped with an additional sparger (Patwardan and Joshi 1997).

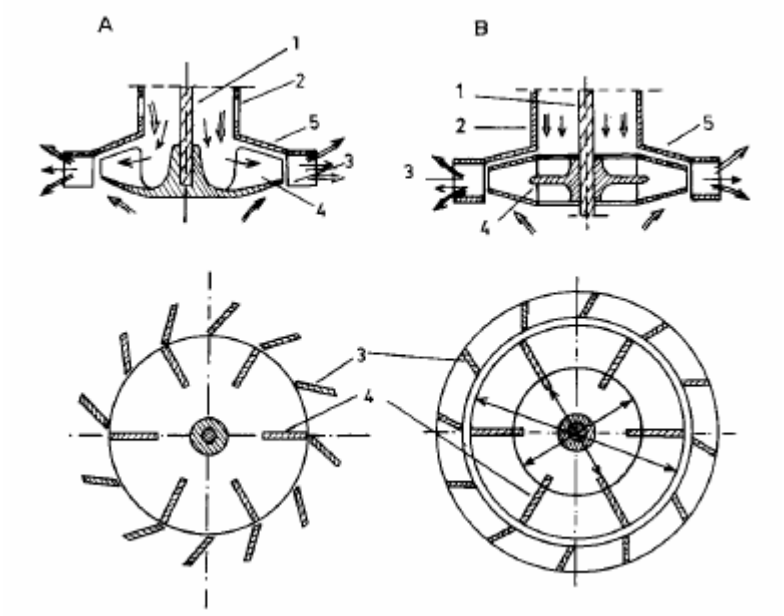

Fig. 3.8: Turboaerator designs (Zundelevich, 1979): (1) solid shaft; (2) standpipe; (3) stator vanes; (4) impeller; (5) stator hood.

The characteristic features of these systems include (i) a rotor impeller, (ii) a standpipe through which the gas induction takes place, and (iii) a stator-diffuser surrounding the impeller.

The basic principle of operation of the stator-standpipe system is as follows. The rotation of the impeller causes a vortex formation in the standpipe. As the impeller speed increases, the vortex formation depth progressively increases. When the vortex is sufficiently near the impeller, the impeller blades shear the gas-liquid interface, entrapping gas bubbles. The entrapped gas bubbles are carried away by the impeller stream. The stator consists of an impeller hood, vanes, and an air ring. The impeller hood prevents the entry of liquid into the impeller zone from above. The air ring prevents the axial downward flow from the impeller. As a result of the impeller hood and the air ring the liquid flow coming out from the stator is radial.

Zundelevich (1979), based his experimental and theoretical analysis of self – inducing turbo aerator on the theory of water jet injector operation. He found that the reactor hydrodynamic behaviour could be based only on two dimensionless groups, C_H and Eu_G, representing the head coefficient and the gas Euler number respectively. Moreover, the aerator performance, at constant submergence, was essentially the same in tanks of different geometry and volume. Consequently he stated that no full geometrical similarity is required for self inducing aerator modelling and scale-up. More importantly, Raidoo *et al.* (1987) found that the scale-up procedure devised by Zundelevich (1979) is not able to relate the performance of different impeller sizes into a single characteristic curve, even for a design that is structurally identical to the design studied by Zundelevich (1979). These considerations render the Zundelevich model very specific to his experiment.

Saravanan *et al.* (1994) designed and studied a gas inducing mechanically agitated contactor (GIMAC) equipped with one pitched turbine impeller covered with a stator-standpipe assembly.

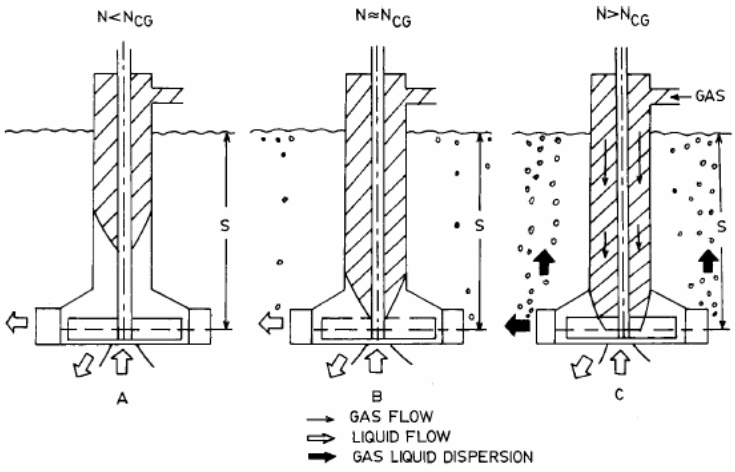

Fig. 3.9: Vortex shapes formed in a stator-rotor system (Saravanan and Joshi, 1995): (A) before the onset of gas induction; (B) at the critical speed for gas induction; (C) at a speed higher than NCG.

They investigated in detail the effect of impeller submergence from the top and impeller clearance from the bottom on gas induction rate and interpreted the various aspects of the process in terms of the phenomenon of vortex formation (Fig. 3.9). Mundale and Joshi (1995) used the same reactor geometry of Saravanan *et al.* (1994), employing several designs of the impeller for optimizing the rate of gas induction with respect to power consumption. They found that a standard 6-bladed 45° pitched bladed downflow turbine was the most energy efficient gas inducing impeller.

Saravan and Joshi (1995, 1996) and Saravanan *et al.* (1996, 1997) further improved the configuration studied by Saravanan *et al.* (1994), by adding a second impeller on the same shaft underneath the stator (Fig. 3.3). They carried out extensive investigation on the multiple impeller systems. They reported that when a single gas-inducing impeller is located close to the top liquid surface for maintaining a high rate of gas induction, it suffers several drawbacks such as poor dispersion of the induced gas, poor solid suspension ability, and so on. These drawbacks were found to become more serious when increasing operation scale. These limitations can be overcome by using a second impeller below the self inducing impeller. The gas inducing impeller can then be kept close to the top liquid surface to induce a high gas rate. The design of the second impeller was optimised for different duties such as gas hold-up, solid

suspension ability, heat transfer etc.. This activity has clearly shown that the optimum design of the lower impeller changes with the design objective. For example to achieve high gas holdup, it was better to use an upflow impeller at the bottom, while to have solid suspension a downflow impeller was desirable.

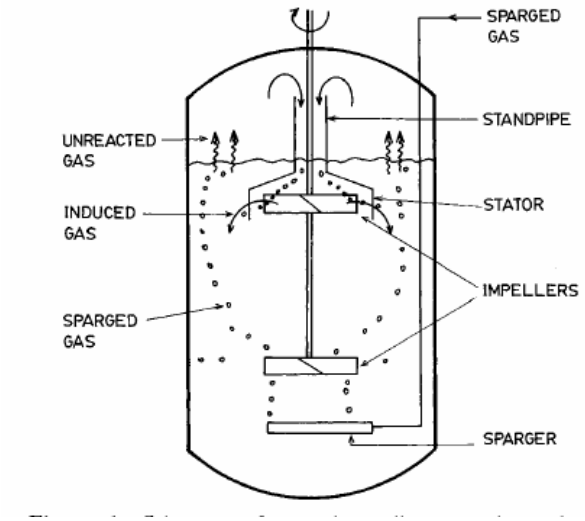

Fig. 3.10: Schematic of a mechanically agitated gas-liquid reactor equipped with a gas-inducing impeller (Patwardan and Joshi 1997).

Patwardan and Joshi (1997) employed a gas inducing impeller in mechanically agitated sparged contactors. Fig. 3.10 shows a schematic diagram of such a contactor. The role of gas inducing impellers in such reactors is, at least to recirculate the unreacted gas from the headspace. If the gas inducing impeller is able to induce gas at a rate grater than the unreacted gas rate, a part of the gas liquid contacting duty is performed by the gas inducing impeller. The productivity of such reactors depends on gas inducing rate, gas holdup and so on. Therefore, the design of the gas inducing impeller plays an important role on the overall performance of the reactor. In the absence of a gas inducing impeller, the system resembles a conventional mechanically agitated contactor and recycle takes place only thanks to gas suction from the headspace.

3.1.3 Vortex ingesting vessels

One of the first examples of a vortex-ingesting system is the "Advanced Gas Reactor" (AGR), developed and patented by Praxair (Litz 1985). It essentially consists of a helical screw in a draft tube as a gas inducing impeller. Fig. 3.11 shows a schematic diagram of the reactor. A baffle arrangement provided at the top of the draft tube generates a number of vortices from which gas induction takes place. When the helical screw rotates, above a certain minimum impeller speed, a downward liquid flow is generated. Gas is drawn into the liquid through the surface vortices and enters the suction side of the impeller, where it is dispersed as fine bubbles within the draft tube. These bubbles are then circulated along the liquid flow through the outer annulus. Litz (1985) found that the ratio of power consumption under gassed and ungassed conditions is 1.0 up to gas holdup of 10%.

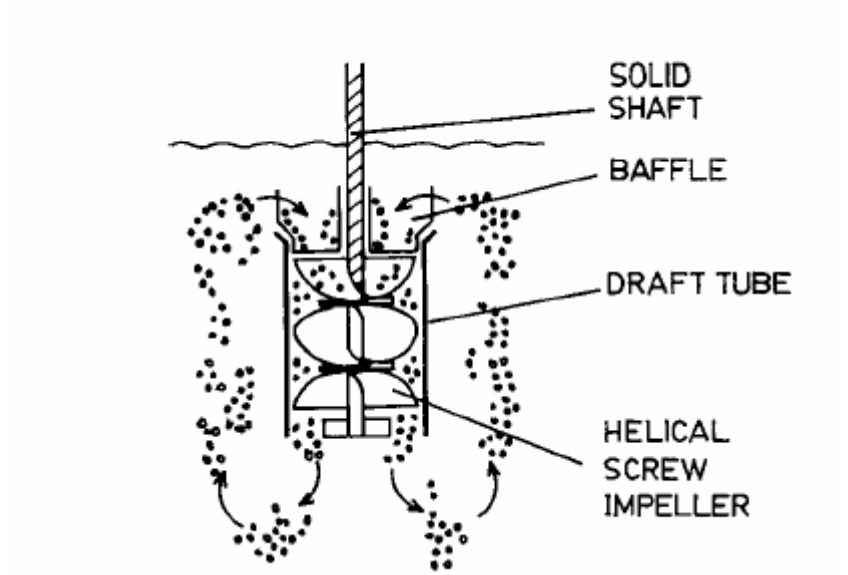

Fig 3.11: Helical screw impeller in a draft tube (Litz 1985)

The geometry details of the reactor were successively improved leading to the AGR adopted by Conway *et al.* (2002) for gas-solid-liquid experimentation (Fig

3.12). In their work, Conway *et al.* (2002) reported results for the effects of solid mass fraction on: (i) the minimum speed for vortex ingestion; (ii) the gas holdup; (iii) the volumetric mass transfer coefficient. Additionally the effects of gas injestion on the just suspended impeller speed were also studied.

The results of the study showed that, unlike many other self-inducing agitators, the AGR was well suited for solid suspension since the discharge flow from the impeller directly impinges on the base of the tank, picking up particles and transporting the into the annulus.

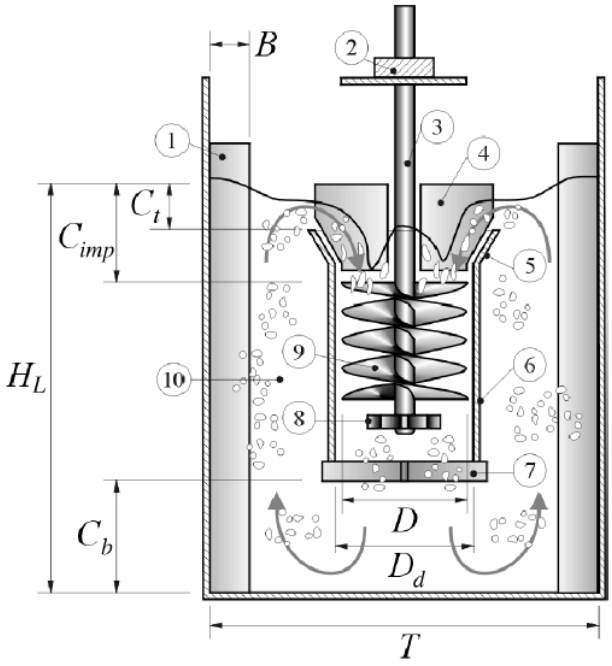

Fig. 3.12: Schematic diagram of the AGR experimental apparatus. 1, wall baffles; 2, motor and shaft bearing; 3, impeller shaft; 4, upper cruciform baffles; 5, draft-tube flare; 6, draft-tube; 7, lower cruciform baffles; 8, radial bladed turbine; 9, helical screw impeller; 10, annulus.

Hsu and Chang (1995), Hsu and Huang (1996, 1997), Hsu *et al.* (2002) proposed a different gas-inducing reactor. The system consists of an unbaffled

tank fitted with one or two impellers. Since the tank is unbaffled, a vortex is generateted in the tank whose depth is progressively increased with increasing impeller speed. At a certain speed the vortex reaches the impeller and is broken up into gas bubbles. Hsu and Chang (1995), Hsu and Huang (1996, 1997), used ozone as the gas phase in the investigations. They report the ozone utilization efficiency as a function of various operating parameters.

Hsu *et al.* (2002) provided correlations for power consumption and critical impeller speed for gas induction. Moreover their work was carried out in small-sized vessels (0.17 m diameter).

Chen *et al.* (2003) used the same optimal design indicated by Hsu and Huang (1997) (Fig.3.13) in a 0.29 m inner diameter vessel (Fig. 3.14). In this case pure oxygen was used for the experimentation and correlations for the onset agitation speed, gas holdup and mass transfer coefficients were provided.

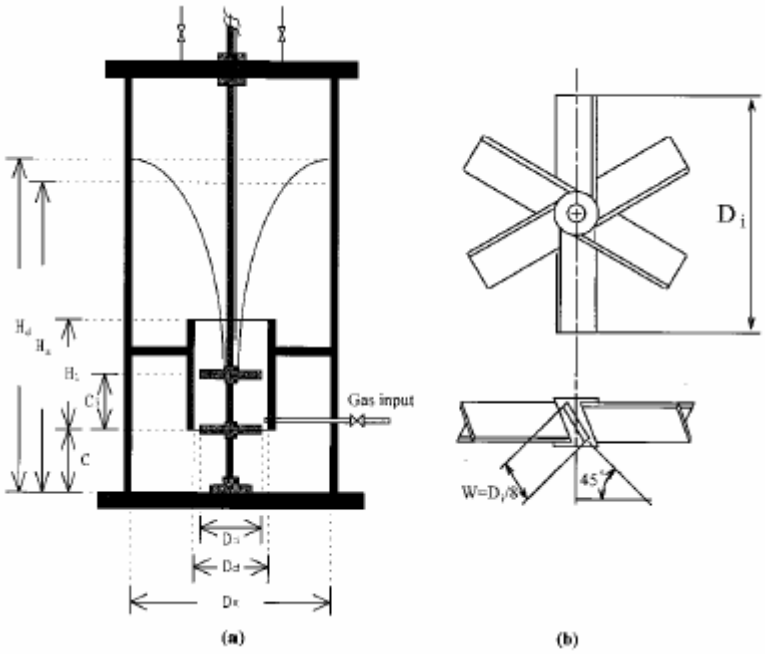

Fig. 3.13: Schemes of the gas-inducing reactor and impeller (Hsu et al. 2002).

Jafari and Mohammadzadeh (2004) measured the onset speed for gas induction at different liquid levels, and power consumption characteristic of a gas inducing reactor with the same design as that by Hsu and Huang (1996, 1997), and an inner diameter of 190 mm. They found that despite high impeller speed required by the gas-induced contactor to initiate gas induction, it consumed less power as compared to conventional gas liquid contactors (radial turbine).

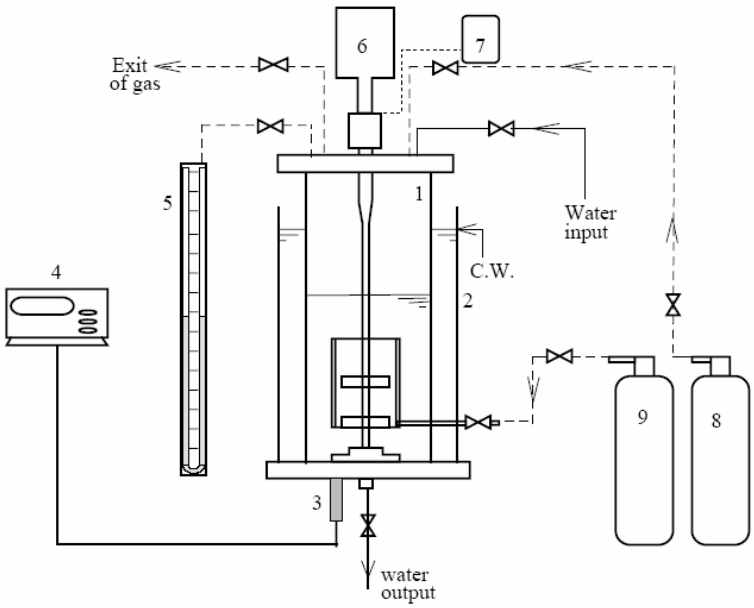

1. Tank body
2. Jacket **6. Motor**
3. DO sensor **7.Torque meter**
4. DO meter **8. Oxygen cylinder**
5. U-tube manometer **9. Nitrogen cylinder**

Fig. 3.14: Experimental set-up used by Chen et al. (2003)

3.1.4 Mass transfer coefficients in gas inducing reactors (GIR).

The considerations on the difficulties involved in the measurement of k_La reported in Chapter 2 clearly apply also to the case of gas inducing reactors (GIR). This section is aimed at reviewing some of the results obtained in this type of contactor. In Table 1 a literature survey on k_La in GIR is reported.

Forrester and Rielly (1994), Forrester *et al.* (1998), Conway *et al.* (2002), determined the volumetric mass transfer coefficients, k_La, from unsteady state experiments using the absorption of oxygen from air bubbles ingested from the head-space.

Poncin *et al.* (2002) evaluated the gas liquid mass transfer coefficient by using two different techniques: the physical dynamic oxygen absorption technique and the coalescence inhibiting sulphite oxidation technique. The dynamic absorption technique was employed both for coalescent systems (air-water) and non-coalescent ones (air-K_2SO_4 solution). The mass transfer coefficient values obtained by the dynamic technique using the coalescent system (water-air) were found to be lower than those obtained with the non coalescent system (K_2SO_4 solution) as well as those assessed by the chemical sulphite oxidation technique, as it could have been expected considering the higher interfacial areas obtained when coalescence inhibiting systems are used.

Hsu and Huang determined the ozone mass transfer coefficient kL,a, formerly by measuring the dynamics of a reactive dye concentration during ozone absorption (Hsu and Huang, 1996), then by a dynamic method where the ozone time dependent concentration was measured by a liquid phase ozone analyser (Hsu and Huang, 1997), unfortunately neglecting ozone decomposition rate. This last was suitably accounted for by Hsu *et al.* (2002).

Joshi and Sharma (1977) determined the liquid side mass transfer coefficient kL,a, in a hollow shaft gas inducing contactor, by using chemical methods. In this case carbon dioxide diluted with air was absorbed in sodium carbonate/sodium bicarbonate buffers.

Tab. 1: Literature survey on k_La in GIR

Authors	Induction type	Gas	Liquid	Method	Experimental procedure
Forrester and Rielly (1994, 1998)	hollow shaft + 6 hollow concave-blades (1 - 4 orifices)	air	water	dynamic	water de-oxigenation with nitrogen. Air absorption
Conway et al. (2002)	vortex ingesting stirred reactor through draft tube elical screw + radial turbine	air	water	dynamic	water de-oxigenation with nitrogen. Air absorption / Oxygen probe time response considered
Heim et al. (1995)	4 and 6 hollow pipes impeller and disk impeller	O_2 / air	water	dynamic	----
Chen et al. (2003)	vortex ingesting stirred reactor through draft tube + 2 PBT	O_2 / air	water	dynamic	----
Poncin et al (2002)	hollow shaft + double disk impeller	air air air	water K_2SO_4 solution water+sod. sulphite	dynamic dynamic chemical	----
Hsu and Huang (1996)	vortex ingesting stirred reactor through draft tube + 2 PBT	ozone	water	chemical (O_3 reaction with dye)	----
Hsu et al. (1997)	vortex ingesting stirred reactor through draft tube + 2 PBT	ozone	water	dynamic	----
Hsu et al. (2002)	vortex ingesting stirred reactor through draft tube + 2 PBT	ozone	water	dynamic, corrected for O_3 decomposition	
Joshi and Sharma (1977)	Hollow shaft + Hollow impeller	CO_2	Na_2CO_3 + $NaHCO_3$	steady state - chemical	----

3.2 LONG DRAFT TUBE STIRRED REACTOR

One of the main aims of this thesis work was that of developing a novel self-inducing gas-liquid contactor. The apparatus was actually devised and consists of a tall cylindrical vessel equipped with a relatively narrow draft tube, into which gas is ingested through a free vortex on the liquid surface, as depicted in Fig. 3.15.

Inside the draft tube a number of axial impellers periodically re-disperses the gas phase and pumps the two phase mixture down to the vessel bottom, where a radial turbine breaks the gas into tiny bubbles that slowly rise with the liquid in the annular portion of the vessel. In some way, this new *"Long Draft Tube Self-ingesting Reactor"* (LDTSR) may be regarded as a self-ingesting bubble column.

3.2.1 Experimental Apparatus

Reactor

The LDTSR actually set up consists of a flat bottomed, perspex made cylindrical tank with an internal diameter of 280 mm and an height of 1450 mm, fitted with four evenly spaced baffles supporting a concentric draft tube with an internal diameter of 100 mm and length of 1200 mm (fitted in turn with four 10 mm wide internal baffles) and off-spaced from vessel bottom by 50 mm, as depicted in Fig. 3.15. Inside the draft tube five identical pitched blade impellers of diameter 0.065 m (Fig.3.16 a) were mounted on the 17 mm dia. shaft, at 50, 150, 450, 750, 1050 mm from the upper brim of the draft tube.

When the stirrer is operated at agitation speeds higher than the minimum impeller speed for gas ingestion, gas is continuously withdrawn from the headspace via the pronounced vortex, resulting in a two-phase mixture that was driven down through the draft-tube. Immediately below the draft-tube a six-flat-blade hub-mounted turbine of diameter 0.095 m (Fig.3.16 b) is situated that breaks the gas phase into tiny bubbles. These slowly rise with the liquid in the annular portion of the vessel and at vessel top either join the gas headspace or are entrained by the liquid that flows down the draft tube, where they mix with the newly ingested gas .

The draft tube was usually fitted with four 10 mm wide internal baffles. For comparison purposes, some experiments were also conducted without baffles in the draft tube (*unbaffled* draft tube configuration). The liquid volume in the system is 0.0769 m^3.

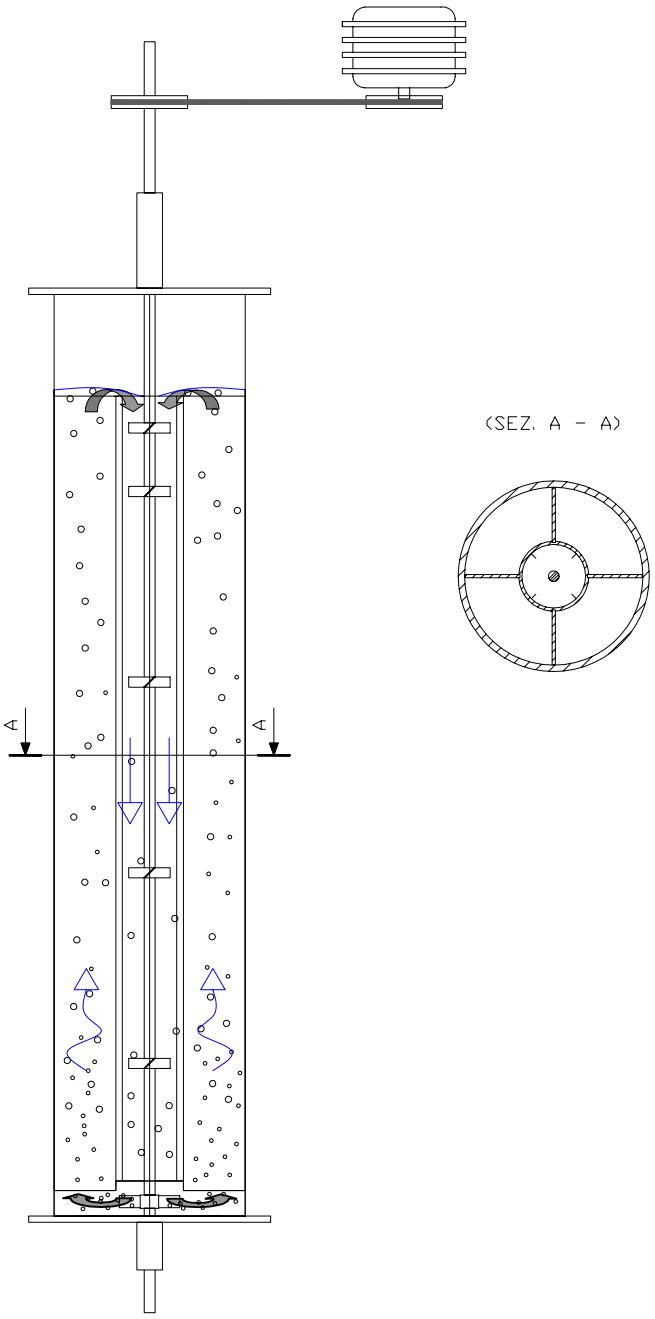

Fig. 3.15: *Schematic diagram of the experimental apparatus*

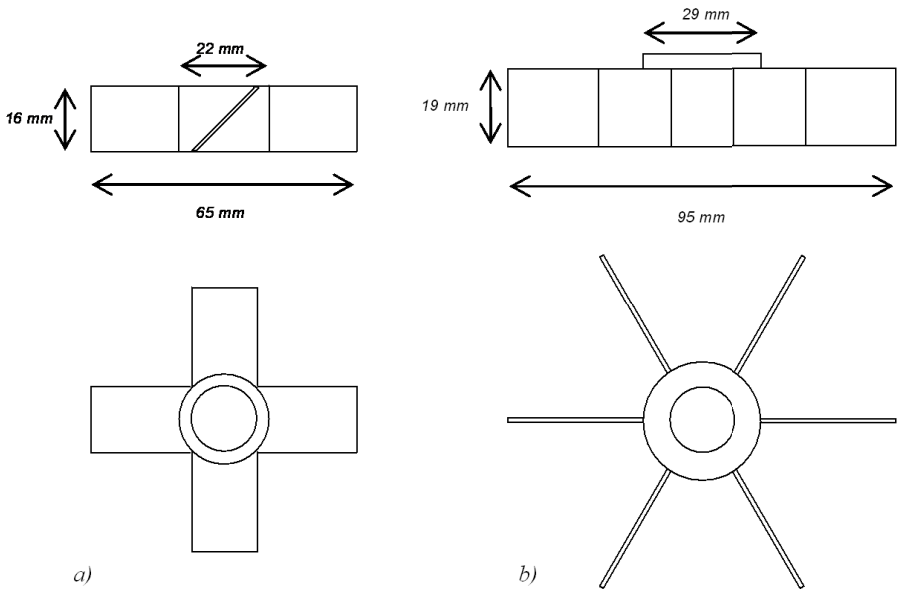

Fig. 3.16: *a) pitched blade turbine; b) radial turbine*

The top plate is 10 mm thick, 400 mm wide and 500 mm high (Fig. 3.17a). Four threaded bushings are arranged on the top of the plate. Two of these are used to for an external circuitry through which, by mean of a peristaltic pump, liquid is continuously withdrawn from the system, passes over the oxygen probe, and is fed back. The other two bushings are used as connections to the vacuum system(made by a barometric column) and/or as inlets/outlets for oxygen and air.

The shaft entered the system from the top through a mechanical seal and crossed the bottom through an other mechanical seal. It was supported by a couple of ball bearings located outside the system, one on the top and the other one on the bottom. It was 2000 mm long and it is stainless steel AISI 304 made (Fig. 3.18).

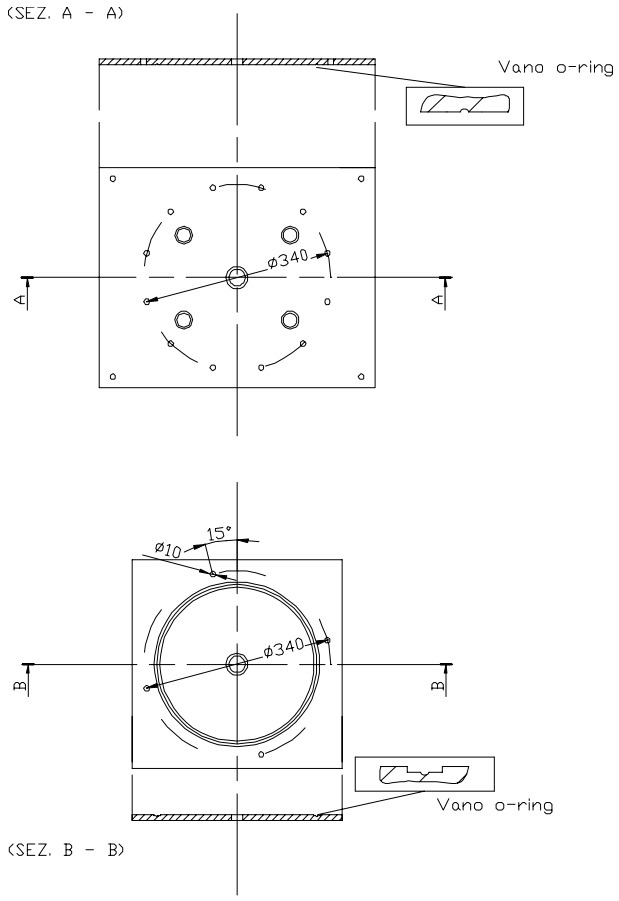

Fig. 3.17.: a) reactor top; b) reactor bottom

External system

The shaft was driven by a 800W DC motor by Mavilor MSS-8 series, equipped with tacho and speed control unit "Infrantor series SMVEN 1510" so that rotational speed is maintained constant, with a tolerance of $\pm$ 0.1%, in a range of 30-3000 rpm.

Industrial oxygen, 99.5 % pure, was used. Oxygen flow was controlled by a "Dynaval" fluximeter with a flow range from 1 to 15 l/mina n upstream pressare of 3.5 bar and a downstream pressare from 0 to 3 bar.

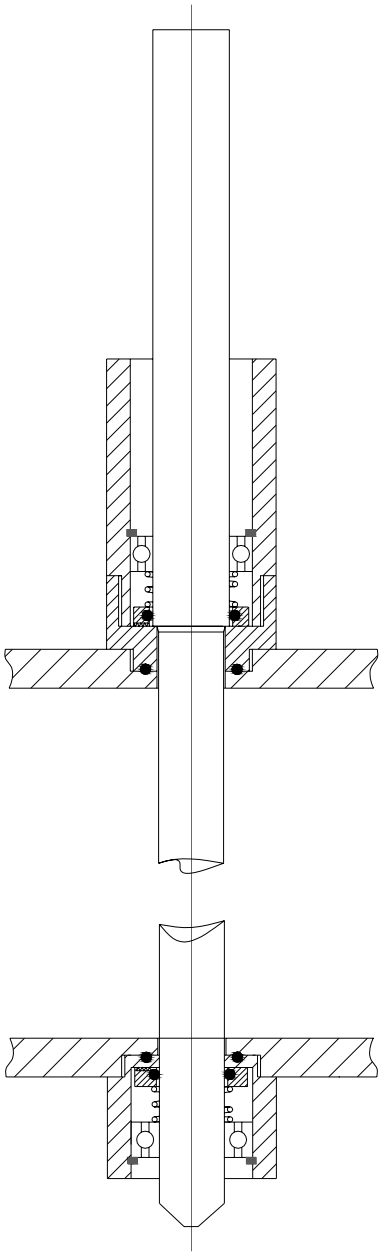

Fig. 3.18: Reactor shaft

Oxygen concentration was measured by means of the same electrode sensor (WTW CellOx 325) and control unit (WTW Oxi 340i) employed for the standard tank experimentation. Once again, by means of a peristaltic pump (Watson-Marlow 501 UR) liquid was continuously withdrawn from the vessel and returned to it after having passed over the oxygen electrode. This external loop added a (negligible) almost-pure delay of the order of few seconds to the measurements made. The output of the oxygen measurement unit were recorded with a data acquisition system and finally processed to yield the relevant value of the mass transfer coefficient k_La.

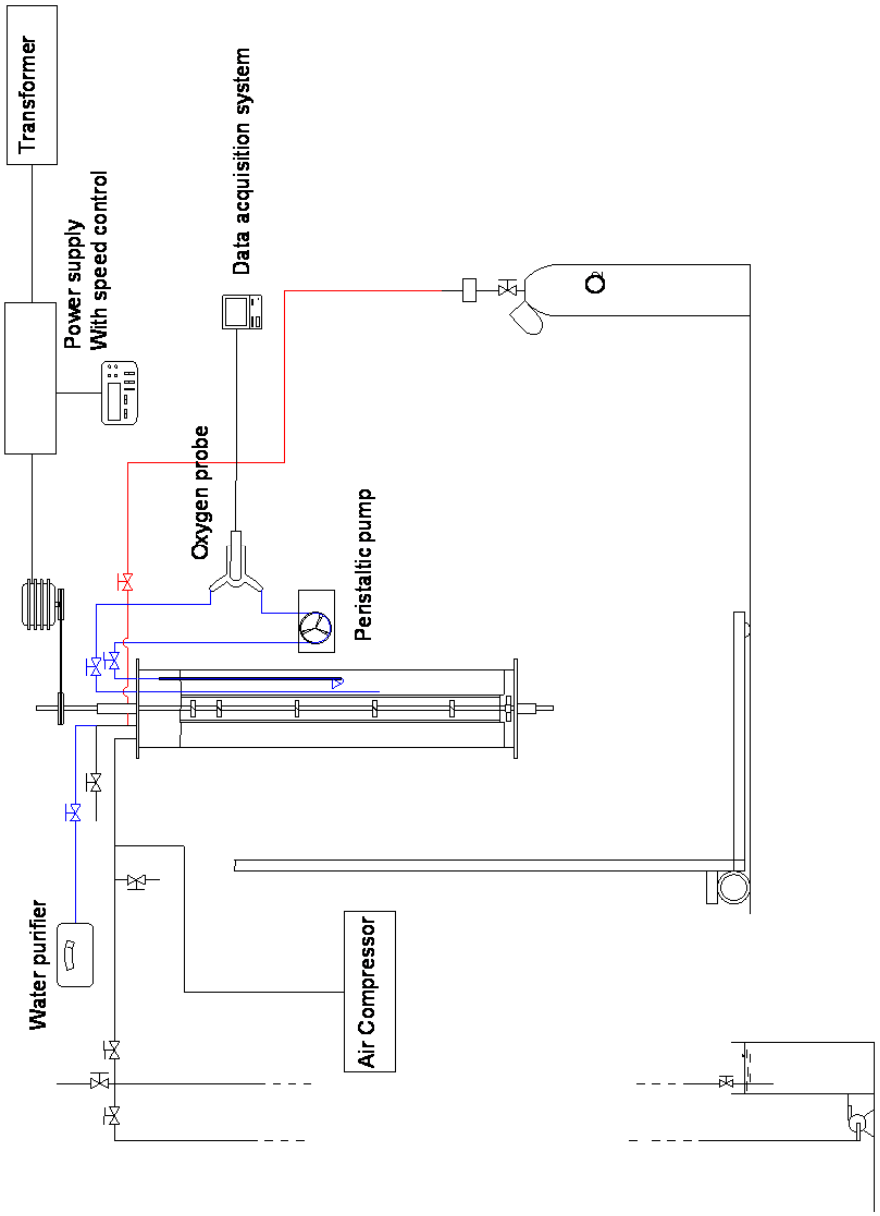

Fig. 3.19: Schematic diagram of the experimental apparatus

3.2.2 Experimental Measurements

Two different liquid phases were employed: deionised water as coalescent system and an aqueous solution of NaCl 0.2 M as non-coalescent system.

Stable hydrodynamic regimes, i.e. stable and reproducible system parameters such as power consumption, gas hold-up and mass transfer coefficients k_La, were only observed at agitation speeds higher than about 700 rpm.

The minimum impeller speed for gas ingestion, as well as gas hold-up and mass transfer parameter, were found to significantly depend on the liquid level above the brim of the draft tube. In particular larger minimum speeds and smaller gas hold-ups and mass transfer performances were observed the larger the level height above the brim. The choice of adopting a liquid height levelled with the draft-tube brim at no agitation conditions stemmed-out from this consideration. There clearly is room for further optimization with lower liquid levels, but this will be the subject of future work.

Five different agitation speeds were explored: 700, 800, 900, 1000 and 1100 rpm. When the agitation speed was lower than 600 rpm, a vortex formed on the liquid free surface and a limited number of relatively large bubbles could be observed inside the draft-tube, but they were unable to reach the bottom of the reactor. At agitation speeds of about 600 rpm a few bubbles started being entrained down to the reactor bottom. However the hydrodynamic behaviour of the reactor appeared to be rather unstable, with very small and continuously changing gas hold-ups.
A stable hydrodynamic regime could only be observed at agitation speeds of about 700 rpm. At this rate all system parameters, such as power consumption, gas hold-up and mass transfer coefficients k_La, were found to be stable and reproducible.

Gas hold-up

Average gas hold-up values were estimated by visual inspection of the liquid level increase with respect to the no-agitation condition, as observed on the transparent vessel side wall. The gas volume in the central vortex was also estimated by visual inspection and considered in the global gas hold-up evaluation. In practice the value of fractional gas hold-up was estimated by means of the following equation:

$$\varepsilon = \frac{\frac{\pi d_{ext}^{\,2}}{4}\left(h_{ext} - h_{rif}\right) - \frac{\pi d_{int}^{\,2}}{4}\left(h_{ext} - h_{int}\right)}{\left(\frac{\pi d_{ext}^{\,2}}{4}\left(h_{ext} - h_{rif}\right) - \frac{\pi d_{int}^{\,2}}{4}\left(h_{ext} - h_{int}\right)\right) + \frac{\pi d_{ext}^{\,2}}{4} h_{rif}} \qquad (3.1)$$

where h_{rif} is the clear liquid height above tank bottom at no agitation conditions, h_{ext} and h_{int} are the levels under agitation conditions in the annular section and the draft tube respectively while d_{ext} e d_{int} are the relevant diameters.

Power consumption

Power consumption was measured by monitoring the temperature rise due to agitation power input. A typical temperature dynamics is shown in Fig. 3.21, where a remarkably constant slope can be observed.

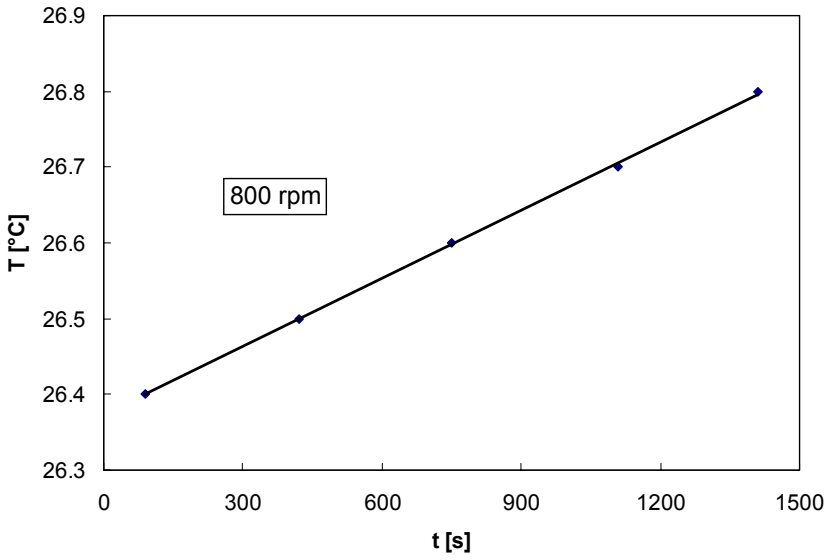

Fig. 3.21: *Typical temperature dynamics (employed for power input determination)*

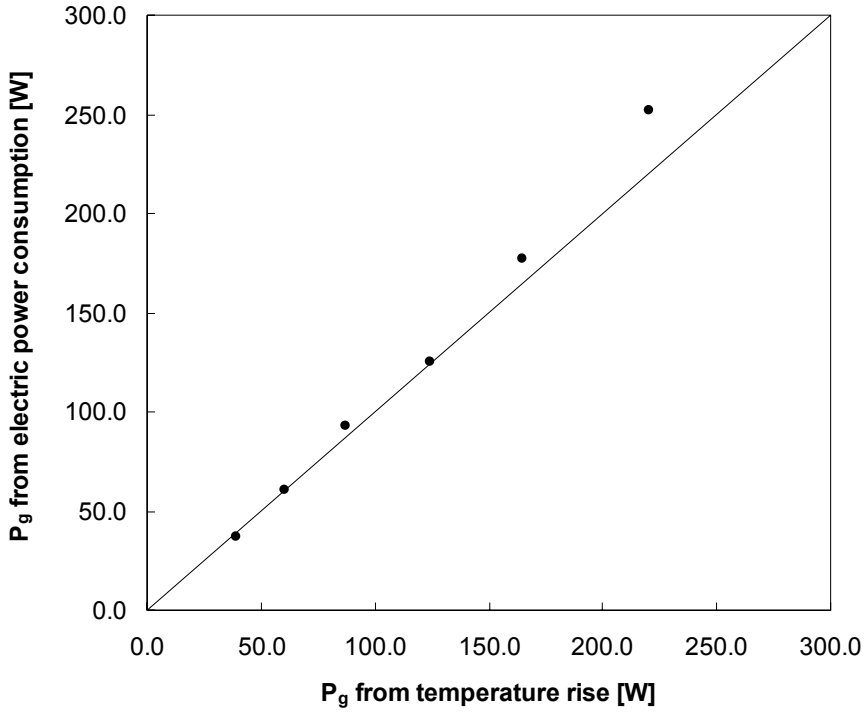

Fig. 3.22: *Comparison between measured power dissipation from electric power consumption and from temperature rise for gassed conditions*

For simplicity, in the computation of power dissipation the heat capacity of vessel walls, shaft and impellers were neglected in front of that of the water mass. This allows to directly convert the observed temperature rise velocity (2.7 10^{-4} °C/s at 800 rpm) into the relevant specific dissipation rate (1130 W/m^3 of liquid phase). It may be guessed that the underestimation of the power consumption incurred because of the quoted simplification accounts for only few percent, being therefore acceptable for most engineering purposes. The total agitation power was finally estimated by multiplying the specific power dissipation by the water volume in the system (0.0769 m^3).

For comparison purposes the agitation power input was also estimated by on-line measurement of voltage current absorption by the DC motor.

Subtracting the relevant electric power absorption with no water in the reactor, and taking into account an overall efficiency of 84% (as indicated in the technical data sheet of the Mavilor, MSS-8 DC motor employed), the measurements practically coincided with those obtained by the temperature rise dynamics, as can be seen in Fig.3.22. The 10 % discrepancy of the datum at the highest agitation speed may be due to a decrease of the DC motor efficiency at the highest power demands. In any case results were considered as a validation of the values obtained from temperature rise.

$k_L a$ measurements

In analogy to what observed in the standard stirred reactor, several variants of the dynamic technique were applied to measure the mass transfer coefficient. As a matter of fact, although in Chapter 2 it was shown that the procedure better suited to provide fundamental results is the one named OApE (see section 2.3.2), the vast majority of data available in the literature were obtained with more questionable techniques and therefore providing here similar data might help performance comparison.

Also, the extent of discrepancies between different experimental techniques may well depend on the type and details of apparatus under investigation. Therefore assessing how such extent may depend on apparatus features was considered to be of general interest.

For these reasons both the previously described OApE and OAS experimental procedures where employed. In addition to these, other commonly employed variants of the dynamic technique were also tested.

Pure oxygen absorption/desorption in air saturated water (procedures "OAS" and "ODA")

A typical "OAS" experimental run started from a condition of air-saturated liquid and no agitation conditions. Pure oxygen then started to be fed to the vessel head space with a flow rate of about 8 l/min, so progressively displacing the air there contained. After 10 minutes the head space was considered to be filled with pure oxygen. Data acquisition was started shortly after agitation, while the head space continued to be flushed with pure oxygen. A transitory followed, in which the difference between the equilibrium concentration to pure oxygen and the time dependent oxygen concentration measured in the liquid phase decayed and eventually vanished.

After the absorption run had been completed, a desorption run was performed (procedure "ODA"), by repeating the above procedure using air (instead of oxygen) as the head-space gas. Once again a simplified model based

on perfectly mixed liquid and gas bubbles all made of air, predicts an exponential decay of the driving force (given this time by the difference between dissolved oxygen concentration and equilibrium concentration with air) with a constant slope coinciding with $(-k_La)$ on logarithmic plots. Clearly the above discussed deviations of reality from model idealisations apply again, though with a reversed nitrogen transfer. In addition, the need to account for the actual behaviour of the gas phase (through a proper gas flow model) may become more stringent.

Pure oxygen absorption in degassed water (procedure OApE)

Once again, pressure inside the reactor was typically brought down to about 0.1 bars while stirring at medium agitation speeds to fasten the degassing process. Vacuum and agitation were maintained for several minutes (typically 5 min) and then atmospheric pressure was restored by admitting pure oxygen to the reactor headspace. To make sure that practically all nitrogen initially dissolved in the liquid phase had been removed, a sequence of at least three evacuation cycles was carried out before beginning the experimental run. This last was then performed in the same way described in procedure "OAS". After the first run, a single evacuation procedure was employed to partially desorb the oxygen dissolved in liquid phase and a new run could be started.

Air absorption in water deoxygenated by nitrogen (procedure "AAN")

In a forth variant the liquid was previously deoxygenated by admitting pure nitrogen to the vessel head-space with a procedure similar to that described in *procedure OAS* for oxygen absorption. When oxygen concentration approached zero, impeller rotation was stopped and air started to be fed to the reactor head-space, thus progressively displacing the nitrogen there contained. After 10 minutes the head space was considered to be filled with air and the stirrer was started, while the head space continued to be flushed with air. Data acquisition of dissolved oxygen concentration was simultaneously started, following the same procedure used in the previous cases. This last is one of the variants more widely employed by experimenters, and was included here for the sake of completeness.

Mixing time τ_{mix} measurements

The liquid phase mixing time measurements, were assessed from unsteady state experiments on the basis of water conductivity dynamics after an instantaneous injection of a high salinity water solution (200 gr/l NaCl) inside the reactor.

Water salinity was measured using a conductivity meter WTW® (Microprocessor Conductivity Meter LF537) with relevant probe (conductibility cell probe TetraCon 96).
The procedure adopted was the following:

1. Set up of the conductimeter in the second range of measurements (0 – 199 μS/cm) (initial water conductibility equal to 30 μS/cm
2. The reactor is brought to regime hydrodynamic conditions at a given agitation speed.
3. Instantaneous injection of 25 cc of high salinity water solution (200 g/l NaCl/water) and contemporaneous start up of data acquisition by LabVIEW®. Data were recorded each 0.1 seconds. ;
4. Data acquisition until the measured value doesn't change any more.
5. Water conductibility is now about 150 μS/cm. A quantity of NaCl is then added so that a conductibility higher than 200μS/cm is obtained and the multimer is brought in the third range of measurements.
6. Set up of the conductimeter in the third range of measurements
7. Second instantaneous injection of 250cc of high salinity water solution and start up of data acquisition until measured values do not change any more.

Conductivity meter delay

The conductivity meter delay was evaluated by imposing an instantaneous step increase of salinity in a water solution. The assumption is that the conductivity meter behaves has a first order system so that by plotting the measured conducibility dynamics vs time in a semi-logarithmic plots will result into straight lines with a slope equal to $(-\tau)$, where τ is the conductivity meter delay.
This was obtained by immerging the probe in a low salinity solution of 30 μS/cm and then passing instantaneously the probe in a high salinity solution at 150 μS/cm, resul

It can be seen that the conductimeter actually behaves as a first order system with an time constant of about 0.5 seconds.

3.3 RESULTS AND DISCUSSION

3.3.1 Gas hold-up

The hold-up values observed at the various agitation speeds are reported in Fig.3.22 as solid circles. As it can be seen, hold-up increases while increasing agitation speed, in agreement with expectations.

In the same graph, the data obtained with the *unbaffled* draft tube have been reported as open squares. As it can be seen, these are much smaller than the gas hold-ups obtained at the same agitation speed with the baffled draft tube configuration. Moreover, the unbaffled draft tube tends to be fairly hydrodynamically unstable. In practice the stirrers tend to be quite easily flooded by the gas, leading to a condition in which below each impeller there is a practically stable gas accumulation that, tending to rise, floods the impeller hence greatly reducing its pumped flow rate.

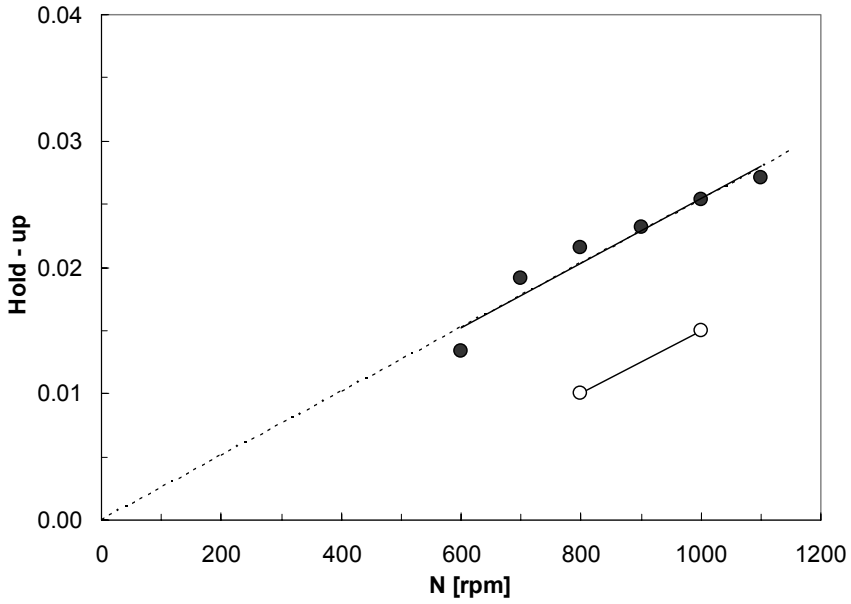

Fig. 3.22: *Experimental gas hold-up versus rotational speed: shaded symbols: baffled draft tube; open symbols: unbaffled draft tube*

The reduced downward flow only manages to keep the gas just underneath the impeller, without succeeding to push it down to the subsequent impeller and to the radial turbine at the base of the vessel, thus failing to circulate the gas phase in the reactor and leaving the annular portion of the vessel substantially ungassed.

The smaller hold-up and mass transfer performance exhibited by the unbaffled draft tube, in conjunction with the similar power demand observed with either baffled or unbaffled configurations and with the wide hydrodynamic instability range that characterises the latter, practically ruled out the unbaffled configuration from further investigation.

It is worth noting that the observed hold-up values range from 1.7 to 2.7 %. These are relatively small values when compared with gas-sparged vessels, but are in the range of values observed with other self-ingesting systems, as it can be observed in Fig. 3.23, where they are compared, versus specific power input, with literature data on other gas inducing reactors. As it can be seen the ability of the LDTSR to bring gas into the liquid phase appears to be somewhat poorer than the other apparatuses, especially at the highest specific power inputs.

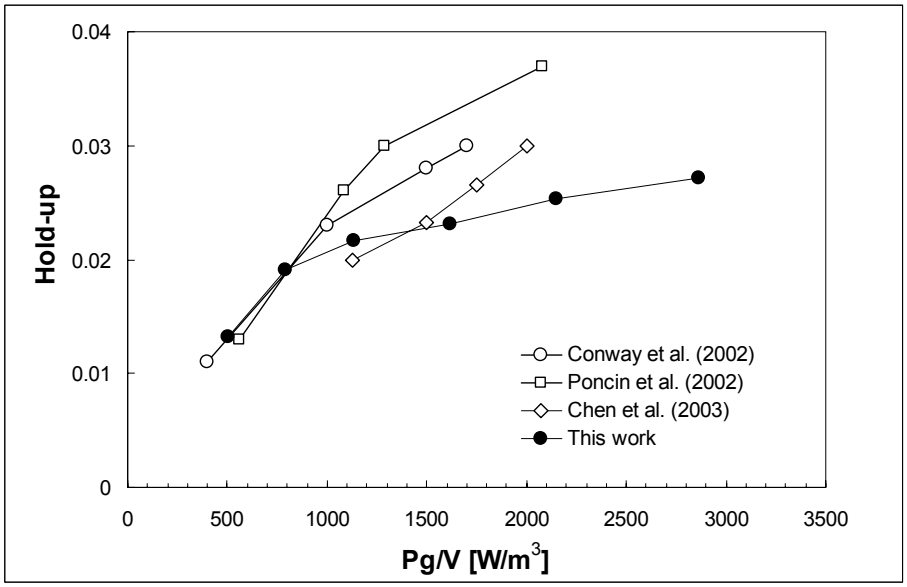

Fig. 3.23: *Comparison between present gas hold-up data with literature results.*

3.3.2 Power consumption

The specific power dissipation values obtained at the various agitation speeds by the temperature rise analysis described in section 3.2.2, are reported in Fig.3.24. A steep increase of power dissipation with agitation speed is observed, as expected.

The relevant total power dissipation was translated into power number (N_p) values, defined as

$$Np = \frac{P}{\rho_L N^3 D^5} \tag{3.2}$$

where P is agitation power, ρ_L is liquid density, N is agitation speed (s^{-1}) and D is the diameter of the radial bottom turbine (D = 0.095 m). The results are also reported in Fig.3.24, where it can be observed that power number slightly decreases when increasing Reynolds number, with values ranging from 5.0 to 4.6. The reason behind the slight decrease is clearly the larger gas hold-up at higher rotational speeds. The relatively constant value observed may anyway be regarded as an indication of hydrodynamic robustness.

It is finally worth noting that if each of the 6 stirrers dissipated the same power as if they were placed in a standard stirred vessel, then the relevant power numbers would have been 4 for the radial impeller [Bates *et al.*, 1967] and 1.27 for each of the axial impellers [Hemrajani and Tatterson, 2004], and the total dissipation by the six stirrers would have resulted in an un-gassed power number (based on the larger impeller diameter) of 4.94. The fact that about the same value was obtained here for the 6 impeller system may be regarded as a validation of the experimental procedure adopted. It also indicates that most of the mechanical power is practically dissipated by the radial impeller alone.

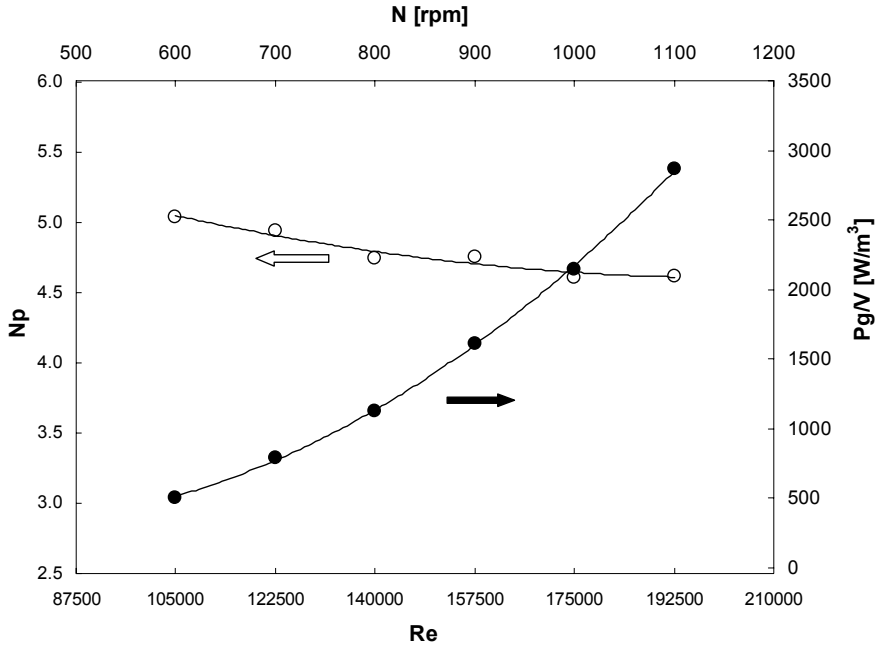

Fig. 3.24: *Specific power dissipation and experimental power numbers for gassed conditions versus agitation speed and* Re *number*

3.3.3 Comparison of k_La values obtained by the four different variants of the dynamic technique

A typical experimental oxygen concentration dynamics obtained by pure oxygen absorption in air saturated water (procedure OAS) is shown in Fig.3.25a, where dimensionless driving force is plotted versus time in a semilog grapgh. Once again, time zero in the figure is meaningless as data acquisition was started first and only after several seconds the agitator was started. As it can be seen, after some time the data points do actually settle on a fairly straight line, so that an estimation of the mass transfer parameter k_La (0.0102 s^{-1}, in the particular case under examination) is obtained.

It is worth noting that an initial transient in which the driving force decay shows a non exponential trend was expected. In particular, taking into account that during this transient gas hold-up, hence interfacial area, is

progressively building up, one would have expected a transient in which the absolute value of the local slope was progressively increasing. In other words, the non-linear portion of the dynamics curve was expected to show a downward concavity. This is not the case of the data in Fig.3.25a, where a distinct upward concavity can be observed instead, after a very short downward concavity. Notably, the same behaviour was consistently observed in all experimental runs when procedure OAS was adopted. The implied progressive decrease of the instantaneous value of k_La is clearly only apparent, and the real reason might well lie on a non negligible variation of oxygen concentration in the gas phase during the absorption process, possibly due to nitrogen counter-diffusion towards the bubbles.

Fig.3.25 b shows the results obtained by Oxygen desorption by means of air (procedure ODA) at the same agitation speed of Fig.3.25a. As it can be seen, a quite similar curve was obtained, with a slope of the final straight line almost coinciding with that obtained with procedure "OAS". Also, a distinct upward concavity is observed again during the transient.

Identical behaviours were found in all the experiments carried out with this methodology, with final slopes practically coinciding with those obtained at the same agitation speed with procedure "OAS".

Pure oxygen absorption in pre-evacuated water (procedure OApE)

A typical result of the almost nitrogen-free procedure is presented in Fig. 3.25c. As it can be seen, this time a very different driving force dynamics was obtained: not only the upward concavity has completely disappeared, but the final slope of the concentration dynamic is strikingly larger than that obtained with procedures "OAS" and "ODA" at the same agitation speed. The same behaviour was observed in all the experiments carried out with procedure "OApE", independently of agitation speed and liquid phase coalescence properties.

As procedure "OApE" is practically identical to the previous procedures, apart from the initial presence of nitrogen in the liquid phase, there can be no doubt that the presence of dissolved nitrogen in the liquid phase was behind the odd initial curve concavities observed with procedures OAS and ODA.

But definitively more important is the strikingly large influence that the initial presence of nitrogen is found to have on the value of the final slope of the driving force dynamics, *i.e.* on the measured value of the volumetric mass transfer coefficient k_La, much larger here than in the previously assessed case of standard stirred vessel.

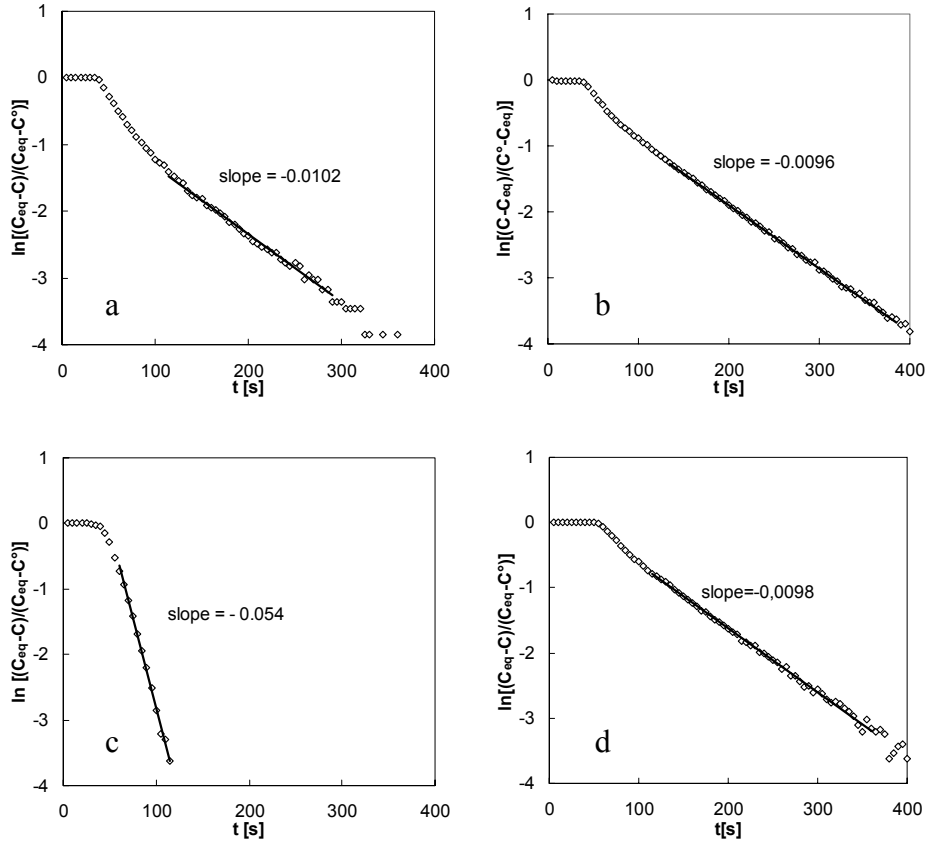

Fig. 3.25:*Typical oxygen concentration dynamics at 1000 rpm: a) Procedure OAS (oxygen absorption in air saturated water); b) Procedure ODA (oxygen desorption with air); c) Procedure OApE (oxygen absorption in pre-evacuated water); d) Procedure AAN (air absorption in nitrogen saturated water).*

In order to understand this result, one may simulate the dynamics of nitrogen concentration in a single bubble initially made of pure oxygen and simply rising in a quiescent air-saturated solution, with constant mass transfer coefficient k_L . In this case a simplified mass balance based on the hypothesis of constant rise velocity shows that after 1.2 m of rise, bubbles larger than 2 mm end up with a negligible nitrogen concentration, while the final oxygen concentration of bubbles smaller than 1 mm is quite strongly affected. An

important presence of bubbles with sizes smaller than 1 mm in the system was actually observed when agitation of the system was suddenly stopped (after the rise of larger bubbles). It has also been experimentally observed in standard stirred vessels, for instance by Barigou and Greaves, (1992) as well as by Laakkonen *et al.* (2005).

Clearly some of these bubbles after reaching the top region are probably recirculated towards the bottom, so either prolonging they exposition to nitrogen counter-diffusion, or mixing with the rest of the gas phase during their travel in the draft tube, in any case leading to a further reduction of the average mass transfer driving force.

On the basis of the above simplified model of single bubble behaviour, one may guess that a great number of tiny gas bubbles (with a diameter smaller than 1 mm) were present inside the reactor. As a matter of fact, the LDTSR is quite effective in generating quite tiny bubbles, as already pointed out. Also its high aspect ratio makes the rise of single bubbles longer and therefore particularly prone to nitrogen counter-diffusion. These considerations imply that the differences in other apparatuses, characterized by larger bubble sizes and/or smaller aspect ratio, the discrepancies between the values obtained in presence or absence of nitrogen may well be much smaller than those observed here. This clearly explains the much larger discrepancies observed with the LDTSR with respect to those observed with the much shorter standard vessel discussed in Chapter 2.

An example of dissolved oxygen dynamics obtained with the commonest variant of the dynamic technique (procedure AAN) is reported in Fig3.25 d, where the upward concavity during the transient and the relatively small value of the final slope are observed again. This implies that, although in this variant the initial nitrogen concentration inside bubbles is relatively high (78 % vol), the presence of dissolved nitrogen is nonetheless able to strongly affect oxygen concentration in the bubbles and therefore the driving force for oxygen transfer to the liquid phase.

All the values of the volumetric gas-liquid mass transfer coefficient k_La obtained by the three variants of the oxygen absorption dynamic technique, are plotted in Fig.3.26 versus agitation speed, both for the coalescing system (oxygen-distilled water) and for the coalescence inhibiting system (oxygen – NaCl solution). As it can be seen, the reproducibility of the measurements at the same hydrodynamic conditions is poorer than in the case of the sparged stirred vessel, yet still acceptable for the purpose of preliminary assessment of apparatus performance.

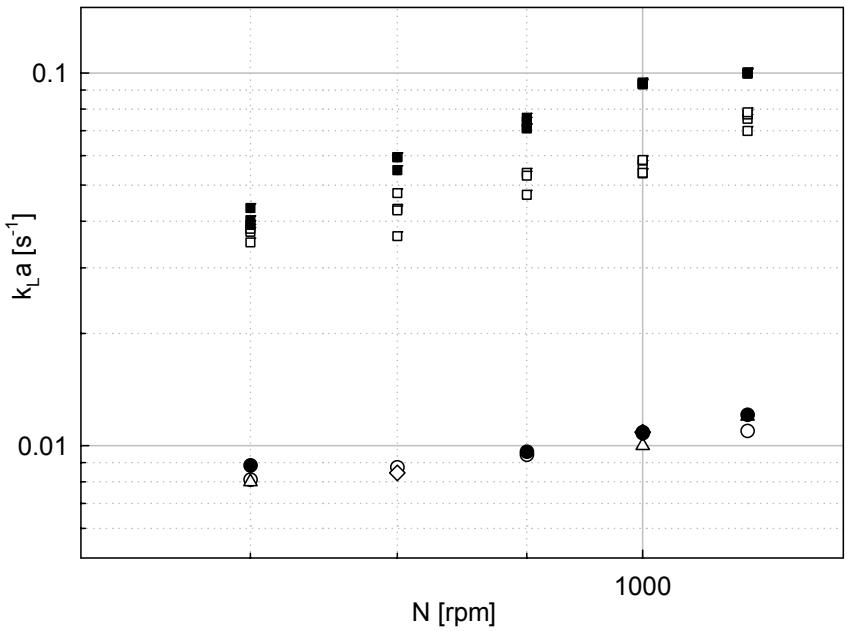

Fig. 3.26:*Comparison between kLa values determined with the four variants of the dynamic oxygen absorption method at various agitation speeds. Circles: procedure OAS ; squares: procedure OApE; diamonds: procedure AAN; triangles: procedure ODA. Solid symbols: Oxygen – NaCl solution system; open symbols: Oxygen – distilled water system.*

Fig. 3.26 confirms that the values of k_La obtained with procedures "OAS", "ODA" and "AAN" are similar for a given agitation speed, while those obtained with procedure "OApE" are about five times larger for coalescing systems and about eight times larger for the non-coalescing system.

The larger difference observed with non-coalescing in comparison with coalescing systems is to be attributed to the smaller average bubble size in the former case. It is worth noting that bubbles whose oxygen concentration has been brought to equilibrium with the liquid at a given time, from then on start acting as oxygen sink instead of an oxygen source. This consideration may further explain the strikingly large differences observed in the LDTSR case.

3.3.4 Dependence of k_La on power dissipation and comparison with other gas inducing reactors

The k_La data obtained with the correct variant OApE of dynamic method are correlated with the specific power input. In Fig.3.27, the k_La values for the coalescing system (water-oxygen) are plotted. The resulting correlation has the form:

$$k_La = 0.0012 * \left(\frac{P}{V}\right)^{0.5} \tag{3.3}$$

The exponent 0.5 compares fairly well with the 0.4 exponent suggested by Van't Riet (1979) for sparged vessels, as the difference is of the right order to compensate for the effect of increasing superficial gas velocity, which is separately accounted for in Van't Riet's correlation. On the same Figure, literature data obtained for coalescent systems by some variant of the dynamic method are also reported. As it can be seen, the system here investigated appears to compare favourably with all other GIR apparatuses. It is worth noting however that All of the literature data reported were obtained in the presence of dissolved nitrogen, and one may guess that had procedure OApE been employed instead, larger values of kLa would have been obtained.. It is unfortunately impossible to predict the extent of the relevant increase, as this depends in a complex way on bubble size distribution (smaller bubbles give larger contributions to it) and rise length (higher aspect ratios increase the effect). The only data obtained with an "OApE" type procedure that the authors were able to retrieve in the literature are those obtained by Linek *et al.* (1987) in a sparged standard stirred vessel. They reported that when previously degassed water was used for the experiments, k_La values larger by 25-30% were obtained. This is a much smaller difference than those observed here; a feature that may easily be explained on the basis of the smaller liquid height that bubbles had to rise through in order to reach the free surface. Clearly for a thorough comparison of results, the availability of data obtained with the simple dynamic method *in absence of nitrogen* with all other apparatuses would be needed.

In Fig. 3.28, the k_La values obtained with procedure OAE for the non-coalescing system (NaCl-water-oxygen) are reported. The resulting correlation has the form

$$k_L a = 0.00042 * \left(\frac{P}{V}\right)^{0.8} \tag{3.4}$$

The exponent of 0.8 compares again reasonably well with the exponent of 0.7 proposed by Van't Riet (1979) taking once again into account the need to compensate for the superficial velocity here implicitly embedded into (P/V). On the same Figure, the results obtained with the non-coalescent system are compared with data by Poncin *et al.* (2002) (sulfite oxidation method) and Joshi and Sharma (1997) (Carbon dioxide absorption in buffer solutions). These last data were normalized with the square root of the ratio of diffusion coefficients (3.42 and 1.91 10^{-9} m^2/s for Oxygen and Carbon dioxide respectively). As it can be seen in this case the present apparatus shows an efficiency comparable with that of the other apparatuses, although the differences in chemical composition may have resulted in different extents of coalescence inhibition. Notably, the above considerations on nitrogen counter-diffusion hardly apply here, and therefore the data obtained by chemical steady state methods should be directly comparable with the data obtained here by means of procedure "OApE" for non-coalescing systems.

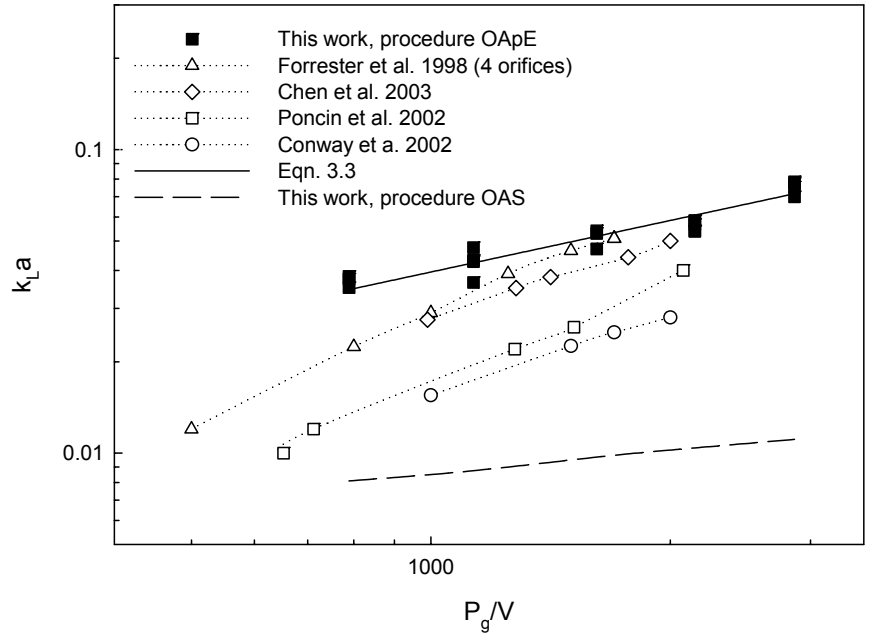

Fig. 3.27: *Mass transfer coefficient vs specific power input in coalescing systems.*

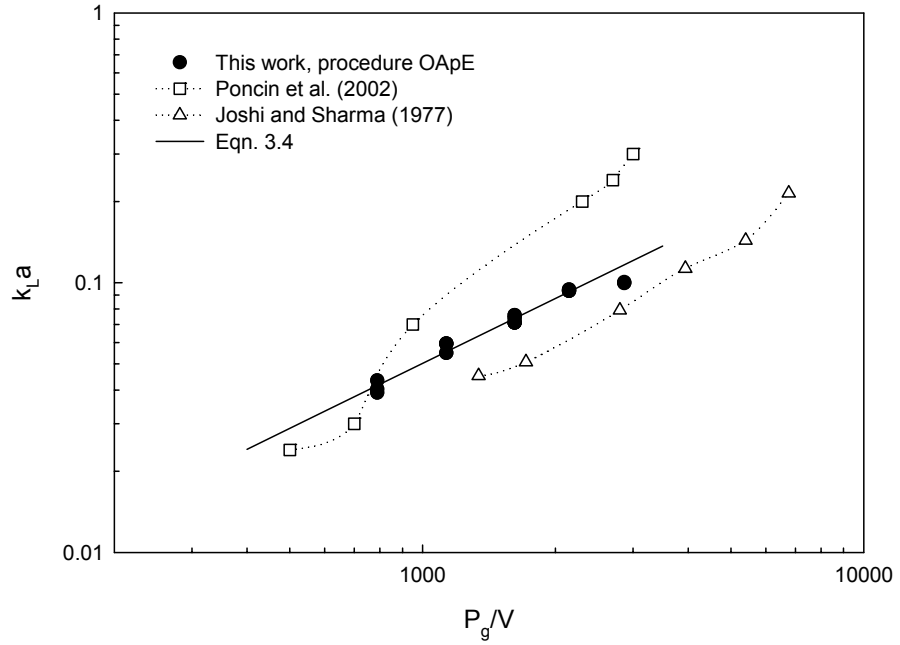

Fig. 3.28: *Mass transfer coefficient vs specific power input in non- coalescing systems.*

Overall, it can be stated that the mass transfer performance of the present apparatus appears to be at least similar to that of similar apparatuses, a finding that encourages its further development.

3.3.5 Mixing time

Water conductivity dynamics after an instantaneous injection of a high salinity water solution inside the reactor were recorded and reported as a graph Fig. 3.29, in which the ratio between the instantaneous and the final voltage was plotted versus time.

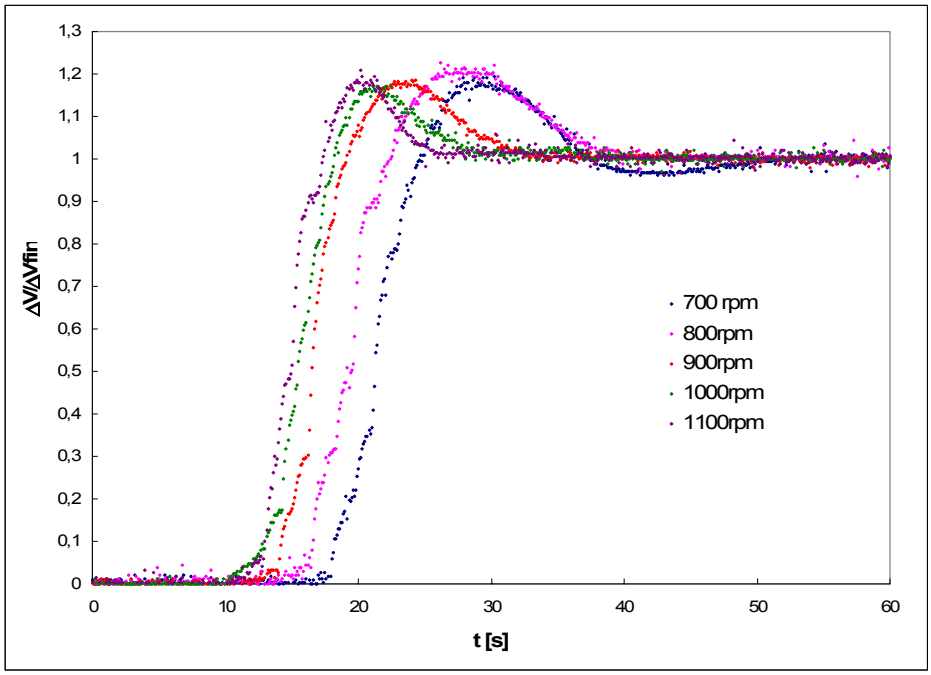

Fig. 3.29: Conductivity dynamics of the system

As it can be seen the dynamic behaviour of the system is similar to that of a *Plug Flow* with a high axial dispersion (Scargiali *et al.* 2004) which is in reasonable agreement with a possible hydrodynamic model of a forced circulation reactor such as the LDTSR under examination.

Information about the average circulation time can be obtained from the voltage dynamics reported in Fig. 3.29 by measuring the whole period length. This last was evaluated as the double of the distance from the first relative maximum of the curve (t_{pick}) and the subsequent relative minimum (t_{valley})

$$\tau_{circ} = 2 * (t_{pick} - t_{valley})$$

The circulation times obtained in such a way are reported in Fig 3.30 as a function of agitation speed.

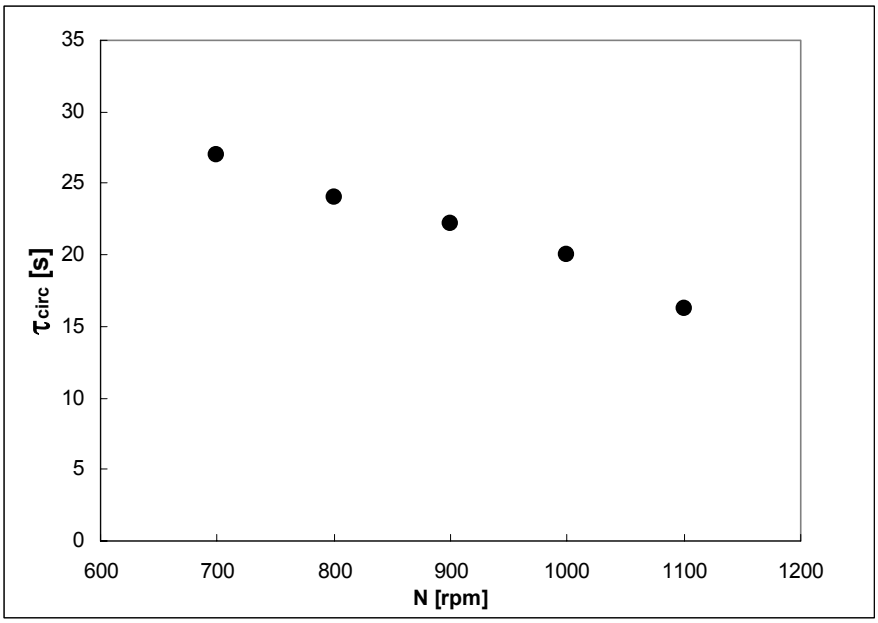

Fig. 3.30: Circulation time of the LDTSR versus agitation speed

As expected circulation time decreases (varying from 27 to 16.5 seconds) while agitation speed increases. The values are much larger than the response time of the probe (about 0.5 s) whose dynamics could therefore be neglected.

Once known the circulation times of the system the pumping number was also calculated from the relation:

$$N_{Qt} = \frac{V}{\tau_{circ} \cdot N \cdot D^3} \tag{3.5}$$

The resulting pumping numbers obtained from the relation reported above are about constant with agitation speed as it is possible to see in Fig. 3.31, a feature that is typical of stirred reactors in turbulent conditions, thus giving of solidity to the measured data. The average value of about 0.8 also agrees well with the typical N_Q of radial turbines (i.e. N_Q=0.75).

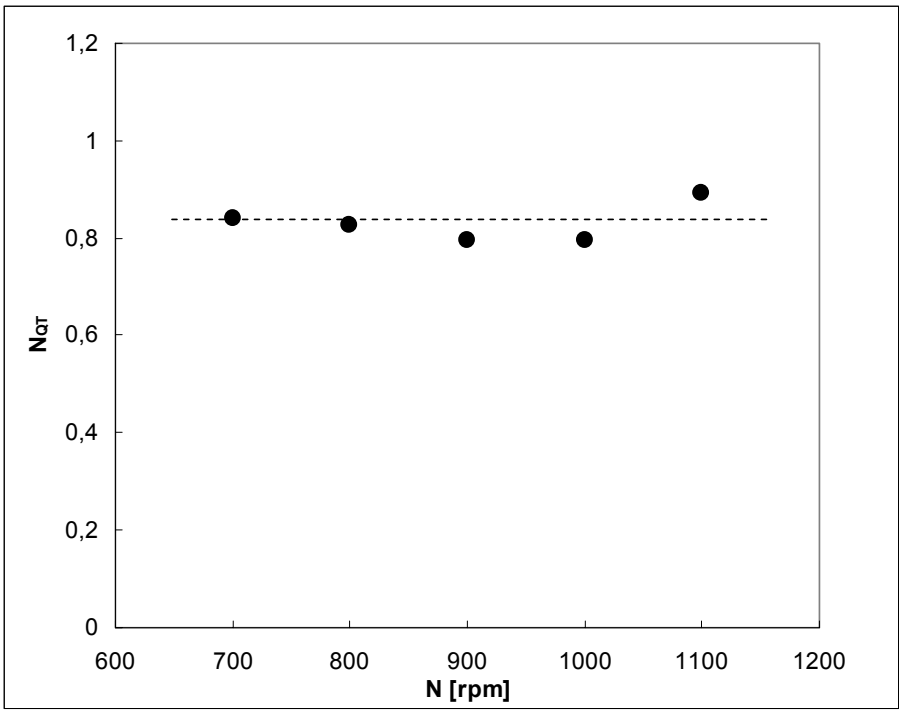

Fig. 3.35: Andamento del numero di pompaggio in funzione della velocità di agitazione.

It may be noticed that the circulation times observed are comparable with the mass transfer characteristic times ($1/k_La$). This consideration suggests that the liquid phase may be far from perfect mixing, and a more complex modellization of liquid hydrodynamics would be needed. Nevertheless, according to Nocentini (1990), it is most likely that the influence of the liquid phase flow behaviour on the accuracy of measurements is negligible.

3.4 CONCLUSIONS ON LDTSR EXPERIMENTATION

A novel self-ingesting gas-liquid contacting device has been proposed. The preliminary results obtained so far show that both gas hold-up and gas-liquid mass transfer coefficient increase while increasing stirrer speed (and therefore specific power input), as it was expected.

Notably the values obtained in this work are comparable with some of the best results reported in the open literature for self-ingesting apparatuses. This is encouraging, especially if one considers that geometrical details of the apparatus here investigated are still to be optimised and that the LDTSR appears to be very well suited for three-phase operations too.

Among the advantages of the present LDTSR it is worth noting that its performance is similar to that of the AGR (Conway *et al.*, 2002) but the mechanical construction of the former is much simpler. It is also believed that the LDTSR scale-up may be simpler and safer, considering that it should be possible to scale it up vertically by simply making it longer while adding further equi-spaced axial impellers to overcome the additional hydraulic head.

Results show that, for the investigated system, gas-liquid mass transfer coefficients obtained according to procedure "OApE" may be several times greater than those measured in the same hydrodynamic conditions but starting with an air-saturated liquid phase. Such differences are much larger than those observed in the standard vessel investigated in Chapter 2; possible reasons behind this discrepancy are discussed. The difference is found to be largest for the non coalescing systems, as these tend to give rise to smaller bubbles, which are the ones most affected by nitrogen counter diffusion effects.

It would clearly be worth extending the investigation with the new variant of the dynamic technique to the other gas inducing apparatuses, for the sake of a thorough performance comparison. In any case, comparison with similar gas inducing devices encourages further development of the presented apparatus.

Finally, the already pointed out importance of using correct methods for $k_L a$ measurement, is further confirmed.

CHAPTER 4

TURBULENCE EFFECTS ON BUBBLE TERMINAL VELOCITY

4.1 INTRODUCTION

Bubble terminal rise velocity in the liquid medium and the related bubble drag coefficient are hydrodynamic parameters of paramount importance involved in the modelling, design and development of such apparatuses. It is especially worth mentioning here the recent developments of computational fluid dynamics (CFD) simulations of multiphase systems, where the interactions between phases are typically modelled on the basis of drag coefficients, which have to be provided as input data (Gosman *et al.*,1992, Brucato *et al.*, 1996, Decker *et al.*,1996, Lane *et al.*,2005).

For still fluids (especially for water) a great deal of information, both experimental and theoretical, is available on bubble terminal velocity for a wide range of bubble sizes and shapes (Clift *et al.*, 1978). Notably, this is the case whether or not the relative motion between the two phases is able to induce turbulence in the liquid phase in the bubble proximities.

On the contrary, almost no information is available on bubble terminal velocities or drag coefficients when the liquid phase exhibits a free stream turbulence which is independently generated by other sources.

This would be a satisfactory situation if one could reasonably expect that free stream turbulence had no effect on liquid-bubble drag forces. Unfortunately this is not the case, as one may guess that the presence of free stream turbulence is bound to significantly affect the flow field in the gas-liquid boundary layer and therefore the extent of the forces exchanged between the two phases. This is known to be true in the case of solid particles freely falling into turbulent fluids, for which free stream turbulence has been observed to significantly affect particle drag forces, by either decreasing them (mainly in the case of relatively large particles falling into air, see for inst. Clamen and Gauvin, 1969) or increasing them (Brucato *et al.*, 1998, Pinelli *et al.*1996, Uhlherr and Sinclair, 1970)

As the latter is typically the case for small particles freely falling into liquid phases, free stream turbulence should be expected to increase also the drag forces experienced by relatively small bubbles freely rising into liquid phases and therefore reduce their terminal rise velocity.

An indirect indication of the actual existence of such effect may be found in the circumstance that neglecting it has been found to result into possible underestimation of the gas hold-up in gas-liquid stirred vessels, as if bubble rise velocity had been significantly overestimated (Lane *et al.*, 2002)

Some direct evidence of the existence of this effect may also be found in the scientific literature. Namely free stream turbulence has been found to

considerably reduce bubble terminal rise velocity in numerical simulations (Spelt and Biesheuvel, 1997) as well as in experiments (Poorte and Biesheuvel, 2002) on bubbles smaller than 1 mm.

It may be concluded that, in spite of the wide scientific and technical interest on the subject, and in spite of the fact that the few data available show that the drag coefficient can significantly be affected by free stream turbulence, there still is a substantial lack of data and reliable correlations on the subject. A reason for this may well lie upon the noticeable difficulties involved in the relevant experimentation.

The present section was aimed at developing a novel experimental technique for measuring free stream turbulence effects on bubble terminal rise velocity. In the followings the technique is described and discussed. Preliminary experimental results are also presented.

4.1.1 Literature survey: bubble terminal velocity in still fluids:

A bubble moving freely in a liquid under the influence of gravity, will rise at a constant velocity after the terminal condition is reached. From the balance of drag and buoyancy forces, the two only forces governing bubble motion at steady state, we have

$$C_D \frac{1}{2}\rho U_T^2 \frac{\pi d^2}{4} = \left(\rho_l - \rho_g\right) g \frac{\pi d^3}{6} \tag{4.1}$$

Solving for U_T^2 yields

$$U_T^2 = \frac{4\left(\rho_l - \rho_g\right) g d}{3 C_D \rho_l} \tag{4.2}$$

Eqn. 4.2 shows that U_T and C_D are strictly related, so that U_T may be estimated if C_D is known and vice versa. For the case of solid spherical partiscles a unique relation called "Standard drag curve" between C_D and particle Reynolds number ($Re=(\rho_l U_p D_p)/\mu_l$) exists.

It should be however noted that reference to the standard drag curve for spheres and relevant analytical correlations, should be avoided when modelling bubbly flows. In fact the standard drag curve concerns spherical particles with a rigid slip-less interface, while bubbles in the millimetres size range are well known to be characterized by a mobile interphase and deformed ellipsoidal shapes, that result into much larger values of the drag force than those pertaining to rigid spheres of equivalent volume (Mendelson, 1967, Clift *et al*, 1978, Tomiyama *et al.* 1998; Tomiyama *et al.* 2002; Celata *et al.* 2006). In those cases in which the presence of impurities inhibits surface mobility, the drag force is further increased (Clift *et al*, 1978; Tomiyama *et al.* 1998).

Data for terminal velocity of bubbles in water are available as a function of bubble equivalent diameter (Fig. 4.1), though a fairly large data dispersion is observed in relation to subtle surface properties, and therefore to the level of water contamination. The data are referred to the ellipsoidal regime and adjacent parts of the spherical and spherical-cap regimes. Some of the spread in the data results from experimental scatter, but the greatest cause is surface contamination. In fact, for a gas bubble there is little viscous resistance to internal circulation, nd hence the drag and terminal velocity are sensitive to the presence of surfactants. The curves converge for small bubbles (spherical),

since even distilled water tends to contain sufficient surfactants to prevent circulation in this range. For large bubbles (spherical cap), where surface tension forces become unimportant. Surface active contaminants affect the rise velocity most strongly in the ellipsoidal regime.

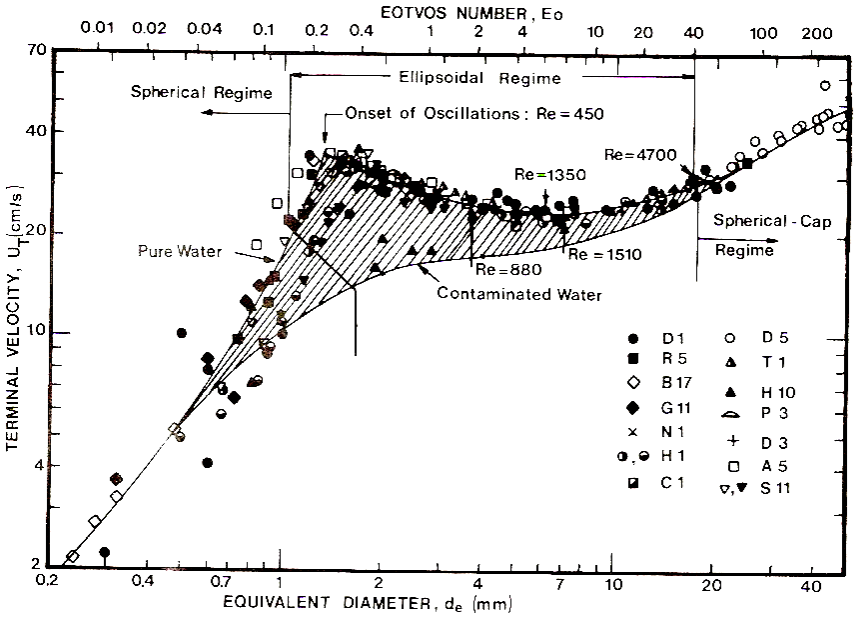

Fig. 4.1: Terminal velocity of air bubbles in water at 20 °C (after Clift et al., 1976, pag. 172)

In Fig. 4.2 (a) and (b) the literature available experimental data for terminal velocity of bubbles in water are compared with the numerous correlations proposed in the literature both for terminal velocity or for drag coefficient.

It is worth noting that, if we compare the experimental data with the relevant terminal velocities derived from the drag coefficient related to rigid spheres (Standard Drag Curve), terminal velocity for bubbles with an equivalent diameter lower than 2.3 mm lies above the rigid sphere when internal circulation is present (pure water), but below if there is no internal circulation (contaminated water) and the drag is dominated by deformation. This last circumstance becomes valid also for pure water when bubbles equivalent

diameter is higher than 2.3 mm and deformation is the main dominant factor on drag coefficient.

In such cases, using correlations for standard drag curve can bring to significant underestimation of the real drag coefficient of the system.
Other correlations have been proposed in the literature and are reported in Fig. 4.2 a e b: the Ishii and Zuber correlation (Fig. 4.2 a) (Ishii and Zuber 1979) and the Grace correlation (Fig. 4.2 b) (Grace, 1976), give very similar results and predict a bubble terminal velocity intermediate between contaminated water and pure water.

In the case of pure water and air bubbles in the range from 1.3 mm to 15 mm, bubble terminal rise velocities may be well correlated by Eqn. 4.3 (Mendelson 1967), that reproduces very well the data for pure water and air, as shown in Fig. 4.2a:

$$U_T = \left[(2.14\frac{\sigma}{\rho d_e}) + 0.505 g d_e \right]^{0.5} \tag{4.3}$$

Eqn. 17, recasted, results in an expression for C_D analogous to the rightmost term of Eqn. 18 a), b) and c) by Tomiyama *et al.* (1998):

(a) for purified systems:

$$C_D = \max\left\{ \min\left[\frac{16}{Re}\left(1 + 0.15 Re^{0.687}\right), \frac{48}{Re} \right], \frac{8}{3}\frac{Eo}{Eo+4} \right\} \tag{4.4a}$$

(b) for a slightly contamined system:

$$C_D = \max\left\{ \min\left[\frac{24}{Re}\left(1 + 0.15 Re^{0.687}\right), \frac{72}{Re} \right], \frac{8}{3}\frac{Eo}{Eo+4} \right\} \tag{4.4b}$$

(c) for a fully contamined system:

$$C_D = \max\left\{ \frac{24}{Re}\left(1 + 0.15 Re^{0.687}\right), \frac{8}{3}\frac{Eo}{Eo+4} \right\} \tag{4.4c}$$

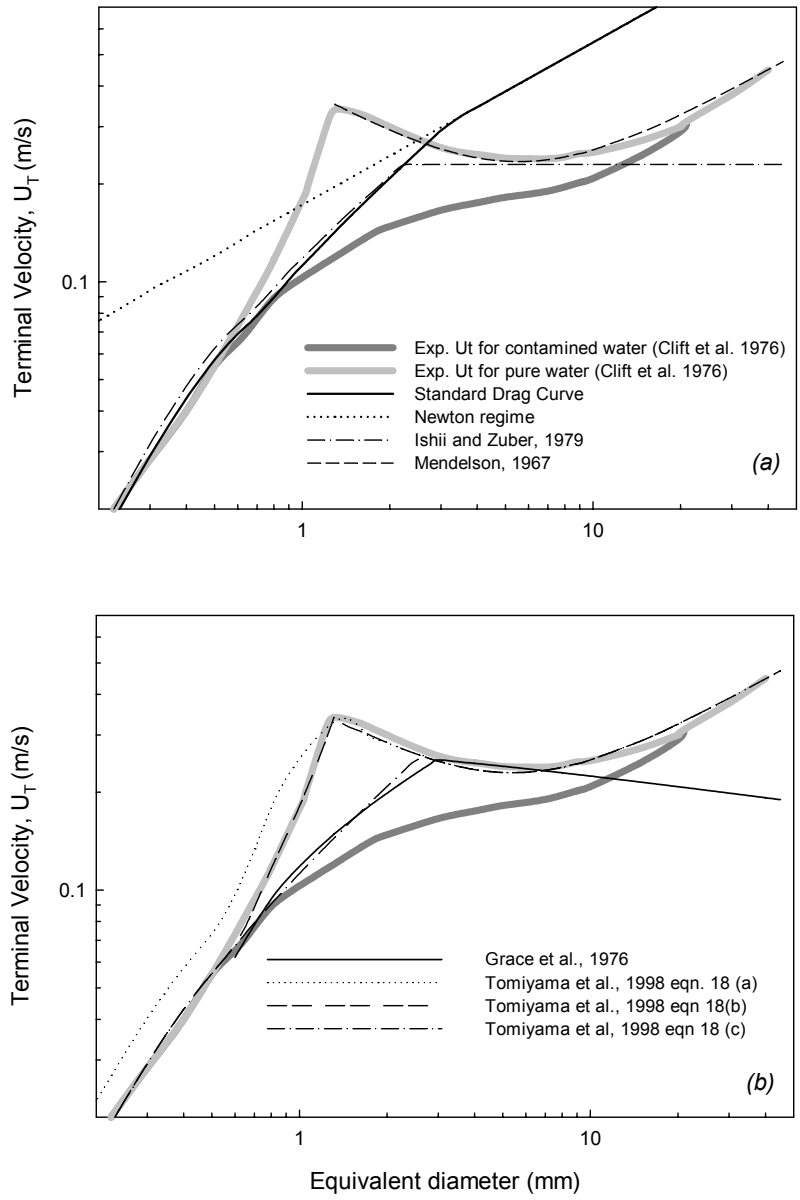

Fig. 4.2 *Comparison between experimental data and available correlations for terminal rise velocity of bubbles in still water versus equivalent diameter.*

Eo is the Eötvös number defined as

$$Eo = \frac{g(\rho_l - \rho_g)d_e^2}{\sigma} \tag{4.5}$$

Eqns 4.4 a. b, and c, solved in conjunction with eqn. 15 allow to obtain the relevant values for bubble terminal velocities at the various equivalent bubble diameters. The corresponding curves are compared with the available experimental data (Clift *et al.* 1976) in Figs. 4.2b, where it can be seen that the data obtained from eqn. 18b nicely fits the available experimental data for pure water over the whole range of bubble sizes. Eqn 4.2a seems a pure theoretical extent of mobile interphase behaviour also for very small bubbles in purified systems.
Recently, many experimental and theoretical studies have also been carried out to take into account bubbles aspect ratio, bubble shape and wake effects (Tomiyama *et al.* 2002, Celata *et al.* 2006) giving sophisticated and more precise correlations though less exploitable in CFD codes.

4.1.2 Literature survey: free stream turbulence effects on bubble terminal velocity

As already pointed out, it is well known that free stream turbulence may significantly affect particle drag (Clamen and Gauvin, 1969, Brucato *et al.*, 1998, Pinelli *et al.*1996, Uhlherr and Sinclair, 1970). For the case of gas bubbles there is much less information in the scientific literature. However the scant information available indicates that such effects may well affect gas bubbles.

Spelt and Biesheuvel (1997) conducted a study about the motion of small bubbles in homogeneous isotropic turbulence. They presented results of numerical simulations of the motion of gas bubbles rising at high Reynolds number through homogeneous isotropic turbulence. The turbulent velocity field was simulated by a large number of Fourier modes with random phases and amplitudes, and by calculating the bubble trajectories from a reasonably well established equation of motion. The forces exerted on a bubble by the surrounding fluid were described by a superimposition of the force on a rigid sphere in an inviscid unsteady non-uniform flow, and the drag experienced by a spherical gas bubble rising steadily at high Reynolds number in still fluid. It was found that the velocity of rise is markedly reduced, down to 50 % of the value in still fluid. In a subsequent work Spelt and Biesheuvel (1998) compared

analytical solutions of the bubble motion equations with results from simulations of bubble motion in a Gaussian random velocity field. They observed that analytical results may have qualitative value for the interpretation of experiments and numerical simulations.

A very interesting experimental study, about the motion of gas bubbles in an isotropic turbulence field was carried out by Poorte and Biesheuvel (2002). In this work the authors tried to obtain experimental validation of the theoretical work previously carried out (Spelt and Biesheuvel, 1997, 1998). The random motion of nearly spherical bubbles in the turbulent flow behind an active grid was experimentally investigated. The roads of this bi-plane grid had agitator wings attached which were actively flapped in a random manner. In this way the structure of the turbulence generated could be suitably modulated. It has higher intensities and larger length scale of a conventional static grid, while the isotropy is not as good as that obtained downwind static grids. Bubbles of 1.0 mm in diameter were studied. These in quiescent water rise rectilinearly with a speed of about 25 cm s^{-1}, while maintaining an approximately spherical shape. The bubbles were let to rise upwards towards the grid through which the water was flowing downwards. By adjusting mean velocity of water the bubbles can be made to move randomly within a relatively small interrogation section at an arbitrary position behind the grid. The trajectory of each bubble was measured with high spatial and temporal resolution with a specially developed technique that makes use of a position sensitive detector. Experimental results were obtained and compared with theoretical predictions. It was shown that the mean rise velocity of bubbles can be significantly reduced, by as much as 35 %, compared with the quiescent conditions. There was reasonable agreement between theory and experiments.

Alves *et al.* (2003) introduced a correction for turbulence on bubble mean rise velocity to fit experimental results obtained on mass transfer coefficients in stirred tanks with traditional correlations for k_L calculation given by the Froessling theory for rigid bubbles and the penetration theory for mobile interface bubbles (Brodkey, 1988). Using a 35 % reduction on bubble rise velocity as calculated from terminal velocity, a good agreement with experimental data was obtained.

As no other information was retreived in the open literature, it may be concluded that it is likely that some turbulence effect on bubble drag exists, but no accurate information on its extent (and dependence on bubble size and turbulence intensity) is available. Clearly there is a need for new experimental data and techniques to fill the gap.

4.2 EXPERIMENTAL TECHNIQUE

4.2.1 Technique fundamentals

Let us consider a vertical channel with water flowing downwards after having passed trough a turbulence generating grid (Fig.4.3). It is well known that the flow field downstream a grid is characterised by a nearly homogeneous and isotropic decaying turbulence (Mohamed and Larue, 1990) the result is therefore a system where free stream turbulence intensity gets larger while moving upwards towards the grid.

A gas bubble injected inside the channel will tend to move upwards or downwards depending on the value of its terminal rise velocity with respect to liquid velocity. With reference to Fig.4.3, let us assume that a bubble is currently moving upwards due to the fact that its terminal rise velocity is larger than the liquid velocity. If the bubble drag coefficient increases with turbulence, then while moving upwards the bubble will experience larger turbulence levels and its terminal rise velocity will progressively be reduced. If the drag increase is sufficiently large, then the bubble will eventually find an equilibrium position where the drag coefficient increase has brought its terminal rise velocity to match the liquid downward velocity.

It is worth stressing that with the system devised a stable equilibrium position for the bubble is possible only under the hypothesis that the bubble drag coefficient increases with increasing turbulence intensity, and therefore the technique can only work if the above hypothesis is satisfied in the real system.
If the above hypothesis holds true, then a given bubble should find a series of quasi-steady elevations when subsequently adjusting the liquid velocity inside the channel. In particular equilibrium positions closer to the grid the smaller the liquid velocity should be clearly observed.

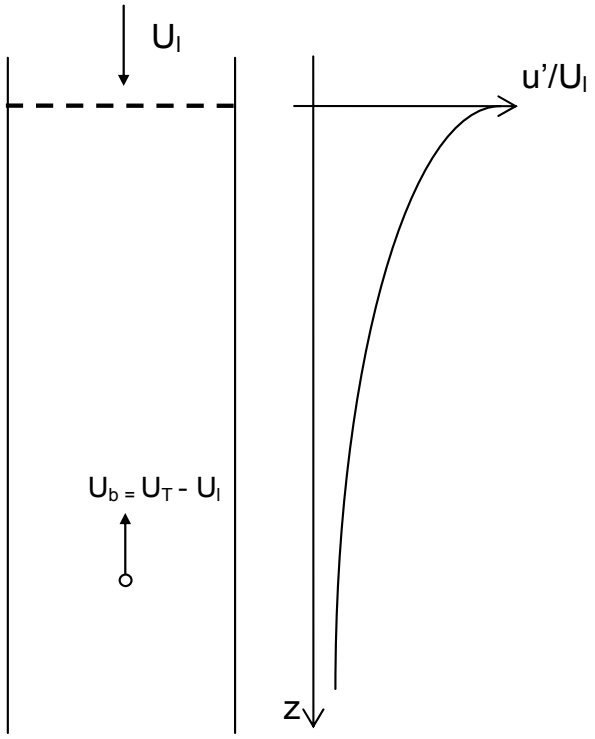

Fig. 4.3: Sketch of a bubble in a water channel with decaying turbulence

4.2.2 Dealing with flow field variations over the channel section

In any finite channel, liquid average velocity and turbulence intensity do vary over the channel section, to become nil at channel walls. Due to turbulence and other causes, bubbles are bound to undergo transversal motion that exposes them to variable flow field conditions, which results in turn in random upwards and downwards movements that may practically impair the technique. To avoid these uncertainties, a centrifugal field was over imposed on the system, with the aim of keeping bubbles near the symmetry axis as a consequence of the density difference between the two phases. This was achieved in particular

by making the circular channel to rotate, resulting in this way in a non-decaying swirling motion that was found to be very effective in stabilizing the bubble in the proximities of the channel axis, hence letting bubbles or light particles to experience well defined flow field conditions.

4.2.3 Experimental apparatus

The experimental apparatus practically set up to explore the viability of the technique under discussion, is depicted in Fig 4.3. It consisted of a square section Perspex container, 200 x 200 mm wide and 1500 mm long, inside which a rotating tube 52 mm wide and 2000 mm long was collocated.

Two ball bearings supported the cylindrical channel from its topmost emerging portion, which accounted for almost 600 mm of its length. A speed controlled DC motor drove the tube rotation by a belt and pulley coupling. A Teflon sliding support was arranged at the bottom of the tube in order to avoid tube oscillations during its rotation.

At the bottom of the channel single bubbles were injected in the tube by means of a syringe. In this way it was possible to obtain relatively large bubbles, 6 - 12 mm in size.
The external circuitry, to obtain the desired flow field in the circular channel, was made of 2.54 mm ID tube and included a centrifugal pump, a flow meter and two flow rate regulation valves.

The turbulence generating grid was collocated at about 800 mm from the top of the tube as depicted in Fig. 4.4. For this preliminary investigation it practically consisted of a perforated Perspex disc, with 3 mm holes and a solidity ratio $\sigma = 0.14$.

Whole Reynolds numbers varied from 5300 to 6600. It is well known (Mohamed and Larue, 1990) that the flow field downstream a grid can be divided basically into three regions. The first is the developing region nearest to the grid where the rod wakes are merging and there is an important production of turbulent kinetic energy. This region is followed by a region where turbulence is nearly homogeneous, isotropic and there are appreciable energy transfers from one wave number to the other. In this region turbulence intensity dependence on downstream distance from the grid may be described by the simple functions including power-laws (Mohamed and Larue, 1990). There finally is a third decay region where viscous effects do directly act on the large energy containing eddies.

In the present case, however, the system differs markedly from the case of an infinitely wide ideal grid. Apart from the fact that the perforated disk employed to generate the desired decaying turbulence is not perfectly equivalent to a proper grid, the system employed involves a quite narrow tube, whose wall is able on its own to promote turbulence in the flowing liquid, as denounced by the relatively high tube Reynolds numbers covered in the present experimentation (Ret = 13000-16000). This means that for, the turbulence intensity u'/U in the proximity of the symmetry axis should be expected to fall in the range of 3-5% (Brodkey and Hershey, 1988).
Clearly, in order to properly assess mean velocity and turbulence distributions in the investigated channel suitable LDA or PIV measurements are to be carried out. This is programmed to be done in the near future. In the mean time and for the present preliminary assessment of the technique viability, it is sufficient to observe that turbulence intensity does surely undergo a decreasing trend downstream the grid, as confirmed by experimental evidence for the similar case of a relatively narrow square channel (Sommerfeld *et al.* 2000).
It is finally worth noting that the time averaged liquid velocity in the proximity of the channel axis does probably undergo a slight increase while moving downstream, as the average velocity radial profile is probably nearly flat in the grid proximities, while sufficiently faraway from the grid it tends towards the typical radial turbulent profile, with central velocity about 1.25 times larger than the liquid mean velocity. It should therefore be expected that the central axis average velocity undergoes a slight increase while moving downstream the grid. Here, for simplicity, the time averaged velocity near the tube axis has been confused everywhere with the liquid superficial velocity (defined as liquid flow rate divided by channel section).

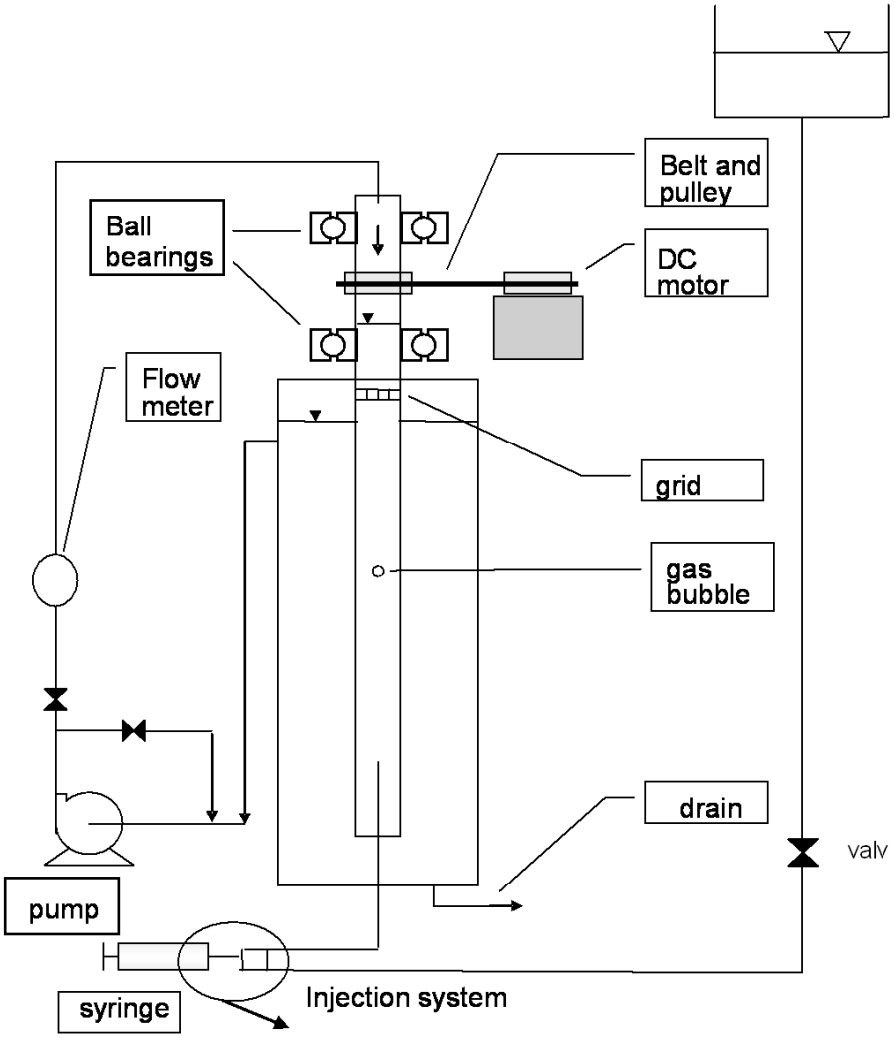

Fig. 4.4 Experimental apparatus

4.3 RESULTS AND DISCUSSION

4.3.1 Technique viability

The first important result is that with the set up devised, bubbles did actually found quasi-steady equilibrium positions at well defined elevations. As previously discussed, apart from making the present technique viable, this observation implies that *a direct dependence of drag (or an inverse dependence of bubble terminal rise velocity) on turbulence intensity does actually hold true.*

In practice for a suitably given liquid flow rate, each bubble occupied a randomly oscillating, yet quasi-steady, position at a given distance from the grid and on the channel axis.

If, starting from these conditions, the liquid flow rate was slightly varied the equilibrium distance from the grid changed accordingly (*i.e.* decreased when decreasing liquid flow rate) as well as smoothly and reproducibly. Typical results obtained with a given bubble are shown in Fig.4.5.

It may be worth noting that the previously mentioned expected increase of the central mean velocity does have a destabilizing effect on the possibility for bubbles to occupy steady elevations. The experimental evidence therefore implies that the increase of drag due to turbulence was in practice large enough to overcome the central velocity increase effect.

When groups of bubbles were injected in the channel, the apparatus behaved as a size classifier and axial bubble distributions (with the biggest bubbles towards the channel top and the smallest towards the bottom of the channel) were often observed.

It may be worth noting that the possibility of obtaining many data with the same bubble, apart from speeding up the experimentation, allows to single out free turbulence effects only. In fact the uncertainties (on the exact bubble size) that would be incurred, if one had to employ a new bubble each time the turbulence intensity was varied, are avoided.

4.3.2 Dependence of bubble terminal rise velocity on free stream turbulence

As previously mentioned, translating the information in Fig.4.5 into the relevant bubble terminal velocity and relating the variations of the latter to the local turbulence quantities would require detailed information on the liquid

flow field that is not available at the moment. If, however, a flat velocity profile is assumed everywhere, first estimates of the bubble terminal velocities can be obtained by dividing the equilibrium flow rates by the channel section. This leads for the same bubble to a sequence of decreasing terminal velocities when the distance of the equilibrium position from the grid decreases, hence at increasing free-stream turbulence levels. The results obtained in this way with a number of bubbles of different sizes are reported as a log-log plot Fig.4.6. As it can be seen, all the bubbles observed behaved in a similar way, with apparent terminal velocities varying bymore than 15 % depending on the steady elevation inside the channel. Notably, if the central velocity variation could have been taken into account, larger actual terminal velocity variations (accounting perhaps for a further 20% variation) would have been found.

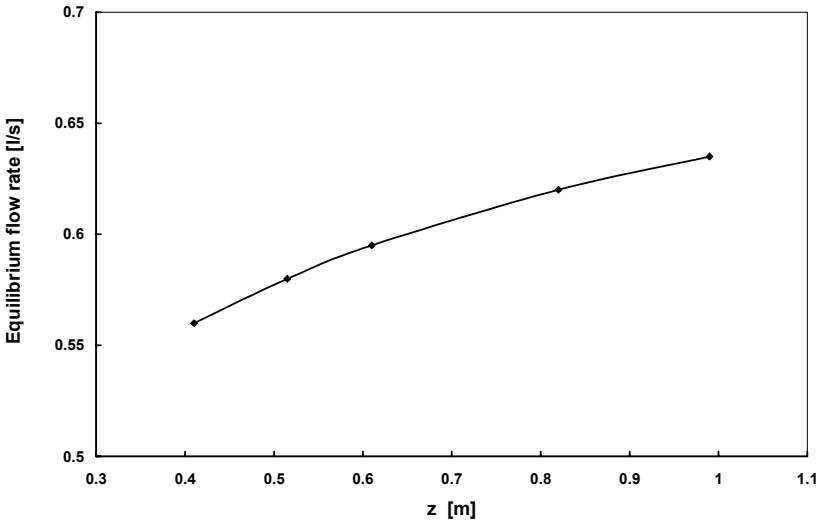

Figure 4.5. Flow rates needed to get quasi-steady (equilibrium) elevations for a given bubble versus distance downstream the grid (z)

It may be observed in Fig.4.6 that in the log-log plot results roughly line up on straight lines with a slope of about 0.1. The relationship with turbulence intensity remains however unknown due to the present lack of data on turbulence intensity dependence on distance from the grid.

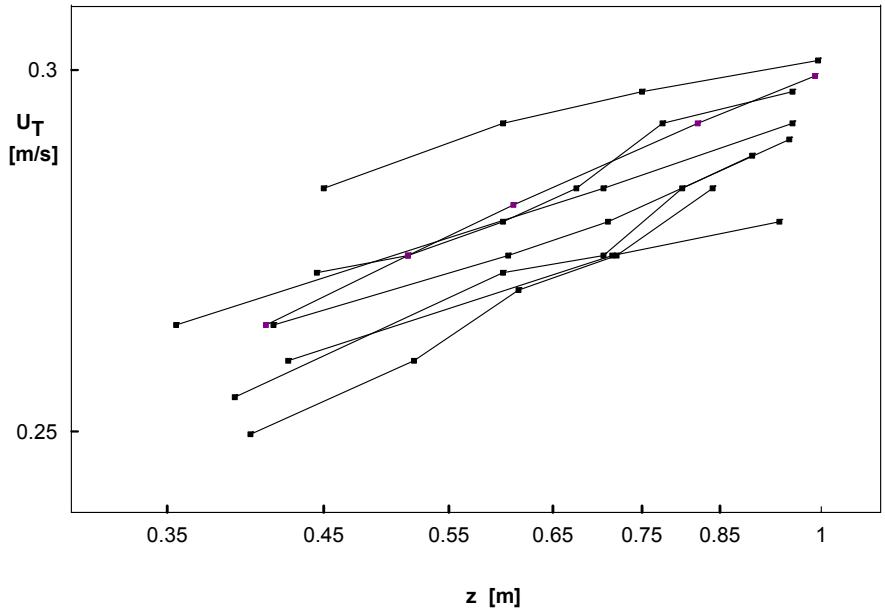

Figure 4.6. Terminal velocities for various bubbles versus distance downstream the grid (z)

For a few bubbles a slightly different experimental procedure was adopted. In particular for each bubble subsequent flow rate variations were adjusted in such a way that each bubble occupied the same equilibrium elevations (0.5, 0.6, 0.7, 0.8, 0.9 and 1.0 m from the grid). The flow rates needed to achieve the desired result were then recorded. Also, pictures of each bubble were recorded by means of a video camera. These allowed a rough estimation of bubble volume and therefore of its equivalent diameter. The four bubbles analysed in this way (Fig.4.7) had estimated equivalent diameters of 6.0, 7.0, 8.3 and 11.6 mm respectively. The results obtained with these bubbles are reported in Fig.6 as bubble terminal velocity versus bubble size. Lines parameter is the distance from the grid, *i.e.* turbulence intensity. As it can be seen, at most distances from the grid, the bubbles exhibited a decreasing trend at the smaller bubble sizes followed by an increasing trend at larger sizes. This is consistent with bubble behaviour in still water, where the same (apparently surprising) behaviour is observed in the same size range, as a consequence of bubble shape changes.

Moving from the 1.0 m line to the subsequent lines, turbulence keeps increasing and terminal rise velocity clearly decreases accordingly. The effect of

turbulence on terminal rise velocity is therefore very clearly observed in this figure, as well as its spread over bubble sizes.
The same results of Fig.4.8 may be put in terms of bubble drag coefficient, which are simply related to bubble terminal rise velocity by the force balance on the bubble:

$$C_D = \frac{4gd_e(\rho_l - \rho_b)}{3\rho} \frac{1}{U_T^2} \tag{4.6}$$

The C_D values so obtained are reported in Fig.4.9 versus bubble Reynolds number. Curve parameter is again the bubble equilibrium position in the rotating tube. Obviously larger C_D values are observed the smaller the equilibrium distance from the grid.
It may be interesting to observe that the increasing trend of drag coefficient with bubble size is in agreement with results for the rise of bubbles into pure water (Fig. 4.1). The C_D values obtained here are however smaller than those observed in still pure water. The reason for this apparent discrepancy is discussed in the following paragraph.

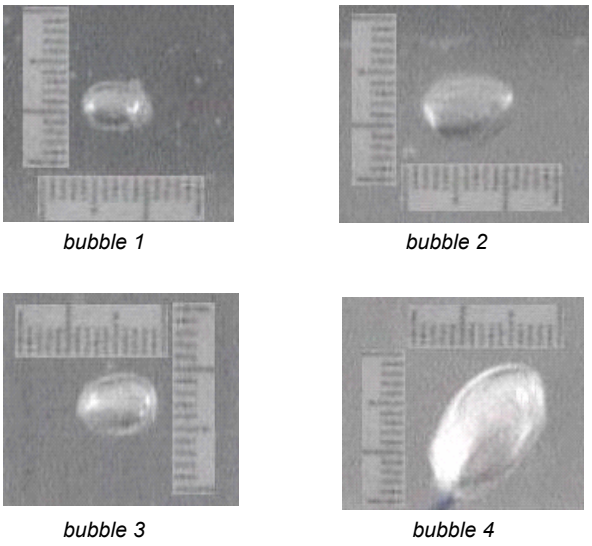

Figure 4.7. Example of bubble shapes inside the channel

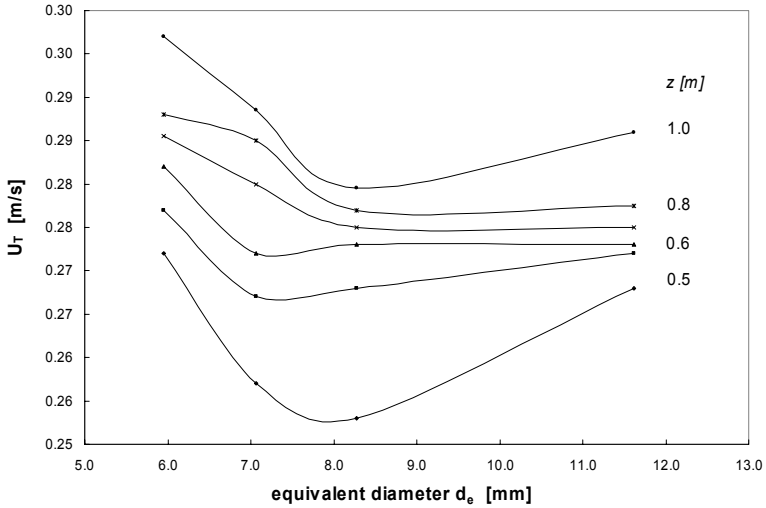

Figure 4.8: Bubble terminal velocity versus bubble size, at various turbulence levels. Curve parameter is the distance from the grid at which bubbles were stabilized

4.3.3 Channel rotation effects on bubble shape and terminal rise velocity

As a consequence of channel rotation, bubbles experienced a centrifugal field that, apart from effectively stabilizing their radial position, could well have modified their shape. In particular some bubble elongation in the direction of the channel axis, which would have reduced the bubble cross sectional area and therefore the liquid-bubble drag, should have been expected.

As a matter of fact, apart from the above observation on the C_D values, the terminal velocity values experimentally obtained under tube rotation conditions (see Figs 4.7 and 4.8) are all larger than the relevant values obtained with bubbles of the same size in still pure water (Fig. 4.1).

To further confirm this effect, a series of runs was carried out with different channel rotational speeds. In Fig.4.10 the terminal velocities (flow rates) needed to maintain a bubble in a given position (0.9 m from the grid) when varying the channel rotational speed are reported. The two curves plotted refer to two different bubbles. As it can be seen, larger equilibrium terminal velocities are observed when increasing the rotational speed, therefore confirming that

centrifugal effects do have a pronounced effect on bubble shape and in turn terminal rise velocity.

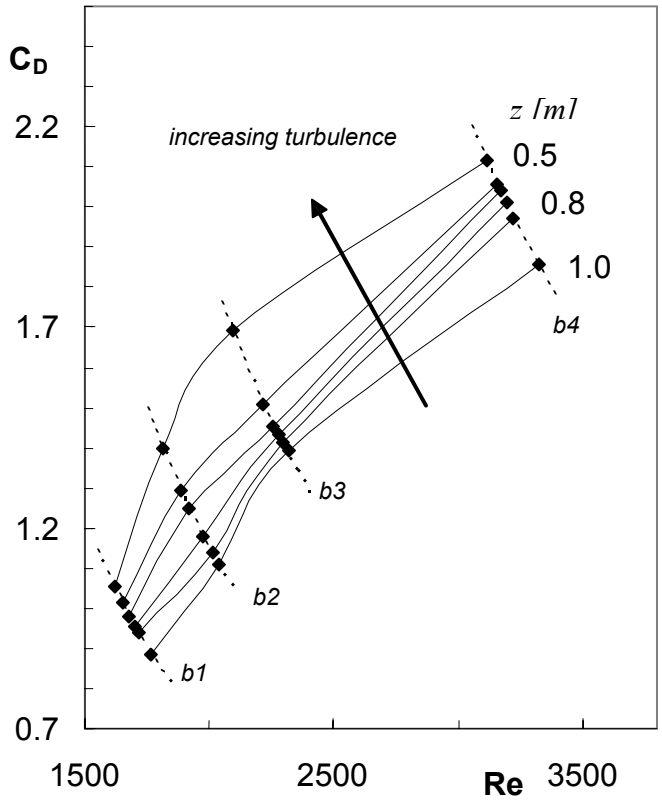

Figure 4.9.Experimental drag coefficients vs. bubble Reynolds number. Curve parameter is the equilibrium distance from the turbulence generating grid [m]. Dotted lines connect data obtained with bubble 1, 2, 3 and 4 respectively

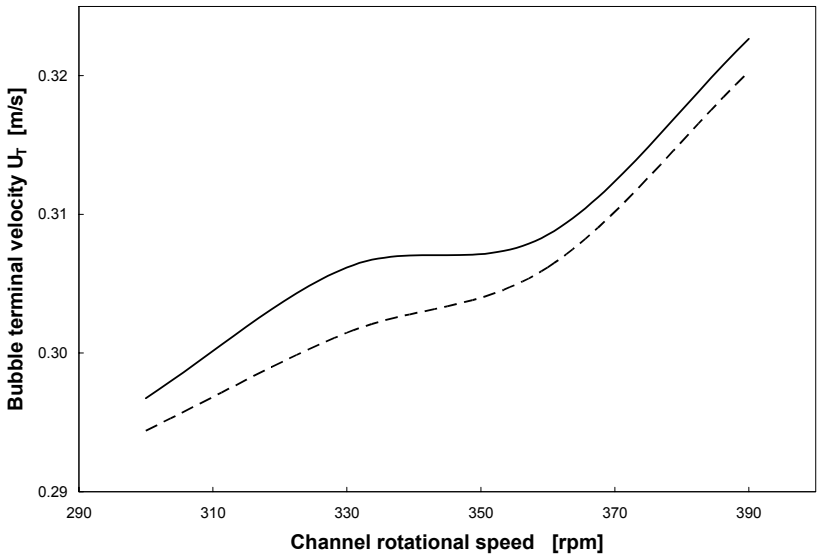

Figure 4.10. Influence of tube rotation on bubble terminal velocity 0.9 m

In Fig.4.11, the results obtained with single bubbles that were allowed to freely adjust their equilibrium positions when varying the channel rotational speed, are reported. In this case the flow rate (terminal velocity) was kept constant for each bubble. For all the bubbles tested, the equilibrium distance from the grid decreased while increasing the channelrotational speed, as a consequence of the fact that a larger drag factor was needed to match again equilibrium conditions under the same flow rate (terminal velocity) as a consequence of bubble shape change.
Clearly further work is to be done for assessing the minimum rotational speed required to make the whole technique viable with minimum deformation of the bubbles.

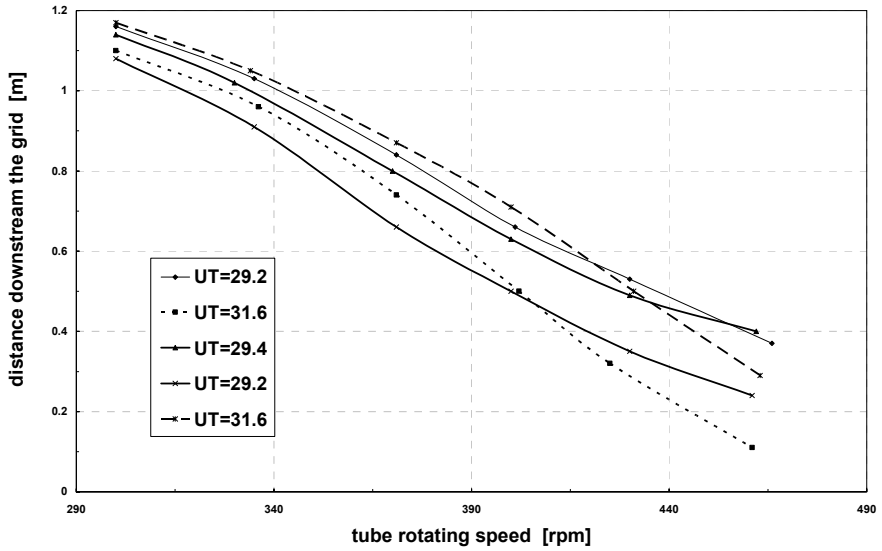

Figure 4.11. Influence of tube rotation on the equilibrium elevation in the channel for fixed flow rates

4.3.4 Flow field inside the tube

In order to relate the observed rise speed velocities to tuirbulence features, preliminary particle image velocimetry (PIV) measurements of flow field inside the tube were carried out. In particular measurements were conducted on vertical planes containing the channel axis, at different distances downstream the grid. Only few data could be taken, due to a number of practical limitations (difficulty to place the camera in the required positions, channel wobbling during rotation due to the deformations occurred during utilization, channel wall transparency heavily reduced by scale and abrasions, etc.) that would have required an almost complete renewal of the apparatus to allow a proper PIV experimentation. The few data that it was possible to collect do not allow firm conclusions to be drawn.

It is worth stressing that for the rise velocity experimental technique here employed, it was important that the flow field was characterized by time averaged axial velocities identical at any distance downstream the grid would and turbulence intensity u'/U decreasing with distance from the grid.

PIV measurements were carried out at 40, 50 and 60 cm downstream the grid. Unfortunately, the time averaged velocity profiles obtained resulted different from each other, as it can be seen in Fig. 4.12, despite the fairly large experimental uncertainties associated with the above mentioned measurement difficulties.

In particular the velocity profile obtained at 60 cm downstream the grid is very different from the velocity profiles at 40 and 50 cm. This might be due to the combination of tube rotation and outlet effects, which may well modify the velocity field from the outlet (120 cm downstream the grid) up to 60 – 70 cm from the outlet, i.e. about 50-60 cm down stream the grid.

This result is in striking contrast with the technique fundamentals reported above, because in this case not only turbulence intensity but also the local time averaged axial velocity would decrease when increasing the distance from the grid. This in turn makes questionable all the experimental results presented in this chapter.

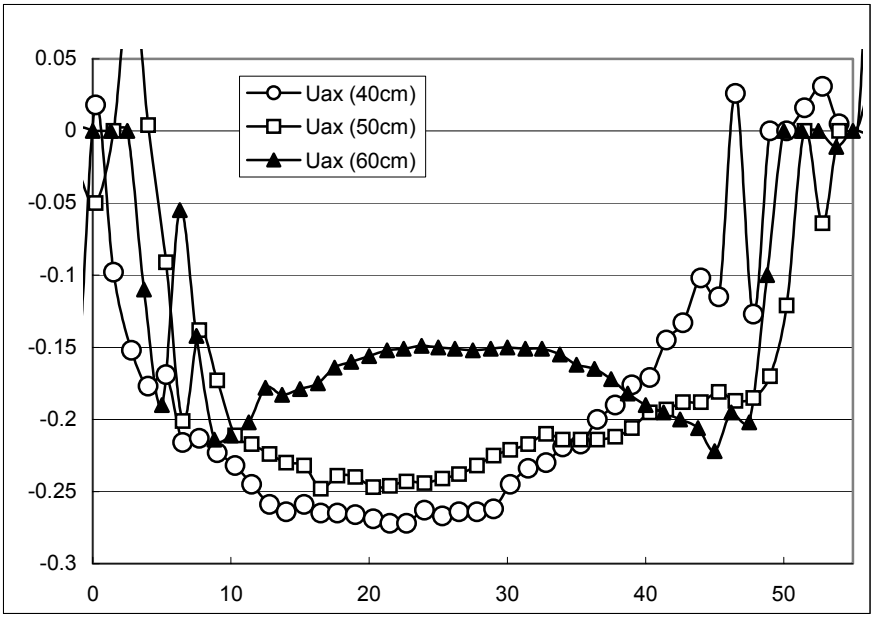

Fig 4.12: Velocity profiles inside the rotating tube. triangles= distance from the grid eq. to 60 cm; squares = distance from the grid eq. to 50 cm; circles = distance from the grid eq. to 40 cm .

There clearly is a need for a thorough PIV analysis of the whole tube flow field at various rotational speeds, in order to properly assess the average velocity and turbulence intensity at the measuring positions at which data were collected. In case it were confirmed that the axial average velocity varies with distance from the outlet, the introduction of a perforated plug at the outlet of the tube aimed at reduce outlet effects might be pursued.

Unfortunately this part of the work could not be completed during the present thesis, but it will be part of future work by the same lab.

4.4 Conclusions on free stream turbulence effects on bubble terminal velocity

The present section was aimed at developing a novel experimental technique that, by easing up the measurements, should allow starting collecting a large number of data on free stream turbulence effect on bubble terminal velocity.

Unfortunately, even though based on a possibly good idea, a lot of practical problems occurred in carrying out the experimental runs, so that no reliable experimental data was, until now, collected.

The most significant problem was the difficulty encountered in maintaining bubbles in an axial position inside the channel. To avoid these uncertainties, a centrifugal field was over imposed on the system, with the aim of keeping bubbles near the symmetry axis as a consequence of the density difference between the two phases.

Unfortunately, channel rotation is suspected to have induced quite heavy outlet effects which probably modified the flow field inside the tube for several equivalent diameters. As a consequence the experimental data obtained in these conditions cannot be considered as reliable.

A possible solution of the problem, if confirmed by more precise PIV measurements, could be the introduction of a perforated plug at the outlet of the tube which should reduce outlet effects. In any case PIV analysis of axial velocity profiles and turbulence intensity distribution downstream the grid will be necessary.

CHAPTER 5

CFD SIMULATIONS OF GAS-LIQUID SYSTEMS

5.1 INTRODUCTION

Due to their practical importance, the capability of reliably simulating gas-liquid reactor characteristics, as for instance gas-hold up, liquid recirculation rate, interfacial area or the possible formation of anoxic zones in biotech fermentations, is of great practical interest. Such modelling needs may well be addressed by suitable developments of Computational Fluid Dynamics (CFD) techniques, though as, a difference from single phase systems, for multiphase systems the development of CFD models is still at its early stages..

The present part of the thesis is aimed at contributing to the field by analyzing the sensitivity of simulation results to main system features such as bubble size, forces exchanged between the two phases, etc. In particular, it is shown that for this kind of physical systems the drag force is predominant with respect to the non drag forces. It is also shown that the inter-phase drag-force exchanged between phases can be conveniently expressed in terms of bubble terminal rise velocity rather than drag coefficient and projected area.

Two different systems were simulated: an internal loop air lift reactor for which experimental information could be retrieved in the literature (Couvert *et al.* 1999), and a stirred vessel employed by Bombac *et al.* (1997), for which the experimental data were also available.

5.1.1 CFD Simulations of gas-liquid systems: Literature Survey

CFD simulations are nowadays possibly the most promising modelling tools for complex process equipment. As a matter of fact, after having been found to be quite reliable for single phase systems, they have also shown good potentialities with both solid-liquid and, to a lesser extent, gas liquid systems. Clearly gas-liquid system are characterised by an additional complexity level, related to the fact that, as a difference with solid-liquid systems, bubble sizes are not known in advance, being rather the result of complex formation-detachment and breakage-coalescence phenomena.

The CFD approach has proven to be successfully applicable to the simulation of the complex flow field existing in a single-phase stirred tank - either baffled (Ranade & Joshi, 1990; Kresta & Wood, 1991; Brucato *et al.*, 1998; Derksen & Van den Akker, 1999) or unbaffled (Armenante *et al.*, 1994; Ciofalo *et al.*, 1996;

Alcamo *et al.* 2005, Gibbardo *et al.* 2006) even for cases where slight modifications of system geometry result in important flow pattern changes (Micale *et al.*, 1999; Montante *et al.*, 2001a) or when chemical reactions occur (Baldyga *et al.* 1997, Brucato *et al.*, 2000).

The situation is much less developed for two-phase systems, due to the intrinsic greater complexity of multiphase fluid dynamics. While the case of solid-liquid systems has successfully been treated for different geometrical configurations with either dilute (Gosman *et al.*, 1992; Micale *et al.*, 2000; Montante *et al.*, 2001b) or dense particle suspensions (Micale *et al.*, 2004), the modelling of gas-liquid systems is more difficult.

A number of CFD simulations of gas-liquid systems have been carried out for non-stirred apparatuses, such as bubble columns (e.g. Delnoij *et al.*, 1997; Lain *et al.*, 1999; Sanyal *et al.*, 1999; Joshi, 2001) and air-lift reactors (Oey *et al.*, 2001; Van Baten *et al.*, 2003). A variety of approaches were used, namely: the Eulerian-Eulerian (Mudde & Simonin, 1999; Grevskott *et al.*, 1996) and the Eulerian-Lagrangian (Lain *et al.*, 1999) schemes and Direct Numerical Simulation (Bunner & Tryggvason, 1999; Tryggvason *et al.*, 2006).

Several attempts have also been made to simulate gas-liquid flow in stirred vessels (Ranade & Van den Akker, 1994; Bakker & Van den Akker, 1994b; Morud & Hjertager, 1996; Lane *et al.*, 2002; Deen *et al.*, 2002; Lane *et al.*, 2005; Khopkar and Ranade, 2006). Some of these were focused on the expression of the inter-phase force term representing the interaction between the two phases (Lane *et al.*, 2005; Khopkar and Ranade, 2006).

Such a characterization is quite difficult due to the complexity of the involved phenomena and currently no comprehensive model of the physics in these systems is available. In particular the appropriate choice of the inter-phase drag term is crucial since it is this term that mostly affects gas hold-up distribution within the vessel. Efforts to model the drag coefficient in gas liquid stirred vessels have been put forward in the past. Bakker and Van der Akker (1994), who defined a turbulence-corrected Reynolds number to be applied to the Morsi and Alexander correlations (Morsi and Alexander, 1972) which approximate the standard drag curve, and Kerdouss *et al.* (2006) who applied the above correction to the well known Schiller and Nauman approximation of the standard drag curve for rigid spheres.

It should be noted however that reference to the standard drag curve for spheres and relevant analytical correlations should be avoided when modelling gas-liquid flows. In fact the standard drag curve concerns spherical particles with a rigid slip-less interface, while bubbles in the millimetres size range are well known to be characterized by a mobile interface and deformed ellipsoidal shapes, that result into much larger values of the drag force than those pertaining to rigid spheres of equivalent volume (Mendelson, 1967, Clift *et al*, 1978, Tomiyama *et al.* 1998; Tomiyama *et al.* 2002; Celata *et al.* 2006). In

those cases in which the presence of impurities inhibits surface mobility, the drag force is further increased (Clift *et al*, 1978; Tomiyama *et al.* 1998).

Recently Lane *et al.* (2001, 2005) tried to model the effect of turbulence on drag coefficients by correcting somehow the drag coefficient calculated for bubbles rising under stagnant fluid condition in contaminated water, namely the Ishii and Zuber correlation (Ishii and Zuber, 1979). Hence in this case a more realistic starting point was adopted. However the proposed turbulence correction was based on "a modification" of experimental data concerning solid-liquid systems, hence rigid interfaces, rather than bubbles. A similar approach was finally adopted also by Khopkar and Ranade (2006). Clearly a specific correlation for bubbles drag accounting also for the possible turbulence modifications would be greatly needed. The only experimental data published on journals of which the authors are aware is that by Poorte and Biesheuvel (2002) which shows that, for bubbles with a diameter between 0.3 and 0.6 mm, turbulence may significantly reduce bubble terminal rise velocity, *i.e.* significantly increase bubble drag. The data available so far are however too scant to allow firm conclusions to be drawn and reliable correlations to be assessed.

As a further complication, for gas liquid systems, population balance tools need to be considered to properly account for bubble size distribution (BSD) effects and improve the accuracy of simulated results, especially when information on interfacial area is needed.

A rigorous integration of bubble population balance equation (PBE) within the reactor is not presently viable, due to its complexity. Nevertheless, a certain number of models are available to predict the coalescence and break-up rates for bubble columns without agitation (Prince and Blanche 1990; Luo and Svendsen, 1996). These models in conjunction with population balance tools have been implemented by some authors for non-stirred systems such as bubble columns and air-lift reactors (Olmos *et al.*, 2001; Chen *et al.*, 2004; Sanyal *et al.*, 1999) and for stirred systems (Lane *et al.*, 2005; Kerdouss *et al.* 2006) but the computational demand is one order of magnitude bigger than for single-diameter simulations. In order to limit the computational effort required for the case of stirred tanks, a simplified approach was adopted by Venneker *et al.* (2002) who over-imposed the population balance equation (PBE) for the gaseous phase on the liquid flow field previously obtained by single-phase CFD simulations.

5.2 MODEL EQUATIONS AND SOLUTION PROCEDURE

5.2.1 Transport equations

A Eulerian-Eulerian framework and the Multi-Fluid approach (Gosman *et al.*, 1992; Morud and Hjertager, 1996) were adopted for simulating gas-liquid flow in the stirred vessel. With this approach continuity and momentum balance equations are separately solved for the two phases. Transported quantities interact via suitable inter phase transfer terms.

In principle the relevant equations could be solved directly. However, since the flow is turbulent in most cases, they are usually solved in averaged form, and require suitable turbulence models for the mathematical closure of the problem. If Reynolds averaging is used, accepting Boussinesq's hypothesis for both phases, the following set of equations is written for each of the two phases:

$$\frac{\partial(r_\alpha \rho_\alpha)}{\partial t} + \nabla \cdot (r_\alpha \rho_\alpha \mathbf{U}_\alpha - \rho_\alpha \frac{\nu_T}{\sigma_T} \nabla r_\alpha) = 0 \tag{5.1}$$

$$\frac{\partial(r_\alpha \rho_\alpha \mathbf{U}_\alpha)}{\partial t} + \nabla \cdot (r_\alpha (\rho_\alpha \mathbf{U}_\alpha \mathbf{U}_\alpha - \mu_{\alpha eff} (\nabla \mathbf{U}_\alpha + (\nabla \mathbf{U}_\alpha)^T))) = r_\alpha (\mathbf{B} - \nabla p_\alpha) + \mathbf{F}_{\beta\alpha} \tag{5.2}$$

where **B** is the resultant of body forces per unit volume and the effective viscosities are computed as:

$$\mu_{\alpha eff} = \mu_\alpha + \mu_{T\alpha} \tag{5.3}$$

Under proper Reynolds averaging, turbulent gas dispersion is modelled by the eddy diffusivity hypothesis, expressed by the last term under parenthesis in eqn 1, where σ_T is the turbulent Schmidt number, whose value has to be suitably specified. It can be noted that turbulent dispersion of volume fraction and

turbulent transport of momentum are supposed to be proportional to the respective gradient according to Boussinesq's hypothesis.

It may be worth noting that when Favre's averaging is adopted instead, the continuity equation remains formally identical to the instantaneous equation (though with averaged values substituted for the instantaneous ones), but a turbulent dispersion force appears in the momentum equation (Viollet and Simonin 1994; Lane 2002). In the present paper the Reynolds averaging approach (RANS) was used troughout.

For the estimation of turbulent viscosities, the standard k-ε model (Launder and Spalding, 1974) has already been proven to be successfully applicable to the simulation of single-phase flow fields in a large number of practical cases. For gas-liquid systems the turbulence models implemented are usually based on a generalisation of the k-ε model, named *multiphase k-ε*. (CFX 4.4 documentation, 1999). As a further simplification, the *homogeneous approximation*, where the two phases are supposed to share the same values of k and ε, has often been used both for bubble columns (Sokolichin and Eigenberger (1999), Joshi (2001)) and gas-liquid stirred vessels (Ranade *et al.* (2001), Lane *et al.* (2005), Khopkar *et al.* (2006)). This is also the approach adopted here. The transport equations for k and ε are:

$$\frac{\partial}{\partial t}(\rho k) + \nabla \cdot (r_\alpha (\rho \mathbf{U} k - (\mu + \frac{\mu_T}{\sigma_k})\nabla k)) = S_k \tag{5.4}$$

$$\frac{\partial}{\partial t}(\rho \varepsilon) + \nabla \cdot (\rho \mathbf{U} \varepsilon - (\mu + \frac{\mu_T}{\sigma_\varepsilon})\nabla \varepsilon)) = S_\varepsilon \tag{5.5}$$

where:

$$\rho = r_\alpha \rho_\alpha + r_\beta \rho_\beta \;\; ; \;\; \mathbf{U} = \frac{1}{\rho}\left(r_\alpha \rho_\alpha \mathbf{U}_\alpha + r_\beta \rho_\beta \mathbf{U}_\beta\right) \;\; ; \;\; \mu_T = r_\alpha \mu_{T\alpha} + r_\beta \mu_{T\beta} \tag{5.6}$$

$$S_k = r_\alpha S_{k\alpha} + r_\beta S_{k\beta} \;\; ; \;\; S_\varepsilon = r_\alpha S_{\varepsilon\alpha} + r_\beta S_{\varepsilon\beta} \tag{5.7}$$

and turbulent viscosities are computed as:

$$\mu_{T\alpha} = C_\mu \rho_\alpha \frac{k^2}{\varepsilon} \tag{5.8}$$

The source terms are the same as their single-phase analogues:

$$S_{k\alpha} = P_\alpha + G_\alpha - \rho_\alpha \varepsilon \tag{5.9}$$

$$S_{\varepsilon\alpha} = \frac{\varepsilon}{k}(C_{1\varepsilon}(P_\alpha + C_{3\varepsilon}\max(G_\alpha, 0)) - C_{2\varepsilon}\rho_\alpha \varepsilon \tag{5.10}$$

where P_α is the shear related production of turbulent kinetic energy while G_α is that due to body forces. These are defined by eqns 11 and 12 respectively:

$$P_\alpha = \mu_{\alpha eff} \nabla \mathbf{U} \cdot (\nabla \mathbf{U} + (\nabla \mathbf{U})^T) \tag{5.11}$$

and

$$G_\alpha = -\frac{\mu_{T\alpha}}{\rho \sigma_\alpha} \mathbf{g} \nabla \rho \tag{5.12}$$

The extra turbulence induced by bubbles in the liquid phase was neglected in view of the partial compensation between the extra dissipation arising from small scale structures and the extra generation due to large bubbles (Ranade, 1997).

5.2.2 Inter phase force term

The interface force term $F_{\beta\alpha}$ represents the interaction forces between the continuous and the dispersed phase. A single particle moving through a fluid experiences forces which affect its motion. If the slip velocity is constant, the force is named "drag". If the motion is non uniform one needs to include various *non drag* terms such as the "virtual mass" and "lift" forces, the" Basset history term" etc, in the interfacial force term :

$$\mathbf{F}_{\beta\alpha} = \mathbf{F}_D \; (+ \; \mathbf{F}_{vm} + \mathbf{F}_{lift} + \mathbf{F}_{Basset} + \mathbf{F}_{wall\ lubrication} ...) \tag{5.13}$$

An appropriate formulation of these inter-phase coupling terms should be provided for comprehensive simulations of gas-liquid systems (Joshi 2001; Lane *et al.* 2005). However it is often found that, when compared to the drag force, the other inter-phase forces are negligible (Sanyal *et al.* 1999; Lane *et al.* 2002).

In the present work, only the drag force was considered first. The main non drag forces, i.e. the lift force and the virtual mass force, were then separately added to evaluate their influence on system hydrodynamics. Wall lubrication and Basset's forces were not considered in the present work as they are usually found to be smaller than lift and virtual mass(Joshi 2001), and therefore negligible in stirred vessels.

Drag Force

If all the dispersed phase particles are assumed to share the same size, the drag force exerted by the continuous phase on all particle present in the unit volume of the two-phase mixture can be written as:

$$\mathbf{F}_D = \frac{r_\beta}{V_p}\left[\frac{1}{2}C_D\rho_\alpha A_p\left|\mathbf{U}_\beta - \mathbf{U}_\alpha\right|(\mathbf{U}_\beta - \mathbf{U}_\alpha)\right] \tag{5.14}$$

where r_β is the dispersed phase volume fraction, V_p is the volume of a single particle, r_β/V_p is the number of particles per unit volume, while the term in squared brackets is the force exerted by the fluid on each particle. This last is expressed in the usual way, where C_D is the drag coefficient and A_p is the particle projected area on a plane normal to the flow direction.

It would appear that in order to use eqn.5.14 one needs to estimate three particle-related parameters, namely C_D, A_p and V_p. This is straightforward in the case of spherical particles. For differently shaped particles, as is the case of most bubbles, one might resort to corrections based on suitable "sphericity" definitions (Clift *et al.* (1978)). Notably, information on C_D is often derived from experimental data on particle terminal velocity, which is an experimentally easily assessable quantity. This is related to C_D by the force balance around a bubble rising in stagnant fluids:

$$C_D = \frac{V_p(\rho_\beta - \rho_\alpha)g}{\frac{1}{2}A_p\rho_\alpha U_T^2} \tag{5.15}$$

by substituting eqn.5.15 into 5.14 one obtains:

$$\mathbf{F}_D = \frac{r_\beta(\rho_\beta - \rho_\alpha)g}{U_T^2}\left|\mathbf{U}_\beta - \mathbf{U}_\alpha\right|(\mathbf{U}_\beta - \mathbf{U}_\alpha) \tag{5.16}$$

Equation 5.16 shows that when terminal velocity is employed to characterize particle drag, any reference to particle diameter, projected area or volume disappears from model equations, to be substituted by particle terminal velocity as the sole parameter really characterizing particle-fluid drag force exchange. To the authors' knowledge, this observation was explicitly made for the first time by Montante (2000) with reference to the solid-liquid dispersions there investigated. The same observation is of great interest for gas liquid-systems as well, as only tiny bubbles (D_b<0.5 mm) are practically spherical while the larger bubbles typically prevailing in gas-liquid contactors are ellipsoidal (Clift *et al.* 1978).

Data for terminal velocity of bubbles in water are available as a function of bubble equivalent diameter (Fig. 4.1), though a fairly large data dispersion is observed in relation to subtle surface properties, and therefore to the level of water contamination. As already mentioned in paragraph 4.1.1 a lot of correlations are also available in the literature to estimate bubble terminal velocity (or the relevant drag coefficient). In the case of pure water and air bubbles in the range from 1.3 mm to 15 mm, bubble terminal rise velocities may be correlated by Eqn. 4.3 (Mendelson 1967), that reproduces very well the data for pure water and air, as shown in Fig. 4.1a.

In this work, having chosen a prescribed bubble diameter in the range from 1.3 mm to 15 mm Equation 5.17 was conveniently adopted.

Lift Force

The lift force considers the interaction of the bubble with the shear field of the liquid. It acts perpendicular to the main flow direction and is proportional to the gradient of the liquid velocity field. It can be expressed as

$$\mathbf{F}_{\text{lift}} = C_L r_\beta \rho_\alpha (\mathbf{U}_\beta - \mathbf{U}_\alpha) \times \nabla \times \mathbf{U}_\alpha \tag{5.18}$$

Where C_L is a suitable proportionality coefficient. According to Lucas *et al.* (2005) C_L may be computed as

$$C_L = \min(0.288 \cdot \tanh(0.121 \cdot \text{Re}), f(\text{Eo}_d)) \qquad \text{if} \quad Eo_d<4$$

$$C_L = 0.00105 \cdot \text{Eo}_d^3 - 0.0159 \cdot \text{Eo}_d^2 - 0.0204 \cdot \text{Eo}_d + 0.474 \qquad \text{if } 4<Eo_d<10 \tag{5.19}$$

$C_L = 0.27$ if $Eo_d > 10$

where Eo_d is the modified Eotvos number defined as

$$Eo_d = \frac{g \cdot (\rho_l - \rho_g) \cdot d_h^2}{\sigma} \tag{5.20}$$

where in turn d_h is the maximum horizontal dimension (in ellipsoidal regime) calculated by an empirical correlation:

$$d_h = d_b \sqrt[3]{1 + 0.163 Eo^{0.757}} \tag{5.21}$$

For 3 mm air bubbles moving into water, the value 0.288 is obtained for C_L.

Virtual mass Force

The virtual mass force stems when bubbles undergo an acceleration different from that of the liquid phase. It takes into account the force required to accelerate part of the surrounding liquid and can be described by the following equation:

$$\mathbf{F}_{VM} = C_{VM} r_\beta \rho_\alpha \left(\frac{D}{Dt}\mathbf{U}_\beta - \frac{D}{Dt}\mathbf{U}_\alpha\right) \tag{5.22}$$

A C_{VM} of 0.5 was adopted in the present work.

5.3 CFD SIMULATION OF A RECTANGULAR AIR–LIFT LOOP REACTOR

Internal loop air-lift reactors are widely used in biotechnology and chemical industry especially in processes where good mixing of large volumes and relatively low shear stresses are requested (e.g.. nitrification/denitrification of wastewater, other bio-processes).

Due to their practical importance, the capability of reliably simulating air-lift reactor characteristics, as for instance gas-hold up, liquid recirculation rate, interfacial area and passive scalar distributions, such as temperature and reactants concentrations, would be of great practical interest.

The simulation of this type of equipment is tackled first, as it does not involve the additional complexities related to agitator rotation in stirred tanks.

5.3.1 Solution domain and boundary conditions

The simulations carried out regarded a rectangular air-lift loop reactor (3.0 m in height, 0.5x 0.5 m in depth and width, with an internal baffle 2.35 m in height positioned in the middle of one side of the reactor) for which experimental information could be retrieved in the literature [Couvert *et al.*, 1999]. In Fig. 5.1 a schematic diagram of the experimental apparatus is reported. The solution domain was discretised by an almost uniform grid encompassing 98696 cells ($r \times \theta \times z = 26 \times 26 \times 146$).

All the simulations were carried out with the help of the commercial code CFX 4.4. Time stepping was set to 0.01 s, which ensured a Courant number smaller than 1 in all cases analysed. This simulation strategy was adopted after having checked that much smaller time steps did not result into significantly different results. The discretization scheme adopted for the convection term was the hybrid upwind that, to prevent numerical instability, switches from 2nd order central to 1st order upwind formulas when the cell Peclet number is greater than two.

The air sparger was modelled as a double series of six superficial mass source cells located at the same geometric position as the two tubular plastic membranes used in the experimental apparatus, whereas the free surface was modelled as a flat "degassing boundary" [CFX User Manual, 1999].

Satisfactory completion of each simulation run was based on several criteria, including sufficient reduction of mass residuals, an accurate balance between rates of gas entering and leaving the reactor, and a constant gas hold

up. Steady state was considered to have been reached when all the above criteria were met.

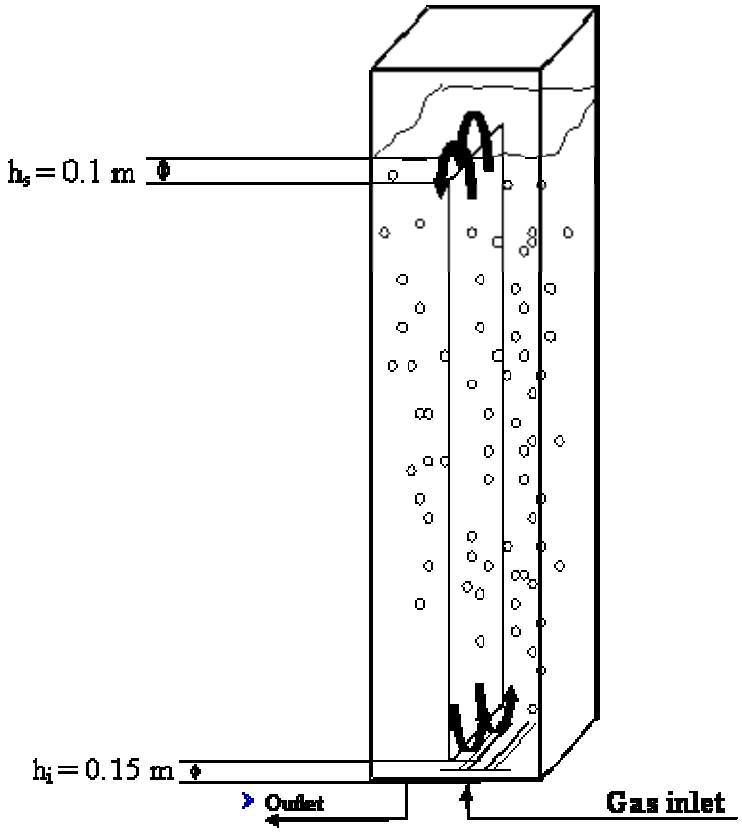

Fig. 5.1: Schematic diagram of the experimental apparatus

5.3.2 Results and discussion

Flow field

Typical simulated vector plots on a vertical plane orthogonal to the baffle are reported in Figs. 5.2 and 5.3, for the liquid and gas phase respectively for the case at maximum gas flow rate (Q_g=7.13 l/s). Although no specific anemometric data are available for the system under consideration, the simulated flow field appears to be in reasonable agreement with expectances. As a matter of fact, the liquid flow-field reported in Fig. 5.3 shows a primary recirculation loop of the continuous phase from the riser to the down-comer and the presence of secondary liquid recirculation loops inside the riser as often experimentally observed [*e.g.* Lucas *et al.*, 2005].

The gas flow-field (Fig. 5.3), shows a strong flux in the riser region and a weak flux in the down-comer due to the entrainment caused by the liquid. An almost uniform outgoing gas flux from the upper surface is also evident. The secondary recirculation loops show the same features of those observed for the liquid phase.

Gas hold-up

Five different gas flow rates (Q_g equal to 0.56, 1.38, 2.75, 5.38 and 7.13 l/s) were simulated. In all cases a prescribed bubble diameter of 3 mm was assumed, somewhat arbitrarily though within the mean Sauter diameter which , according to Couvert *et al.* (1999) ranged from 2.5 to 4 mm depending on the gas flow rate injected.

Figures 5.4 *a, b, c, d, e* show normalised contour plots of the simulated volumetric gas fraction (local hold-up) on a vertical plane orthogonal to the baffle for the five different Q_g values explored. Contour lines are referred to 0.4, 0.8, 1.2, 1.6, 2 times the average gas hold-up (ε_{av}), where ε_{av} is defined as

$$\varepsilon_{av} = \frac{V_g}{V_g + V_l} \tag{5.23}$$

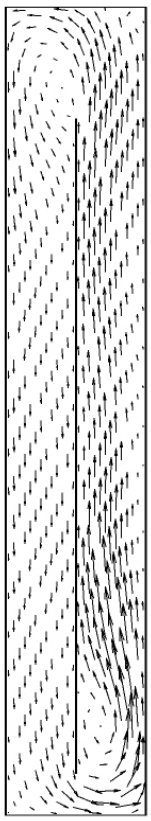

Fig. 5.2: Vector plot for liquid phase: Q_g = 7.13 l/s; U_g=0.057 m/s

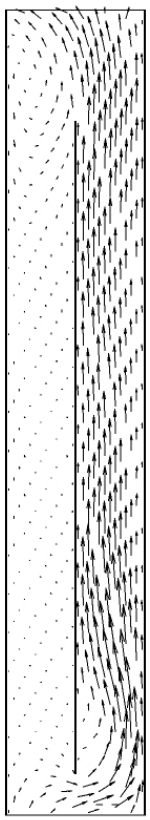

Fig. 5.3: Vector plot for gas phase: Q_g = 7.13 l/s; U_g=0.057 m/s

Although no specific experimental information is available about local gas hold-up distribution, the main patterns of the gas distribution obtained in all the simulations appear to be in agreement with expectances: for instance in the riser a higher gas concentration than in the down-comer and a waving bubbly plume which departs from the sparger to rise the liquid surface is observed. It is worth noting that when increasing the gas flow rate (from case *a* to case *e*), an increasing gas hold-up is obtained in the down comer region resulting in a more even distribution of gas fraction inside the reactor.

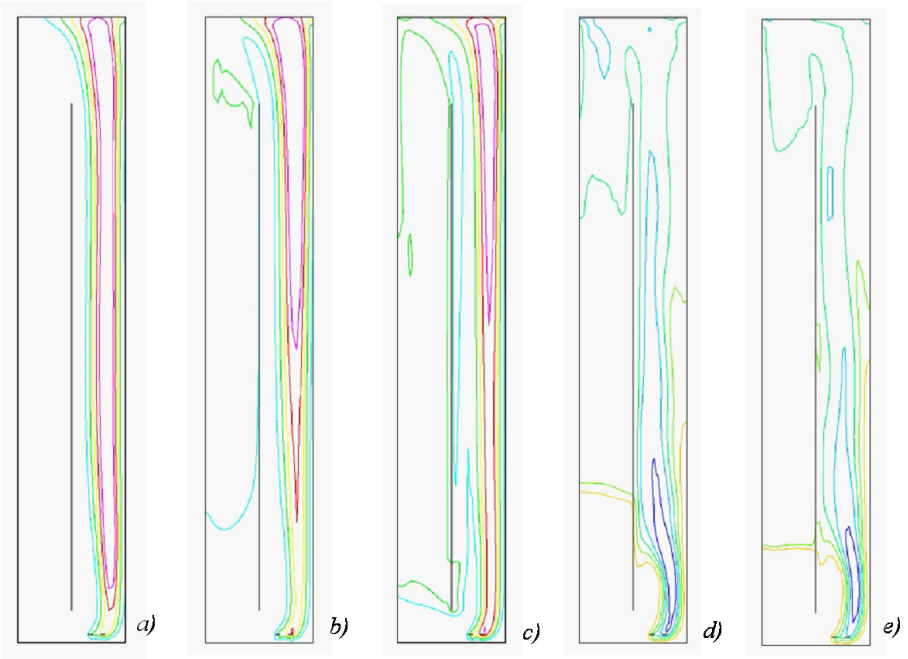

Fig. 5.4: Normalised contour plots of the simulated volumetric gas fraction on a vertical plane orthogonal to the baffle: a) Q_g = 0.56 l/s, b) Q_g = 1.38 l/s, c) Q_g = 2.75 l/s, d) Q_g = 5.38 l/s and e) Q_g =7.13 l/s.

In Fig. 5.5 the simulated steady state average gas hold-up (ε_{av}) is compared with the relevant experimental data by Couvert *et al.* [1999]. It can be observed that, apart from an almost constant slight underestimations, the match is very good, especially in view of the many simplifications and approximations adopted..

Average liquid velocity

Experimental information on liquid recirculation rate was available, as it had been obtained by measuring liquid recirculation time inside the reactor (by a tracer injection technique). In particular, Couvert *et al.* (1999) presented the data in terms of average liquid velocity, obtained by dividing some average tracer route by the experimentally assessed recirculation time. In the present

simulations the circulation time of the continuous phase along the reactor was estimated by dividing reactor volume by the simulated liquid flow rate.

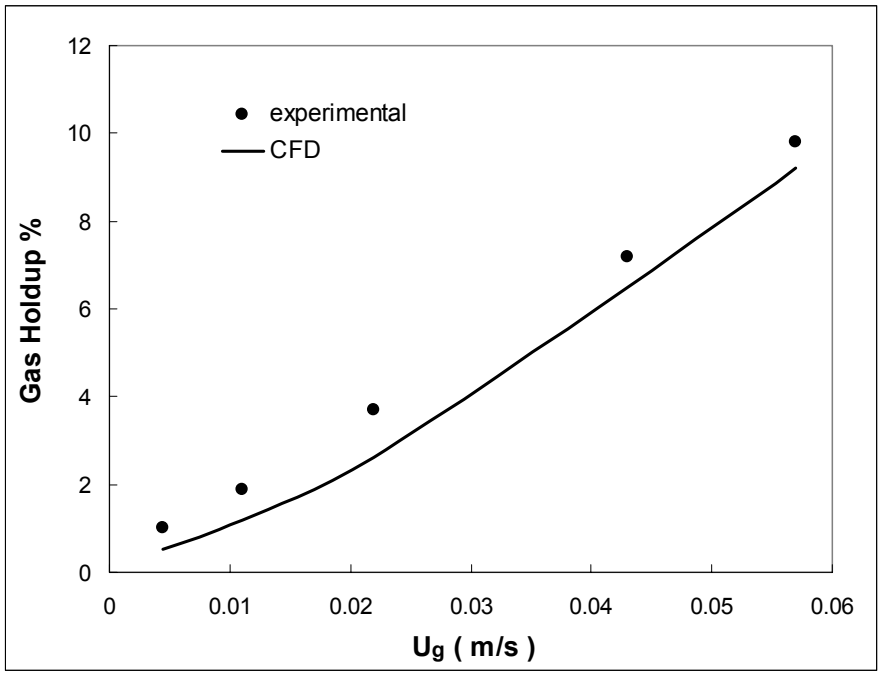

Fig. 5.5: Comparison between experimental global gas hold-up and simulation results at various superficial gas velocities

In Fig. 5.6 simulation results are compared with the experimental data. As it can be seen, simulation results reproduce very well the trend experimentally observed. In particular, both data sets show an initial increase in global liquid velocity, when superficial gas velocity is smaller than 0.02 m/s, and a sort of plateau when superficial gas velocity is larger than 0.02 m/s. Over the entire gas velocity range, simulated values are somewhat underestimated, a discrepancy consistent with the relevant underestimation of the average gas hold-ups (Fig.5.5).

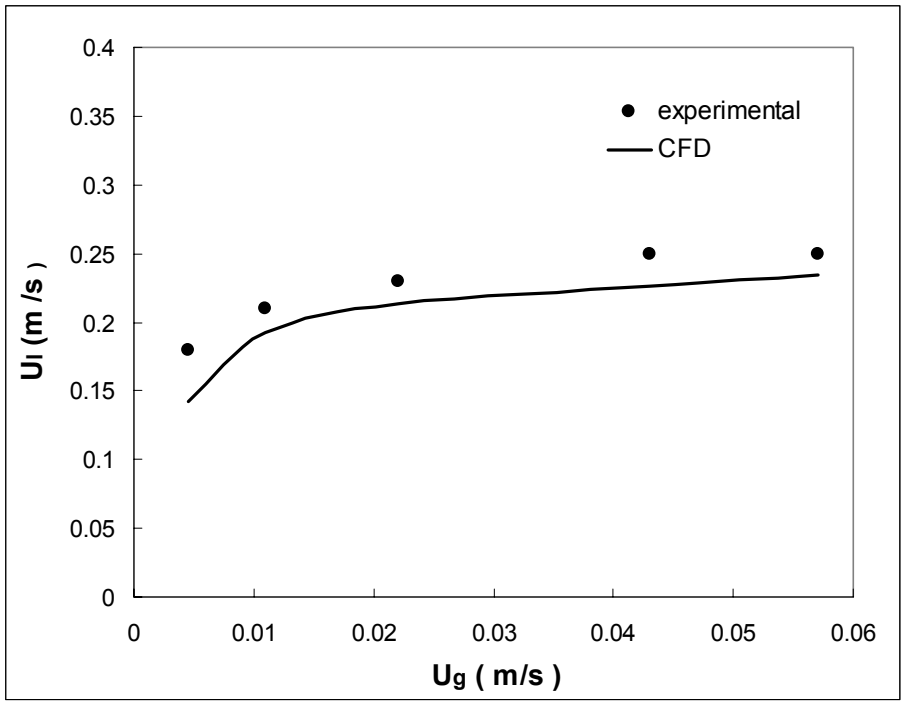

Fig. 5.6: Comparison between experimental liquid recirculation rate and simulation results at various gas flow-rates

Effect of bubble diameter

One may wonder whether a different value for the prescribed bubble diameter in the simulations would have brought to different results. For this reason a simulation with a prescribed bubble size of 4 mm (at the top of experimental values) was carried out for the same conditions of Fig. 5.6d. In Fig. 5.7 normalised contour plots of the simulated volumetric gas fraction (local hold-up) on a vertical plane orthogonal to the baffle for Q_g equal to 5.38 l/s are reported and compared with the relevant contour plot obtained with a prescribed bubble diameter of 3 mm. As it can be seen, gas distribution appears to be only slightly affected by the choice of bubble diameter in the simulation. As regards a quantitative comparison with experimental data, the simulated average gas hold-ups obtained were 6.5 % and 7 % for the simulations based on D_b = 3 and 4 mm, respectively, while the global liquid velocities obtained

were 0.23 and 0.26 m/s respectively. These results are to be compared with the relevant experimental data of 7.2 %. for gas hold-up and 0.25 m/s for liquid velocity. It can be concluded that the effect of adopting a single bubble size of 4 mm is that of slightly improving simulation accuracy.

It is however worth noting that results are only slightly affected by the choice of bubble diameter in the simulations, as it could have been expected on the basis of the relatively small decrease of terminal rise velocity (0.26 – 0.24 m/s for D_b=3.0 and 4.0 mm respectively).

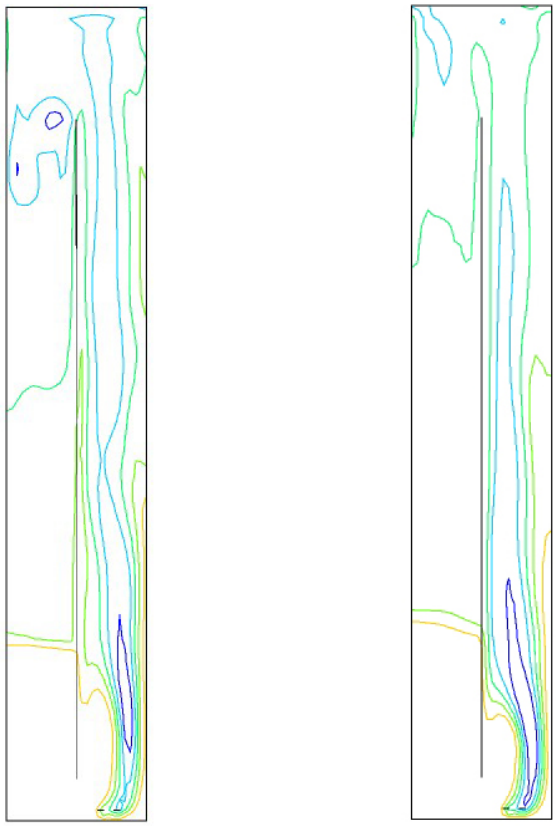

*Fig. 5.7: Comparison between normalised contour plots obtained with prescribed bubble diameter of 4 mm and 3 mm respectively, at Q_g = 5.38 l/s. Contour lines are for 0.4, 0.8, 1.2, and 2 * ε_a*

It may be concluded that the hydrodynamics of a rectangular air-lift loop reactor was satisfactorily simulated by a fairly simple Computational Fluid Dynamics model, based on the "homogeneous" k-ε Multi-Fluid approach.

The use of bubble terminal rise velocity to characterize bubble drag is also confirmed to be sound as well as viable. This, in conjunction with the fact that bubble rise velocity varies only a little over a wide bubble size range encompassing most actual situations, helps understanding why single-bubble-size CFD simulations may give rise to reasonable results despite the strong simplification with respect to reality, were a quite wide bubble size distribution exists at any time.

5.4 CFD SIMULATION A MECHANICALLY STIRRED TANK

5.4.1 Solution domain and boundary conditions

The simulations performed concerned the stirred vessel employed by Bombac *et al.* 1997, for which literature experimental data were available. It was a standard cylindrical vessel of diameter T=0.45 m, impeller diameter D=T/3, baffles width b=T/12. The impeller was offset from the bottom by C=T/4 and a ring sparger was used to introduce the air stream into the vessel. Further geometrical details regarding the apparatus can be found in Bombac *et al.* (1997) where a thorough complete descriptions of the measurement techiques and a comprehensive explanation of gas liquid cavity regimes can also be found.

Different grids were used to reproduce the geometry of the system in order to assess simulation grid dependence. In particular the solution domain was discretised either by coarse or a fine grid (r x θ x z = 37 x 36 x 53, 70596 cells; 106 x 74 x 36, 282384 cells). In Fig. 5.8 the coarse grid is depicted. In both cases, in order to impose periodic boundary conditions in the azimuthal direction, the computational domain included an integer number of blades and baffles; thus it was half tank including three blades initially located at 30°, 90° and 150° and two baffles located midway between the blades (45° and 135°).

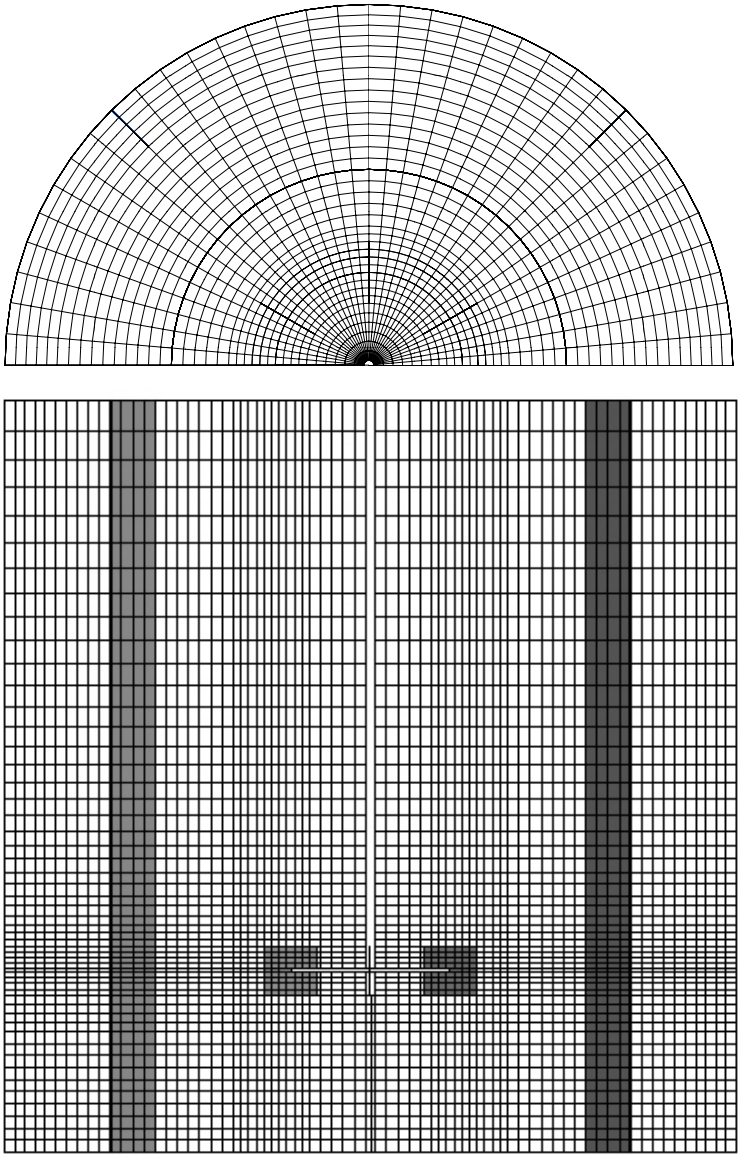

Fig 5.8. *Domain discretisation in azimuthal, radial and vertical directions*

The computational domain was also subdivided in two sub-domains, as required by the *sliding-grid* algorithm, that was employed to get a fully predictive simulation of impeller motion. All the simulations were carried out with the help of the commercial code CFX 4.4. Time stepping was such that the impeller rotated by 60 degrees at each step. With such a large time interval, the impeller position is practically reproduced at each time step, so that a steady state solution (rather than a periodic one) is to be obtained. In practice this simulation strategy makes the *sliding grid* approach to get close to the *Multiple Frames of Reference* (MFR, Luo *et al.* 1994) approach. This strategy results in considerable savings of CPU time and was adopted here after having checked that much smaller time steps (e.g. set in order to let cells to slide azimuthally by just one at a time) did not result into significantly different results.

The discretization scheme adopted for the convection term was the *hybrid upwind* which, in order to prevent numerical instability, switches from 2nd order central to 1st order upwind formulas when the cell Peclet number is greater than two.

The air sparger was modelled as a superficial continuous mass source located at the same geometric position as the sparger, whereas the free surface was modelled as a flat *degassing boundary* (CFX 4.4, User Manual)

Satisfactory completion of each simulation run was based on several criteria, including sufficient reduction of mass and other residuals, an accurate balance between rates of gas entering and leaving the tank, and a constant gas hold up. Steady state was considered to have been reached when all the above criteria were met. About 100 stirrer revolutions were typically found to be amply sufficient to satisfy all the above-mentioned criteria.

5.4.2 Results and Discussion

Flow field

Typical simulated vector plots obtained with the coarse grid are reported in Figs. 5.9 and 5.10, for the liquid and gas phase respectively. Although no specific anemometric data are available for the system under consideration, the simulated flow fields appears to be in reasonable agreement with expectances. As a matter of fact, a triple loop configuration, with two recirculation loops above and one below the stirrer can be observed. Such a configuration is in agreement with previous gas-liquid experimental and CFD simulation results (Khopkar *et al.,* 2005). Also the slight inclination towards the

top of the vessel of the impeller discharge stream appear to be in agreement with previous findings.

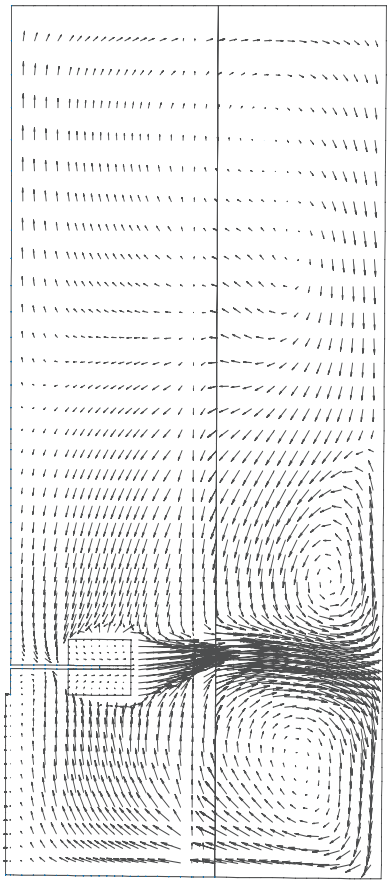

Fig 5.9. *Liquid flow field*

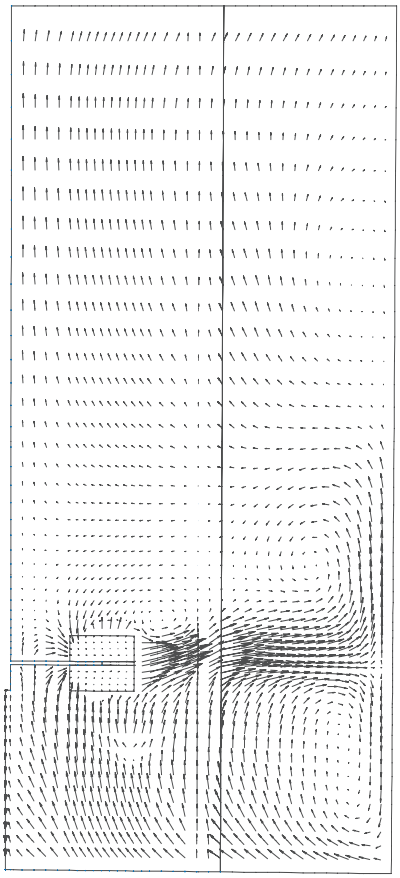

Fig 5.10. *Gas flow field*

Gas hold-up

The simulated gas fraction distribution is reported in Fig.5.11b as a contour plot of the simulated volumetric gas fraction (local hold-up) on a vertical plane 12° upstream a baffle. Values in the internal (rotating) domain were azimuthally averaged. Comparison with the relevant experimental data by Bombac *et al.* (1997), reported in Fig. 5.11a, shows that the main patterns of the gas distribution appear to be quite well predicted. For instance, the accumulation of gas near vessel walls below the impeller plane and the high concentration area immediately above the impeller, which are clearly observable in the experimental data, are both predicted by the simulations. The shape of contour lines is also in reasonable agreement with experiment in all two cases.

On the other hand, some discrepancies can be observed also, especially in the vessel volume below the impeller, where the gas penetration is always significantly under-predicted. This discrepancy may depend on the modelling assumption of a single bubble size, whereas in reality bubbles show a size distribution down to rather small bubbles, which are more easily carried down by the liquid streams.

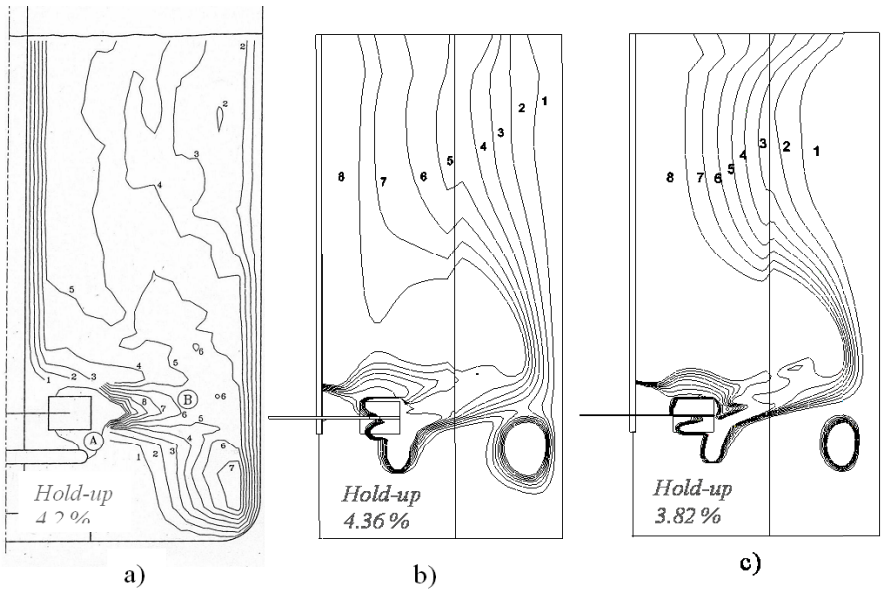

Fig. 5.11: *Gas hold up distribution, Q=1.67 E-3 m3/s; n=6.27 rps: (a) Bombac et al. (1997), (b) CFD results with coarse grid; (c) CFD results with refined grid.*

In the region above the impeller, the relative maxima are somewhat over-predicted, probably due to the fact that, in the real system, in those zones bubbles tend to heavily coalesce, up to the point of increasing their terminal velocity and, as a consequence, decreasing local air volume fraction, a feature that, again, cannot be captured by the present "single-sized" simulations.

It may be worth noting that the resulting total gas hold-up, reported in Figs 5.11b and 5.11a (4.36 and 4.2 %, respectively), is very well predicted, especially in view of the many simplifications adopted to reach the solution. It should be noted, however, that the good agreement on the global parameter is the result of underestimations in certain zones that are compensated by overestimations in other zones. This consideration confirms that, in general, good results on global parameters should never be considered as thorough indications of the simulation quality.

Grid sensitivity

The effect of grid size on the major characteristics of the system (global gas hold-up and gas hold-up distribution) may be estimated by comparing simulation results obtained by the previously described coarse (Fig. 5.11b) and fine (Fig. 5.11c) grids. As it can be seen, the gross characteristics of the local gas hold-up distribution within the vessel remain substantially unaffected by grid refinement. However, global gas hold-up appears to be somewhat affected by grid changes, as increasing cells number a reduction of the predicted gas hold-up from 4.36% to 3.82% is observed. It is worth noting that the simulated results for both cases are in similar agreement with the experimental global gas hold-up (4.2%).

On the basis of the above considerations, the coarse grid was used throughout the present work to take advantage from its lighter computational demand (CPU times of the order of 24 h instead of 72 h required by the finer grid) with negligible loss of accuracy in the assessment of the results sensitivity to modelling choices.

Influence of the prescribed bubble size

To investigate the influence of the prescribed single size, two further simulations were carried out for the same conditions of Fig. 5.11 a, but with bubble sizes set to 2 and 4 mm. Results are reported in Figs 5.12 (a) and (b) respectively, where it can be seen that results are only slightly affected by the choice of bubble diameter in the simulation. This outcome reflects the relatively small decrease of terminal rise velocity while increasing bubble diameter in the size range here explored (0.29 – 0.24 m/s)

It is worth noting that the relatively small influence of bubble size on total gas hold up as well its distribution implies that vessel hydrodynamics is not too affected by bubble sizes. As a consequence a simulation strategy like that adopted by Venneker te al. (2002) where coalescence/breakage computations are conveniently carried out off-line, after having assessed the vessel flow field. The two steps are then to be iterated, nevertheless large savings of computational demand may be expected.

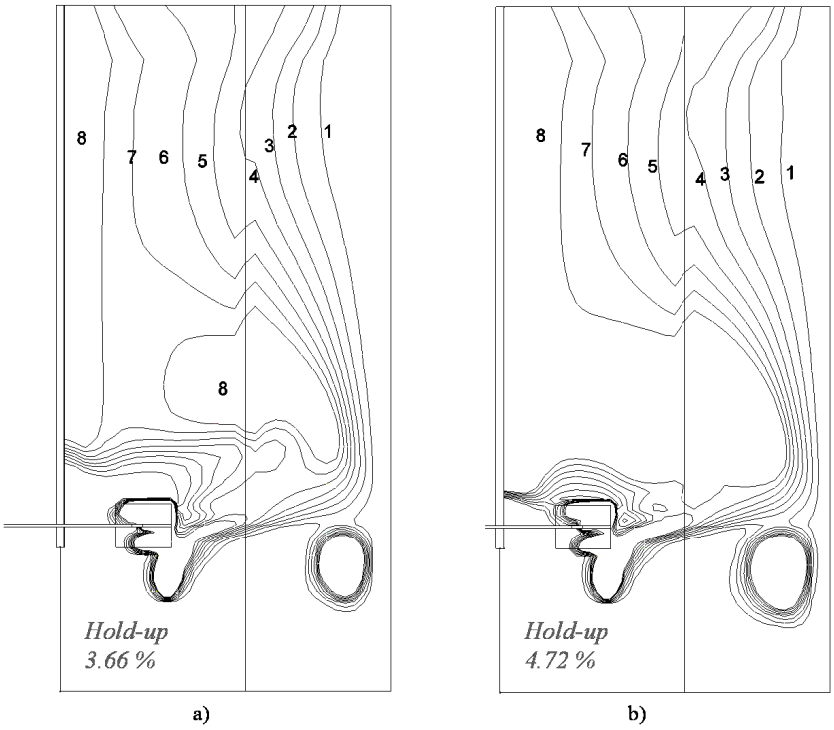

Fig .5.12 Gas hold up distribution, Q=1.67 E-3 m3/s; n=6.27 rps: (a) db = 2 mm; (b) db = 4 mm

Influence of stirrer speed and gas flow rate

The modelling approach adopted in the *base case* was then applied to two other operating conditions about which experimental data by Bombac et. al (1997) were available. Simulation results are compared with experimental data in Figs. 5.13 and 5.14. For the case relevant to a reduction in agitation speed (about 30%) the simulated global gas hold-ups (3.06%) perfectly reproduce the experimental datum of 3.2%, while the simulated local gas hold-up distribution follow quiet well the experimental one (Fig. 5.13).

The effect of a reduction in gas flow rate of about 66% is reported in Fig. 8. It can be observed that as in the experimental figure, contours levels are fewer and more distant than in the base case, which it is physically reasonable due to more uniform distribution of the gas. The simulated global gas hold-ups (2.15%) perfectly reproduce the experimental datum of 2.2%

Simulation sensitivity to turbulent dispersion and non drag forces

The notable variations on modelling approach, such as turbulent gas dispersion and non drag forces, were firstly evaluated separately while maintaining the same physical conditions (agitation speed and gas flow rate) and simulation parameters employed in the base case, to understand their effects on system hydrodynamics.

The effect of including turbulent gas phase dispersion by setting a value of 0.8 (Yakhot *et al.*, 1987) for the turbulent Schmidt number σ_T is shown in Fig. 5.15 (a) . By comparing Fig.15a with Fig.11b, one may note that the two figures almost coincide, as well as the global gas hold-ups (4.35% vs 4.36% of base case). It may be concluded that the gas phase turbulent dispersion is practically negligible for the system under examination, in agreement with Khopkar *et al.* (2003) findings.

Fig 5.15 (b) shows the effect of lift force. Notably its effect on global gas hold-up is slightly greater than turbulence dispersion (4.67% vs 4.36% base case). Also in this case a more uniform distribution within the vessel can be observed

Results regarding the effect of virtual mass force are reported in Fig. 5.15 (c). Global gas hold-up is practically the same (4.6% vs 4.36% base case) while a slight effect on local gas hold-up distribution is present: the main effect of virtual mass force may be visualized near the rotating devices where the two phases seem to be accelerated differently due to their different density.

These results allow to conclude that for this kind of physical systems the drag force is predominant with respect to the non drag forces.

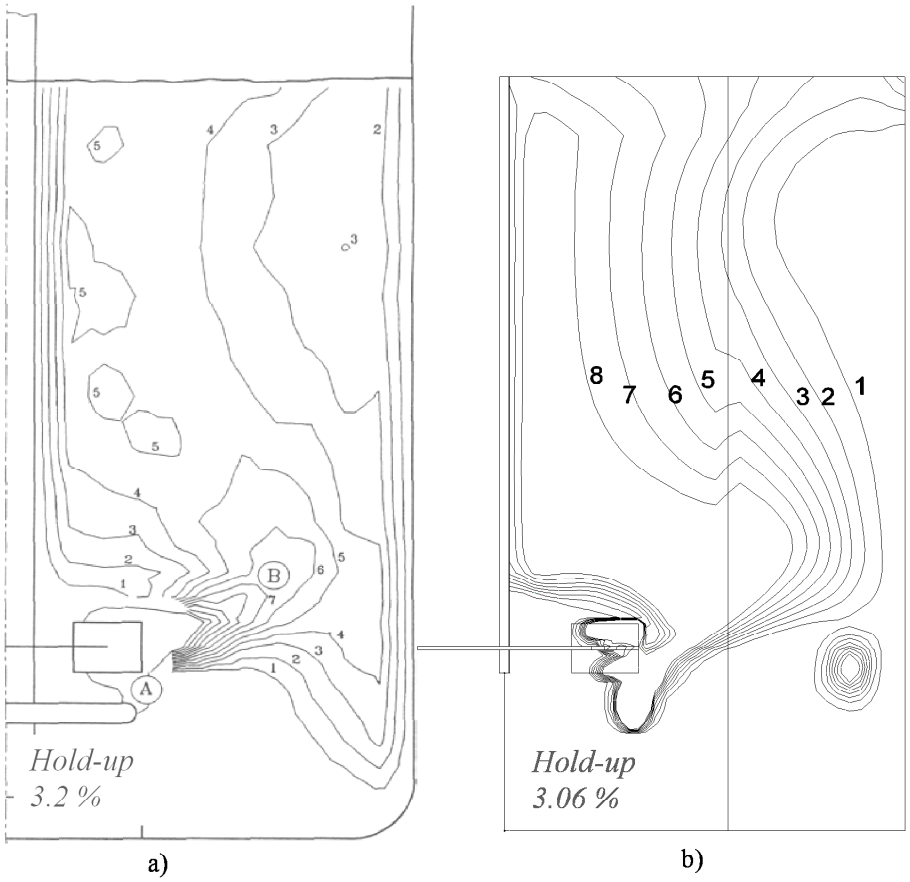

Fig .5.13: *Gas hold up distribution Q=1.67 E-3 m^3/s; n=4.43 rps:*
(a) Bombac et al. (1997); (b) CFD results d_b = 3 mm and coarse grid

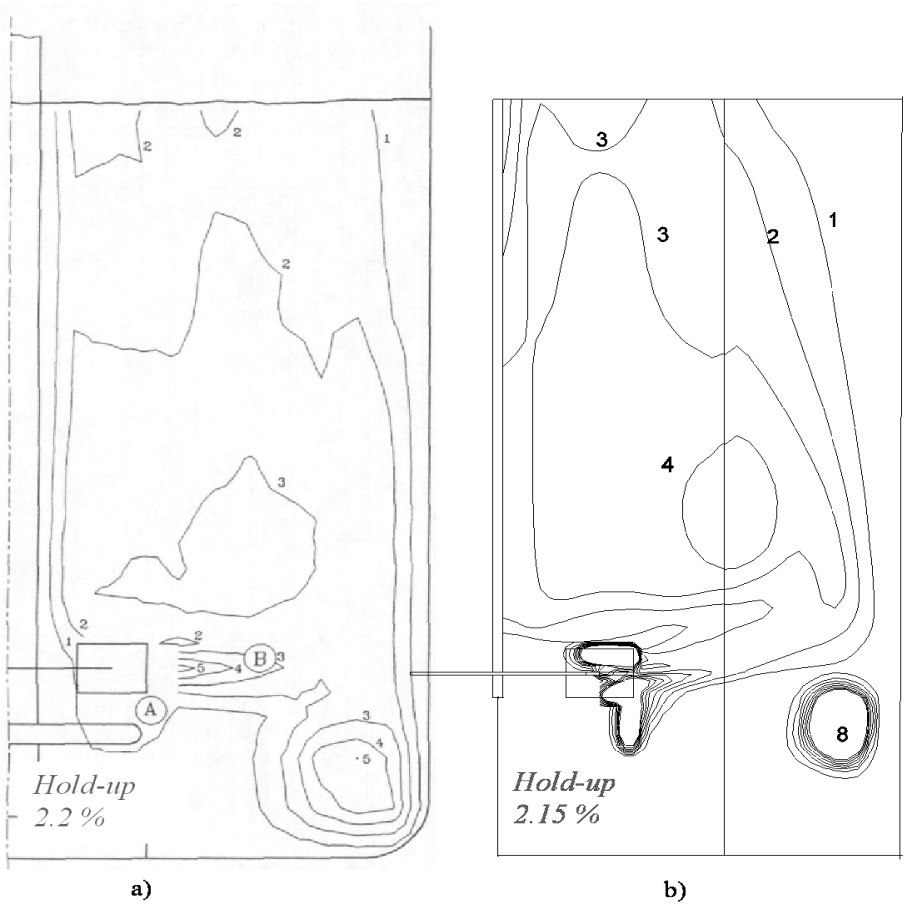

Fig .5.14 *Gas hold up distribution Q=0.556 E-3 m^3/s; n=6.27 rps:*
(a) Bombac et al. (1997); (b) CFD results d_b = 3 mm and coarse grid

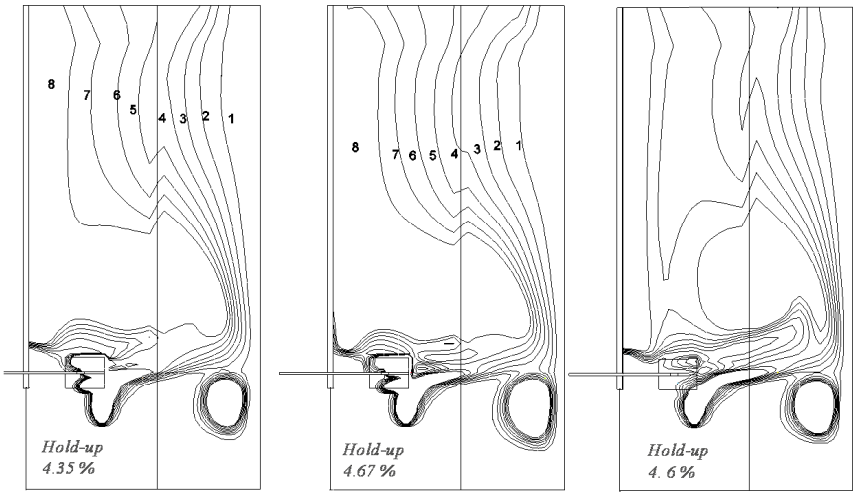

Fig .5.16:*Gas hold up distribution, Q=1.67 E-3 m^3/s; n=6.27 rps: (a) Effect of turbulent dispersion of volume fraction (σ_T=0.8); (b) effect of lift force; (c) effect of virtual mass force*

Gas cavities

It is well know that in gas-liquid stirred vessels gas tend to accumulate behind the blades up to forming pockets called gas cavities (Middleton, 1985). Such cavities act like blade streamliners and in this way they significantly reduce the power drawn by the impeller under gassed conditions with respect to the power drawn by the same impeller under ungassed consitions. One may wonder whether this phenomenon is reproduced by the Multi-Fluid CFD simulations carried out in this wok. To this end the simulation results obtained for N=376 rpm and Qg = 6.27 m^3/s, i.e. under conditions for which it S33 gas cavities were actually present in the real system (Bombac *et al*, 1997), were reported in Fig.5.16 as isosurfaces of several values of the volumetric gas fraction (0.2, 0.3, 0.4 and 0.5). As it can be seen, the simulations do actually predict the accumulation of gas behind the blades, as they are able to account for the relative motion between bubbles and liquid induced by pressure gradients. However, by looking at Fig.5.16 it is clear that the actual cavities are

not properly simulated, as in the real system they are made of 100% gas and there is an abrupt gas fraction change across their boundaries, while the simulated accumulation never gets any close to 100% and also no neat boundary exists between the gas rich region and the rest of the dispersion.

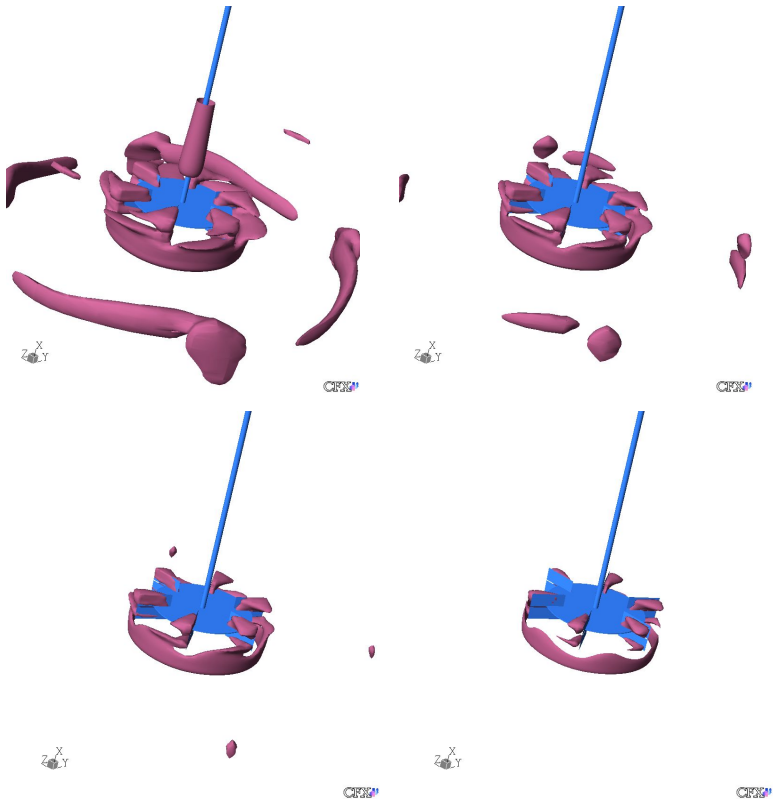

Fig 5.16: *Isosurfaces of gas volume fraction at 0.2 (a), 0.3 (b), 0.4 (c) and 0.5 (d) VF.*

This is not surprising, as the simulation of the gas-liquid transition, as well as that of the gas coalescence to form the pockets are clearly out of reach for MFM simulations. The question however arises whether the main effect of the

presence of cavities, *i.e.* the already quoted reduction of power demand by the stirrer, is reproduced to some extent.

To answer this question, a single phase simulation of the ungassed system stirred at 376 rpm, was carried out, and the relevant power number was computed on the basis of the simulated torque on the impeller. The result was a power number Np= 4.24, hence a reasonable value for the Rushton turbine here employed. The power number resulting from the gassed simulation (Qg=6.27 m^3/s) at the same agitation speed was instead 3.0, with a reduction of about 30% with respect to the ungassed value. Unfortunately no specific experimental value of power numbers are available for the investigated system. However, on the basis of other published information (Nienow *et al*, 1985; Middleton ,1985), the predicted reduction of the power drawn by the impeller appears to be quite realistic. It may be concluded that MFM simulations of gas-liquid stirred vessels may well result into reasonably accurate estimations of the power drawn by the impeller, despite their lacks in the simulation of the actual gas cavities. A struggle to better simulate these last, for instance by means of "Volume of Fluid" (VOF) techniques, may therefore be less needed than expected.

5.3.3 Average terminal velocity vs. average bubble size

It was pointed out that the main parameter for inter phase drag force is bubble terminal velocity and not bubble size. As a consequence, in the case of a bubble size distribution, the resulting drag force per unit volume will be given by:

$$F_D = \sum_i \frac{r_i \cdot (\rho_\beta - \rho_\alpha) \cdot g}{U_{Ti}^2} \left| \overline{U}_\beta - \overline{U}_\alpha \right| \tag{5.24}$$

where U_{Ti} are terminal velocities of bubbles of equivalent diameter d_i. This may be put in the equivalent form

$$F_D = \frac{(\rho_\beta - \rho_\alpha) \cdot g}{U_{Tav}^2} \left| \overline{U}_\beta - \overline{U}_\alpha \right| \tag{5.25}$$

if, instead of an averaged bubble diameter, a suitably averaged terminal velocity is used. This has clearly to be defined as:

$$U_{Tav}^2 = \frac{1}{\sum_i \frac{r_i}{U_{Ti}^2}} = \frac{1}{r_\beta \cdot \sum_i \frac{f_i}{U_{Ti}^2}} \tag{5.26}$$

where f_i are the volume fractions pertaining to each bubbles size class), to correctly reproduce the total drag force exchanged .

This is an important point as, by observing the shape of the experimental curve giving bubble terminal velocity *vs* bubble diameter in Fig.4.1, it becomes clear that considering a drag coefficient (or a bubble terminal velocity) obtained from any average bubble diameter may lead to serious mistakes, especially if a significant fraction of bubbles smaller than 1 mm is present.

5.5 CONCLUSIONS

CFD simulations of an air lift reactor and of a stirred vessel were carried out under an Eulerian-Eulerian Multifluid approach in conjunction with the simplest two phase extension of the k-ε turbulence model. For both apparatuses simulation results were found to be in good agreement with experiment, despite the many simplifications adopted in the model, including the assumption of a single prescribed bubble size.

It was pointed out that the real parameter affecting gas distribution in gas liquid systems is bubble terminal rise velocity. This approach is quite simple and facilitates physical understanding of simulation results. Also, considering that bubble rise velocity varies only a little over a wide bubble size range encompassing most actual situations, it becomes clear why single-bubble-size CFD simulations may give rise to reasonable results. As a matter of fact, good agreement between simulations and experiment was found here by prescribing bubbles sizes of either 2, 3 or 4 mm.

The effect of the main non drag forces was considered. The modellization of the system does not seem to be significantly affected by them which reflects the fact that gas-liquid equipment, regardless of the presence of impellers are essentially drag and buoyancy dominated, being also turbulence dispersion of the gas phase of secondary importance for gas distribution.

Notably, the effect of turbulence on terminal rise velocity was not considered in this study, but it is an effect which could significantly change the gas distribution, and should be given further consideration in the future, as more information on turbulence effects becomes available.

More accurate results will certainly require suitable modelling of coalescence and break-up phenomena. The relevant much larger computational demand may, however, be more easily dealt with by recognizing that flow field simulation and bubble coalescence/breakage phenomena may be conveniently carried out subsequently rather than contemporaneously. In fact, as the drag force exchanged between bubbles and liquid depends only on bubble terminal velocity, which undergoes only moderate changes for the bubble sizes prevailing in gas liquid contactors, gas distribution is not severely affected by bubble size distribution. This in turn justifies the above statement on the decoupling of population balances and flow equations.

CHAPTER 6

CONCLUSIONS AND PERSPECTIVES

6. Conclusions and perspectives

The general scope of the present work was an investigation on agitated gas-liquid systems, which are important in the chemical, process and biotechnological industry as well as in environmental remediation. The investigation was directed to a better comprehension of the principles of the underlying physical and fluid-dynamic processes, to obtain more reliable design methods for typical equipment and to improve their knowledge based on scientifically grounded approaches. Attention was focused on selected equipment of remarkable interest for application purposes, namely stirred vessels, either sparged or self-induced.

The main results obtained can be summarised as follows:

- A novel self-ingesting gas-liquid stirred reactor, the Long Draft Tube Self-inducing Reactor (LDTSR), was conceived and set up. Its main features are a high aspect-ratio and a fairly narrow multiple-impeller draft tube, through which the gas phase is ingested and drowned down to the vessel bottom, where it is dispersed into the rising liquid. The preliminary results obtained show that both gas hold-up and gas-liquid mass transfer coefficient increase while increasing stirrer speed (and therefore specific power input), as it was expected. Notably the values obtained are comparable with some of the best results reported in the open literature for self-ingesting apparatuses.

  Possible future developments of the proposed device include design modifications of the axial impellers adopted, in order to enhance the recirculated gas-liquid flow rate and the global gas hold-up. Finally, preliminary tests showed that solid particles introduced in the gas-liquid vessel tend to stay suspended in the annular region and do not reach the draft-tube brim. As a consequence, recirculation through the stirrers and the relevant mechanical attrition is avoided while still effectively promoting solid-liquid mass transfer. In a way, for three phase applications too, the vessel devised may be regarded as being akin to a bubble column, a feature

that might make the present apparatus a good choice for three-phase applications.

- A convenient variant of the dynamic technique for the k_La measurements was developed and compared with other traditional dynamic techniques. With this variant the simplest two component system (water-oxygen) is dealt with, and therefore the k_La data obtained cannot be affected by gas phase concentration variations. As a consequence there is no need to resort to flow models for the gas phase and reliable information on the mass transfer parameter is obtained.

  Results show that, for the investigated standard stirred vessel, gas-liquid mass transfer coefficients obtained in the absence of species other than water and oxygen, are about 30 % - 50 % greater than those (less reliable) measured in the same hydrodynamic conditions but starting with an air-saturated liquid phase, i.e. in the presence of dissolved nitrogen. The data obtained by the new variant of the dynamic technique were also validated by comparison with the (quite scant) literature information available.

  The investigation with the new variant of the dynamic technique was extended to the LDTSR. In this last case, gas-liquid mass transfer coefficients obtained in absence of dissolved nitrogen were found to be several times greater than those measured in the same hydrodynamic conditions but starting with an air-saturated liquid phase. Such differences are much larger than those observed in the standard vessel investigated. The reason behind this discrepancy is likely to lie in the much larger rise height of bubbles before escaping from the system. The difference is found to be largest for the non coalescing systems, as these tend to give rise to smaller bubbles, which are the ones most affected by nitrogen counter diffusion effects.

  As a last remark, results clearly show that is very important to use correct methods of k_La measurement, able to produce physically consistent data, as only such data with clear physical interpretation can lead to successful design and scale-up of process apparatuses.

- An attempt to develop an original experimental technique to evaluate free stream turbulence effects on bubble terminal velocity was put foreword. A number of practical problems occurred in carrying out the experimental runs, so that the data collected cannot be considered as reliable. The most significant problem was the difficulty in maintaining bubbles on the channel axis. To avoid these uncertainties, a centrifugal field was over imposed on the system, with the aim of keeping bubbles near the symmetry

axis as a consequence of the density difference between the two phases. Unfortunately, channel rotation induced heavy outlet effects which probably modified the flow field inside the tube to a large extent, so compromising the assumption of constant axial velocity, and therefore the data collected so far.

- CFD simulations of the gas liquid dispersion in an air-lift reactor and of a sparged stirred vessel were carried out with a standard Euler-Euler Multifluid approach. The effect of including in the model the main non-drag forces (lift and virtual mass forces) was found to be quite small. Also, turbulent dispersion of the gas phase seems to play a negligible role in gas distribution.

  As concerns drag, it was pointed out that the real parameter needed for its correct description is bubble terminal rise velocity, which allows a simpler expression, with lesser uncertainties, for the drag force term in the momentum balance equation. It also makes for an easier physical understanding of system behaviour and provides a way for correctly taking into account bubble drag in the presence of a bubble size distribution.

  Simulation results were found to be in acceptable agreement with experiment, for average bubble sizes between 2 and 4 mm. Notably, had other bubble sizes been chosen in the range between 2 and 15 mm, in view of the almost constant terminal velocity in such range, similar results would have been obtained. Notably, the effect of turbulence on terminal rise velocity was not considered in this study due to the lack of reliable data (see 3), but it is an effect which could significantly change the gas distribution, and should be given further consideration in the future, as more information on turbulence effects becomes available.

NOTATION

AAN	Air Absorption in Nitrogen treated water
OApE	Oxygen Absorption in pre-Evacuated water
OAS	Oxygen Absorption in air Saturated water
ODA	Oxygen Desorption by Air
$A_{p,}$	particle surface, m^2
B	vector body force N m^{-3}
C_D,	drag coefficient, dimensionless
C_L	constant in lift force expression, dimensionless
$C_{1\varepsilon}$,	constant in k-ε model, dimensionless
$C_{2\varepsilon}$,	constant in k-ε model, dimensionless
$C_{3\varepsilon}$,	constant in k-ε model, dimensionless
C_μ ,	constant in k-ε model (eqn 4), dimensionless
C_{vm},	constant in virtual mass expression, dimensionless
Eo	Eotvos number, dimensionless
D	diameter of the radial bottom turbine (D = 0.095 m)
$\mathbf{F}_{\beta\alpha}$,	inter-phase force term, N m^{-3}
$\mathbf{F}_D$,	drag force term, N m^{-3}
$\mathbf{F}_{vm}$,	virtual mass force term, N m^{-3}
$\mathbf{F}_{lift}$,	lift force term, N m^{-3}
$\mathbf{F}_{Basset}$,	Basset history term, N m^{-3}
$\mathbf{F}_{wall\ lubrication}$,	wall lubrication force term, N m^{-3}
G_α,	term in turbulent kinetic energy transport equation due to b. forces
LDTSR	Long Draft Tube Stirred Reactor
$N_{P,}$	power number, dimensionless
$N_{Q,}$	pumping number, dimensionless
N	agitation speed

Np	Power number
P	Agitation Power
P_{α},	term in turbulent kinetic energy transport equation due to shear
Q_g	gas flow rate, $m^3\ s^{-1}$
Re,	Reynolds number, dimensionless
S,	source or sink term in transport equation
U,	vector of velocity field, $m\ s^{-1}$
$\mathbf{U}_T$,	bubble terminal rise velocity, $m\ s^{-1}$
V	Reactor volume
$V_{p,}$	particle volume, m^3
c_L^*	equilibrium oxygen concentration
c_L	oxygen concentration in the bulk
c_0	oxygen concentration in the bulk at time $t=t_0$
d_e,	equivalent bubble diameter, mm
d_h,	modified bubble diameter, mm
d_{ext}	reactor diameter in the annular region
d_{int}	draft tube diameter
g ,	gravity acceleration, $m\ s^{-2}$
h_{ext}	clear liquid height in the annular region
h_{int}	clear liquid height in the draft tube
h_{rif}	clear liquid height above tank bottom at no agitation conditions
k_La	volumetric mass transfer coefficient
k,	turbulent kinetic energy , $m^2\ s^{-2}$
n,	agitation speed, rps
p,	pressure, $N\ m^{-2}$
r ,	volume fraction, dimensionless
t	time

t_0 initial time

Greek symbols

α, pedix for continuous phase

β, pedix for dispersed phase

ε gas hold-up

ρ_L liquid density

ρ_λ, density of the liquid phase, Kg m^{-3}

ρ_γ, density of the gas phase, Kg m^{-3}

μ, viscosity, Pa s

μ_T, turbulent viscosity, Pa s

ν_T, turbulent cinematic viscosity, Pa s

θ, azimuthal direction, rad

ε, dissipation of turbulent kinetic energy, m^2 s^{-3}

σ, surface tension, N m^{-1}

σ_K, σ_ε k–ε model parameters, dimensionless

σ_T, Turbulent Schimdt number, dimensionless

REFERENCES

Alcamo R., Micale G., Grisafi F., Brucato A., Ciofalo M., 2005, Large-eddy simulation of turbulent flow in an unbaffled stirred tank driven by a Rushton turbine, *Chemical Engineering Science*., 60, 2303-2316.

Alves S.S., Maia C.I., Vasconcelos J.M.T., 2003, Effect of bubble contamination on the liquid film mass tramsfer coefficient in stirred tanks, Proceedings of *11th European Conference on Mixing,* 15-17 October 2003, Bamberg, Germany

Armenante P., Chou C.-C., Hemrajani R.R., 1994. Comparison of experimental and numerical fluid velocity distribution profiles in an unbaffled mixing vessel provided with a pitched-blade turbine. *IChemE Symposium Series* 136, 349–356.

Bakker A., H.E.A. Van den Akker, 1994b. A Computational Model For The Gas-Liquid Flow In Stirred Reactors, *Chem. Eng. Res. Des.*, 72, 594-606

Baldyga J, Bourne JR, Hearn SJ, 1997, "Interaction between chemical reactions and mixing on various scales", *Chemical Engineering Science* , 52 (4): 457-466.

Barigou M., Greaves M., 1992, Bubble-size distributions in a mechanically agitated gas-liquid contactor, *Chemical Engineering Science* 47, 2009-2025.

Bates R. L., Fondy P. L., Corpstein R. R., 1963, An examination of some geometric parameters of impeller power, *I&EC Process Design and Development*, 2 (4), 310-314.

Bombac A., Zun I., Filipic B., Zumer M., 1997, "Gas-filled cavity structures and local void fraction distribution in aerated stirred vessel", *AIChE J*., 43, 2921-2931.

Brodkey R.S., Hershey, H.C., Transport Phenomena, *McGraw-Hill,Inc.Cap 6,* 1988

Brucato A., Ciofalo M., Grisafi F. and Micale G., 1998, "Numerical prediction of flow fields in baffled stirred vessels: a comparison of alternative modelling approaches", *Chemical Engineering Science*., 53, 3653-3684.

Brucato A.,. Ciofalo M., Grisafi F., Tocco R., 2000, On the simulation of stirred tank reactors via computational fluid dynamics *Chemical Engineering Science,* 55, 291-302

Brucato a., Ciofalo M., Gofrey J., Micale G., 1996, Experimental detrmination and CFD simulation of solid distributions in stirred vessels, *Proc. of 5th Int.*

Conf. on Multiphase flow in Ind Plants, Amalfi, Italy, 26-27 Sept., 1996, 323-334.

Brucato A., Grisafi F., Montante G., Particle drag coefficients in turbulent fluids, *Chem. Eng. Science*, 53, 3295-3314, 1998.

Bunner & Tryggvason, 1999, Direct numerical simulations of three-dimensional bubbly flows, *Physics of Fluids*, 1967-1969.

Celata G.P., D'Annibale F., Di Marco P., Tomiyama A., Zovini C., 2006, Effect of gas injection mode and purity of liquid on bubble rising in two-component systems, *Experimental Thermal and Fluid Science,* 31, 37–53.

CFX4.4 Documentation, 1999 AEA Technology.

Chen, J.-H., Hsu, Y.-C., Chen, Y.-F., Lin C.-C., 2003, Application of Gas-inducing Reactor to Obtain High Oxygen Dissolution in Aeration Process, *Water Research* 37, 2919-2928.

Chen P., Sanyal J., Dudukovic M. P., 2004, CFD modelling of bubble columns flows: implementation of population balance, *Chemical Engineering Science*, 5201-5207

Ciofalo M., A. Brucato, F. Grisafi, N. Torraca, 1996, Turbulent flow in closed and free-surface unbaffled tanks stirred by radial impellers, *Chemical Engineering Science* , 50, 3557-3573

Clamen A., and Gauvin W.H., 1978, Effects of turbulence on the drag coefficients of spheres in a supercritical flow regime, *Am. Inst. Chem Engng. J.*, 15, 184-189, 1969.

Clift R., Grace J.R., Weber M.E., Bubbles, drops and particles, Academic Press, London.

Conway K., Kyle A., Rielly C. D., 2002, 'Gas-liquid-solid operation of a vortex-ingesting stirred tank reactor', *Trans IChemE Part A*, 80, 839-845.

Couvert A., Roustan M.., Chatellier P., 1999, "Two phase hydrodynamic of a rectangular air-lift loop reactor with an internal baffle", Chem. Eng. Sci., 54, 5245-5252.Delnoij E., Kuipers J.A.M., vanSwaaij W.P.M., 1997, "Computational fluid dynamics applied to gas-liquid contactors", *Chem. Eng. Sci.*, 52 (21-22), 3623-3638.

Decker S., Sommerfeld M., 1996, Calculation of particles suspension in agitated vessel with the Euler Lagrange approach, *Inst. Chem Engrs Symp Ser*, 140, 71-82, 1996.

Derksen J.J. and H.E.A. van den Akker, 1999, Large eddy simulations on the flow driven by a Rushton turbine, *A.I.Ch.E Journal* : 45, 209-219

Forrester, S. E. and Rielly, C. D. 1994, "Modelling the increased gas capacity of self-inducing impeller". *Chemical Engineering Science* 49, 5709-5718.

Forrester, S. E., Rielly, C. D. and Carpenter, K. J. 1998, "Gas-inducing impeller design and performance characteristics". *Chemical Engineering Science* 53, 603-615.

Forrester, S. E. and Rielly, C. D. 1998, "Bubble formation from cylindrical, flat and concave sections exposed to a strong liquid cross-flow". *Chemical Engineering Science* 53, 1517-1527.

Gibbardo B., Micale G., Grisafi F., Brucato A., Ciofalo M., 2006, "Numerical simulation of low-Reynolds flow fields in unbaffled stirred vessels", Proceedings of the *12th European Conference on Mixing*, Bologna, June 27-30 2006, pp. 57-64

Gosman A.D., Issa R.I., Lekakou C., Looney L.K., Politis S., 1992, "Multidimensional modelling of turbulent two-phase flow in stirred vessels". *AIChE J.,* 38, 1946-1956

Grevskott S., Sannæs B.H., Dudukovic M.P., Hjarbo K.W., Svendsen H.F., 1996, Liquid circulation, bubble size distributions, and solids movement in two- and three-phase bubble columns, *Chem. Eng. Sci.*, 51(10), 1703-1714.

Grisafi F., Brucato A., Rizzuti L., 1998, "Solid-Liquid Mass Transfer Coefficients in Gas-Solid-Liquid Agitated Vessels", *The Canadian Journal of Chemical Eng.*, V.76, 446-455.

Harnby N., Edward M.F. and Nienow A.W. 1985, (Eds.) Mixing in the Process Industries, Butterworth

Heim A., Kraslawski A., Rzyski E., Stelmach J., 1995, Aeration of Bioreactors by Self-Aspirating Impellers, *Chem. Eng. Journ.* 58, 59-63.

Hemrajani R.R. and Tatterson G.B., 2004, "Mechanically stirred vessels" in E.L. Paul, V.A. Atiamo Obeng and S.M. Kresta (eds.) "Handbook of Industrial Mixing", Wiley and Sons, Table 6-4 p. 365.

Hsu Y.-C., Huang C.-J., 1996, 'Characteristics of a new gas-induced reactor', *A.I.Ch.E. Journal* 42, 3146-3152.

Hsu, Y.-C., and Huang, C.-J. 1997, "Ozone transfer with optimal design of a new gas-induced reactor". *A.I.Ch.E. Journal* 43, 2336-2342.

Hsu, Y.-C., Chen, J.-T. and Yang, H.-C. 2001, "Decolorization of dyes using ozone in a gas-induced reactor". *A.I.Ch.E. Journal* , 47(1), 169-176.

Hsu, Y.-C., Chen, J.-T., Chen, J.-H., Lay C.-W., 2002, Ozone Transfer into Water in a Gas-Inducing Reactor, *Ind. Eng. Chem. Res.*, 41, 120-127.

Ishii M., Zuber N., 1979, Drag coefficient and relative velocity in bubbly, droplet or particulate flows, *AIChE Journal,* Vol. 25, Issue 5, 843-855

Joshi J. B., Sharma M. M., 1977, 'Mass Transfer and Hydrodinamic Characteristics of Gas Inducing Type of Agitated Contactors', *The Canadian Journal of Chemical Engineering*, Vol. 55, 683-695.

Joshi J.B., 2001, "Computational flow modelling and design of bubble column reactors", *Chem. Eng. Sci.*, 56, 5893-5933.

Kerdouss F., Bannari A., Proulx P., 2006, CFD modelling of gas dispersion and bubble size in a double turbine stirred tank, *Chem. Eng. Sci.*, 61, 3313-3332.

Khopkar A.R., Rammohan A.R., Ranade V.V., Dudukovic M.P., 2005, "Gas–liquid flowgenerated by a Rushton turbine in stirred vessel: CARPT/CT measurements and CFD simulations", *Chem. Eng. Sci.*, 60, 2215-2229.

Khopkar A.R., Ranade V.V., 2006, CFD Simulation of Gas-Liquid Stirred Vessel: VC, S33 and L33 Flow Regimes, *A.I.Ch.E. Journal*, Vol. 52, No. 5, 1654-1672.

Kresta S.M. and P.E. Wood, 1991, Prediction of the 3-dimensional turbulent flow in stirred tanks, *A.I.Ch.E. Journal*, 37, 448-460.

Lain S, Broder D, Sommerfeld M., 1999, "Experimental and numerical studies of the hydrodynamics in a bubble column", *Chem. Eng. Sci.*, 54 (21), 4913-4920

Laakkonen M., Honkanen M., Saarenrinne P., Aittamaa J., 2005, Mocal bubble size distributions, gas-liquid interfacial areas and gas hold-ups in a stirred vessel with particle image velocimetry, *Chemical Engineering Journal* 109, 37-47.

Lane G. L., Schwarz M.P., Evans G.M., 2002, "Predicting gas-liquid flow in a mechanically stirred tank", *Applied Mathematical Modelling* , 2, 223-235.

Lane G.L., Schwarz M.P., Evans G.M., 2005, "Numerical modelling of gas-liquid flow in stirred tanks", *Chem. Eng. Sci*, 60, 2203-2214.

Lara Marquez A., Wild G., Midoux N., 1994, A review of recent chemical techniques for the determination of the volumetric mass transfer coefficient kLa in gas-liquid reactors*, Chem. Eng. Proc.*, 33, 247-260.

Launder BE, Spalding, DB, 1974, "The numerical computation of turbulent flows", *Comp. Meth. Eng.*, 3: 269-289.

Linek V., Benes P., Vacek V., Hovorka F., 1982, Analysis of differences in kLa values determined by steady state and dynamic methods in stirred tanks, *Chem Eng. Journ*, 25, 77-88.

Linek V. , Vacek P., Benes P., 1987, A critical review and experimental verification of the correct use of the dynamic method for the determination of oxygen transfer in aerated agitated vessels to water, electrolyte solutions and viscous liquids, *Chem Eng. Journ*, 34, 11-34

Lucas, D., Prasser, H.-M., Manera, A.,Influence of the lift force on the stability of a bubble column, (2005) *Chemical Engineering Science*, 60 (13), pp. 3609-3619.

Luo J. Y., Issa R. I., Gosman A. D., 1994, Prediction of impeller induced flows in mixing vessels using multiple frames of referenc, *IChemE Symposium Series*, N. 136, 549-556.

Luo H., SVendsen H.F., 1996, Theoretical Model for Drop and Bubble Breakup in Turbulent Dispersions, *AIChE Journal*, Vol. 42, n.5, 1225-1233

Manna L., 1997, A method to study gas-liquid mass transfer using a slow chemical reaction, Recent Progres en Genie des Procedes (Ed. Lavoisier, Paris), 11, No. 52, 209-214.

Mendelson H.D., 1967, The Prediction of Bubble Terminal Velocity from Wave Theory, *A.I.Ch.E. Journal*, Vol. 13, N. 2, 250-253

Metha V.D., Sharma M.M., 1971, Mass Transfer in mechanically agitated gas-liquid contactors, *Chemical Engineering Science* 26, 461-479.

Micale G., A. Brucato, F. Grisafi and M. Ciofalo, 1999, Prediction of flow fields in a dual-impeller stirred vessel, *AIChE J*., 45 (3), 445-464

Micale G., G. Montante, F. Grisafi , A. Brucato, J. Godfrey, 2000, CFD simulation of particle distribution in stirred vessels, *Chem. Eng. Res. Des*., 78, 435-444.

Micale G., Grisafi F., Rizzuti L., Brucato A., 2004, "CFD simulation of particle suspension height in stirred vessels" *Chem. Eng. Res. Des*., 82 (A9), 1204-1213.

Middleton J.C., 1985, 'Gas-liquid dispersion and mixing' in Harnby N., Edward M.F. and Nienow A.W. (Eds.) Mixing in the Process Industries, Butterworth, pp 322-355

Mills P.L., Chaudari R.V., 1999, Reaction engineering of emerging oxidation processes, *Catalysys Today*, 48, 17-29

Mohamed M. S. and Larue J., 1990, The decay power law in grid generated turbulence, *Journal of Fluid Mechanics*, 219, 195-214.

Montante G., 2000, "Modelling and simulations of single-phase and solid-liquid stirred vessels", PhD Thesis, Università di Palermo.

Montante G., Lee K.C.,. Brucato A and Yianneskis M., 2001a, Numerical simulations of the dependency of flow pattern on impeller clearance in stirred vessels *Chem. Eng. Sci.*, 56, 3751-3770.

Montante G., Micale G., Magelli F., Brucato A., 2001b, "Experiments and CFD predictions of solid particle distribution in a vessel agitated with four pitched blade turbines", *Chem. Eng. Res. Des.*, 79, .1005-1010.

Morud K.E., B.H. Hjertager, 1996, LDA measurements and CFD modelling of gas-liquid flow in a stirred vessel, *Chem. Eng. Sci.*, 51, 233-249

Mudde R.F., Simonin O., Two- and three-dimensional simulations of a bubble plume using a two-fluid model, *Chem. Eng. Sci.*, 54, 5061-5069 (1999).

Mundale V. D., Design of gas inducing type agitated reactors. PhD (Technology) Thesis, Bombay University, 1993.

Mundale V.D. and Joshi B.J., 1995, 'Optimization of impeller design for gas inducing type mechanically agitated contactors', *Can. J. Chem. Eng.*, Vol. 73, 161-172.

Nienow A.W., Warmoeskerken M.M.C.G., Smith J.M., Konno M., 1985, On the flooding/loading transition and the complete dispersal condition in aerated vessels agitated by a Rushton turbine, *5th European Conference on Mixing*, Wurzburg, West Germany: 10-12 June, 1985, p. 143-154.

Nocentini M., 1990, Mass Transfer In Gas-Liquid, Multiple-Impeller Stirred Vessels: A Discussion about Experimental Techniques for kLa Measurement and Models Comparison, *Trans. IChemE, Part A*, 68,287-294.

Olmos E., Gentric C., Vial Ch., Wild G., Midoux N., 2001, Numerical simulation of multiphase flow in bubble columns reactors. Influence of bubble coalescence and breakup, *Chemical Engineering Science*, 6359-6365.

Patil S.S., Joshi J.B., 2003, Optimum Design of Multiple-Impeller Self-Inducing System, *Ind. Eng. Chem. Res.*, 42, 1261-1265

Patwardhan, A. W. and Joshi, J. B. 1997, "Hydrodynamics of a stirred vessel equipped with a gas-inducing impeller". *Ind. Eng. Chem. Res.*, 36, 3904-3914.

Patwardhan, A. W. and Joshi, J. B. 1999, Design of Gas-Inducing Reactors, *Ind. Eng. Chem. Res.*, 38, 49-80.

Paul E.L., Atiamo Obeng V.A., Kresta S.M., 2004, "Handbook of Industrial Mixing", Wiley and Sons, Table 6-4 p. 365

Pinelli G., Nocentini, and Magelli F., Modelling of the solid distribution in slurry reactors stirred with multiple impellers: influence of suspension

characteristics, *Proceedings of CHISA* '96, Paper D1.2 [515], Praha 25-30 August (1996)

Poncin, S., Nguyen, C., Midoux, N. and Breysse, J. 2002, "Hydrodynamics and volumetric gas-liquid mass transfer coefficient of a stirred vessel equipped with a gas-inducing impeller". *Chemical Engineering Science* 57, 3299-3306.

Poorte R.E.G., Biesheuvel A., 2002, Experiments on the motion of gas bubbles in turbulence generated by an active grid, *Journal of Fluid Mechanics*, 461, 127-154.

Prince M.J., Blanch H.W., 1990, Bubble Coalescence and Break-up in Air-Sparged Bubble Columns, *AIChE Journal*, Vol. 36, N.10, 1485-1499.

Ranade V.V. and J.B. Joshi, 1990, Flow Generated by a Disk Turbine .2. Mathematical-Modelling And Comparison With Experimental-Data*, Chem. Eng. Res. Des.* 68 (1): 34-50

Ranade V. V., Deshpande V. R., 1999, Gas-liquid flow in stirred reactors: Trailing vortices and gas accumulation behind impeller blades, *Chemical Engineering Science*, 2305-2315.

Ranade V.V. and Van den Akker H.E.A., 1994, A computational snapshot of gas-liquid flow in baffled stirred reactors, Chem. Eng. Sci. 49, 5175-5192

Ranade V.V., 1997, Modelling of turbulent flow in a bubble column reactor, *Chem. Eng. Res. Des.*, 75, 14.

Ranade V.V., R. Perrard, N. LeSauze, C. Xuereb, J. Bertrand, 2001, Influence of gas flow rate on the structure of trailing vortices of a Rushton turbine: PIV measurements and CFD simulations, *Chem. Eng. Res. Des.*, 79, 957-964.

Rielly, C. D., Evans, G. M., Davidson, J. F. and Carpenter, K. J. 1992, "Effect of vessel scaleup on the hydrodynamics of a self-aerating concave blade impeller". *Chemical Engineering Science* 47, 3395-3402.

Sanyal J., Vasquez S., Roy S., Dudukovic M.P., 1999, "Numerical simulation of gas-liquid dynamics in cylindrical bubble column reactors", *Chem. Eng. Sci.*, 54, 5071-5083.

Saravanan, K. and Joshi, J. B. 1995, "Gas-inducing type mechanically agitated contactors : hydrodynamic characteristics of dual impeller system". *Ind. Eng. Chem. Res.*, 34, 2499-2514.

Saravanan, K. and Joshi, J. B. 1996, "Fractional gas holdup in gas-inducing type of mechanically agitated contactors". *Can. J. Chem. Eng.* 74, 16-30.

Scargiali F, Grisafi F., Chermakova J., V. Machoň, A. Brucato, 2004, "Particle flow modelling in slurry-fed stirred vessels", *Chemical Engineering & Technology*, VOL 27, N° 3, 249-256

Scargiali F., Grisafi F., Brucato A., 2005, On the Performance of a Long Draft Tube Self-Ingesting Reactor for Gas-Liquid Operations, *Inzynieria Chemiczna i Procesowa* 26 (3), 499-511

Sokolichin A., Eigenberger G., 1999, "Applicability of the standard k- turbulence model to the dynamic simulation of bubble columns: part I. Detailed numerical simulations", *Chem. Eng. Sci.*, 54, 2273-2284.

Sommerfeld M., Kartushinskii, G.K., Rudi, Y.A., Khusainov, M.T., Shcheglov,I.N., 2000, "Experimental investigation of the effect of coarse particles on decaying grid-generated turbulence in a two-phase flow", *Fluid Dynamics*, vol.35, N°6, 872-882.

Spelt P.D.M., Biesheuvel A., 1997, On the motion of gas bubbles in homogeneous isotropic turbulence, *Journal of fluid Mechanics*, 221-224.

Stelmach, J. and Kuncewicz, C. 2001, "A comparison of the efficiency of self-aspirating and flat-blade impellers". I. *Symp. on Mixing in Ind. Proc.*, Toulouse, France.

Tomiyama A., Kataoka I., Zun I., Sakagichi T., 1998, Drag coefficients of single bubbles under normal and microgravity conditions, *JSME International Journal*, Series B, 41, 472-479.

Tomiyama A., Celata G.P., Hosokawa S., Yoshida S., 2002, Terminal velocity of single bubbles in surface tension force dominant regime, *Int. Journ. Mult. Flow,* 28, 1497-1519

Tryggvason G., Esmaeeli A., Lu J., Biswas S., 2006, Direct numerical simulations of gas/liquid multiphase flows, *Fluid Dynamics Research* 38 660–681

Uhlherr P.H.T., and Sinclair C.G., The effect of free styream turbulence on the drag coefficient of spheres, Proceedings *Chemeca '70*, Vol. 1, Butterworths, Melbourn, 1-13, (1970).

Van't Riet, 1979, Reviewing of measuring method and results in nonviscous gas-liquid mass transfer in stirred vessels, *Ind. Eng. Chem. Proc. Des. Dev.,* 18, 357-364.

Vasconcelos J.M.T., Nienow A.W., Martin T., Alves S.S., Mc Farlane C.M., 1997, Alternative ways of applying the hydrogen peroxide steady state method of kLa measurement, *Trans IChemE, 75, Part A*, 467-472.

Venneker B. C. H., Derksen J. J., Van den Akker H. E. A., 2002, Population Balance Modelling of Aerated Stirred Vessels Based on CFD, *AIChE Journa*l, Vol. 48, N. 4, 673-685.

Viollet P.L:, Simonin O., 1994, "Modelling dispersed two phase flows: closure, validation and software development", *Appl., Mech*., Rev.,47, 880-884.

Yakhot V., Prsza A., Yakhot A., 1987, "Heat transfer in turbulent fluids: I Pipe flow", *Int. J H M* T ,30, 15-22.

Zundelevich, Y. 1979, "Power consumption and gas capacity of self-inducing turbo aerators", *A.I.Ch.E. Journal* 25, 763-773.

List of publications strictly related to the present thesis

ISI journals

1. Francesca Scargiali, Franco Grisafi, Alberto Brucato, "On the Performance of a Long Draft Tube Self-Ingesting Reactor for Gas-Liquid Operations", *Chemical and Process Engineering* (INŻYNIERIA CHEMICZNA I PROCESOWA), VOL **26**, 499-511 (2005)
2. Scargiali F., Russo R., Grisafi F. Brucato A, "Mass Transfer and Hydrodinamic Characteristics of a High Aspect Ratio Self-Ingesting Reactor for Gas-Liquid Operations", *Chemical Engineering Science*, VOL **62**, N° 5, 1376 – 1387 (2007)
3. Scargiali F., D'Orazio A., Grisafi F., Brucato A., "Modelling and simulation of gas-liquid hydrodynamics in mechnically stirred tanks", Accepted for publication on *TransIChemE-Part A* (*ChERD*) (2007).

Conference Proceedings

4. Scargiali F., Riguccio D., Brucato A., "A novel self-ingesting stirred vessel for gas-liquid and three-phase operations", *5th International Symposium on Mixing in Industrial Processes, ISMIP5,* Seville, Spain, June 1-4 2004
5. Scargiali F., Di Maggio R., Brucato A., "Free turbulence effects on bubble terminal velocity", Proceedings of *3rd International Symposium on Two-Phase Flow Modeling and Experimentation*, Pisa, ISBN 88-467-1075-4, September 22-25, 2004
6. Scargiali F., "Misure di coefficienti di trasporto di materia in un reattore gas-liquido agitato autoaspirante", Proc. *PharmChem&Tech, Meeting di Dottorandi,* pag. 35-37, Palermo, 23-24 giugno 2005.
7. Scargiali F., Salvaggio S., Grisafi F., Brucato A. CFD simulation of gas-liquid hydrodynamics in a rectangular air–lift loop reactor, Proceedings of *10th Int. Conf. 'Multiphase Flow in Industrial Plant'* Tropea (Italy), pag. 515-526. ISBN 88-7458-049-5, Sept.20-22, 2006.
8. F. Scargiali, R. Russo, F. Grisafi, A. Brucato "On the measurement of mass transfer coefficient k_La in gas-liquid contactors via oxygen concentration dynamics" Proceedings of *17th*

International Congress of Chemical and Process Engineering, 27-31 August 2006, Prague

9. Scargiali F., "CFD simulations of Bio-reactors", Atti di *PharmChem&Tech 3, Meeting di Dottorandi,* Palermo, 12-13 luglio 2006, pag. 114-118.
10. Scargiali F, D'Orazio A, Grisafi F, Brucato A, CFD simulation of gas-liquid stirred vessels, Proceedings of *12th European Conference on Mixing*, pag. 463-470. ISBN 88-901915-9-7, Bologna, 27-30 June 2006

List of other publications

ISI journals

11. Piccarolo S, Scargiali F, Crippa G, Titomanlio G. "Relation between packing flow and mechanical properties of weld zones in injection-moulded thermoplastic polymers" *Plastics Rubber and Composites Processing and Applications;* VOL 19; N° 4 ,. 205-209 (1993, UK)
12. La Mantia FP, Valenza A, Scargiali F, "Nonisothermal Elongational Behavior of Blends With Liquid Cristalline Polymers". *Polymer Engineering and Science*; VOL 34; N° 10 Pag. 799-803 (1994, USA)
13. Scargiali F, Grisafi F., Chermakova J., V. Machoň, A. Brucato. "Particle flow modelling in slurry-fed stirred vessels", *Chemical Engineering & Technology*, VOL 27, N° 3, 249-256 (2004)
14. Scargiali F, Grisafi F., Chermakova J., V. Machoň, A. Brucato. "Residence Time Distribution of solid particles in a continuous, high-aspect ratio multiple-impeller stirred vessel" *Chemical Engineering Science,* VOL 59, N° 17, 3601-3618 (2004)
15. Scargiali F., Di Rienzo E., Ciofalo M., Grisafi F., Brucato A., "Heavy gas dispersion modelling over a topographically complex mesoscale: a CFD based approach." , *TransIChemE-Part B* (Process Safety and Env. Prot.), VOL 83 (B3), 242-256, (2005)
16. J. Čermáková, F. Scargiali, N. Siyakatshana, V. Kudrna, A. Brucato, V. Machoň, Axial dispersion model for solid flow in liquid suspension in system of two mixers in total recycle, *Chemical Engineering Journal*, 117, 101–107 (2006)

Conference Proceedings

17. Piccarolo S, Scargiali F, Crippa G, Titomanlio G, Gennaro "On improving weld line properties by effect of packing flow. Experiments with fibres filled polyamide." *European Regional Meeting of Polymer Society,* Palermo 18 Settembre 1991, P24, pag 295-296.
18. F Scargiali, E Di Rienzo, F Grisafi, A Brucato, M Ciofalo, M F Milazzo, G Maschio, "Modelling and Simulation of Heavy Cloud Atmospheric Dispersion in Semi Confined Urban Areas" *ACHEMA 2003 - 27th International Exhibition Congress on Chemical Engineering, Enviromental Protection and Biotechnology*, Frankfurt am Main/Germany, 19-24 May 2003, pag. 122.
19. J. Čermáková, N. Siyakatshana, V. Kudrna, V. Machoň, S. Castellino, F. Scargiali, A. Brucato, "Application of dispersion model on flow mixers with liquid and solid-liquid systems", *ECCE 4th European Congress of Chemical Engineering,* Granada (Spain), 21-25 September 2003
20. F. Scargiali, E. Di Rienzo, F. Grisafi, A. Brucato, M. Ciofalo, "Dense-Cloud Atmospheric Dispersion In Complex-Terrain Sites" Proceedings of *The sixth Italian Conference on Chemical and Process Engineering*, ICheaP-6, Pisa 8-11 June 2003, *Chemical Engineering Transaction*, Vol. 3, 2003, ISBN 88-900775-2-2, pag. 671-676.
21. Scargiali F., M. Ayrault*, F. Grisafi, L. Rizzuti, A. Brucato, "Dense plumes simulation by Computational Fluid Dynamics", *6° Congresso INCA,* Palermo, 2 - 4 Ottobre 2003, P28, 125-126..
22. F. Scargiali, G. Micale, A. Brucato, G. Maschio, M.F. Milazzo, "CFD simulation of Heavy Cloud Dispersion in Semi-confined Urban Areas", *6° Congresso INCA*, Palermo, 2 - 4 Ottobre 2003, O14, 49-50.
23. Brucato, F. Grisafi, G. Micale, L. Rizzuti, F.Scargiali, "Misura della concentrazione di solidi particellari mediante laser pulsato e analisi di immagini", *6° Congresso INCA*, Palermo, 2 - 4 Ottobre 2003, P31, 131-132.
24. F. Scargiali, J. Cermakova, F. Grisafi, V. Machon, A. Brucato, "Particle RTD assessment by means of twin system: application to a triple impeller stirred reactor", *6° Congresso INCA*, Palermo, 2 - 4 Ottobre 2003, P29, 127-128.
25. F. Grisafi, G. Micale, F. Scargiali, A. Brucato, L. Rizzuti, "PIV measurements of the flow field in the impeller discharge zone of an unbaffled stirred tank", *6° Congresso INCA*, Palermo, 2 - 4 Ottobre 2003, P36, 139-140.
26. Scargiali F., Conti M., Grisafi G., Brucato A., Maschio G., Milazzo M. F., "CFD simulation of dense cloud dispersion in urban areas", Proc. *Convegno GRICU 2004, Nuove Frontiere di Applicazione delle Metodologie dell'Ingegneria Chimica*, Porto d'Ischia (Napoli), 12-15 settembre 2004, ISBN 88 87030 80 4, pag. 533-536.

27. Castellino S., Chermakova J., Scargiali F., Grisafi F., Machon V., Brucato A., "Residence Time Distribution of Solid Particles in a High-Aspect Ratio Multiple-Impeller Stirred Vessel", Proceedings of *11th European Conference on Mixing,* 15-17 October 2003, Bamberg, Germany, ISBN 3-931384-45-4, pag. 145-152.
28. Francesca Scargiali, Franco Grisafi, Giorgio Micale, Alberto Brucato, "CFD simulation of dense plumes in an atmospheric wind tunnel", Proceedings of *11th International Symposium Loss Prevention and Safety Promotion in the Process Industries,* LP 2004, 31 May – 3 June 2004, Praha, Czech Republic, paper n. 0935, ISBN 80-02-01574-6, pag. 3137-3142.
29. Brucato A., Grisafi F., Scargiali F., Bonfiglio A., Cipollina A. "Heavy gas dispersion modelling by means of computational fluid dynamics" Proceedings of *The 1st Italian Convention on Safety & Environment in Process Industry,CISAP-1,* Palermo, Italy, 28-30 November 2004 *Chemical Engineering Transaction*, Vol. 5, 2004, ISBN 88-900775-5-7, pag. 241-248.
30. F. Scargiali, F. Grisafi, M. Ayrault, A. Brucato, "Comparison between experimental data and CFD simulations of a continuous heavy gas plume in an atmospheric wind tunnel", Proceedings of *The 2nd Italian Convention on Safety & Environment in Process Industry,CISAP-2, Napoli,* Italy, 21-24 May 2006, ISBN 88-901915-1-1, pag. 159-164

ACKNOWLEDGEMENTS

I wish to express my sincere gratitude to my supervisor Prof. Alberto Brucato for his excellent scientific supervision and for his enthusiastic assistance in this work.

I also wish to thank Prof. Franco Grisafi for his precious guidance in all aspects of my thesis work, Prof. Lucio Rizzuti, Prof. Giorgio Micale and Prof. Nino Sclafani for their excellent suggestions and friendship.

Finally I wish to thank all the students and colleagues, Giacinta Conte, Bartolomeo Cosenza, Cosimo D'Aiello, Roberto Di Maggio, Alessandro D'Orazio, Ignazio Macaluso, Roberta Messina, Mariella Mulè, Davide Riguccio, Riccardo Russo, Salvatore Salvaggio, Giuseppina Vella, Antonio Busciglio and Bruno Gibbardo, who in many ways contributed to this thesis.